University of South-Eastern Norway

www.usn.no

FMH606 Master's Thesis 2021

Energy and environmental technology

Modelling temperature transition and co-digestion in VEAS biogas process

Veronika Mikelsone

Faculty of Technology, Natural sciences and Maritime Sciences

Campus Porsgrunn

University of South-Eastern Norway

www.usn.no

Course: FMH606 Master's Thesis, 2021

Title: Modelling temperature transition and co-digestion in VEAS biogas process

Number of pages: 99

Keywords: Anaerobic digestion, mesophilic condition, thermophilic condition, modelling ADM-1, temperature transition, co-digestion, thermal hydrolysis, aircraft de-icing fluid.

Student:	Veronika Mikelsone
Supervisor:	Wenche Hennie Bergland and Gamunu L. Samarakoon Arachchige
External partner:	Espen Govasmark

University of South-Eastern Norway

www.usn.no

Summary:

Anaerobic digestion (AD) is a well-established way to stabilise concentrated sludge produced in wastewater treatment (WWT) plants. The benefit of the process is the production of biomethane and digestate that can be used as biofertiliser in land application. AD is a biological process, and many environmental parameters can influence its stability. One way to aid in the prediction and control of the process is to use mathematical modelling. This work aimed to assess the modelling of the transition from mesophilic to thermophilic AD by evaluating microbial adaptation to temperature shift. Also, evaluate the effects of co-substrate addition with the help of simulation. Consider the effect of Thermal Hydrolysis (THP) pre-treatment on AD and substrate. Additionally, assess if a potential increase of energy production by 50% is possible for VEAS.

In this work, a study of AD modelling was done to simulate the transition from mesophilic to thermophilic AD process and co-substrates. Anaerobic Digestion Model No. 1 (ADM1) was used as base model and modified to simulate the temperature transition and evaluate co-digestion. Two models temperature transition models, ADM1_CTM1 and ADM1_FTnew, were tested and evaluated same cases. Model ADM1_FTnew had a better match with data from the two laboratory-scale experiments than ADM1_CTM1. Modelling of additional co-substrate was done by implementing the input parameter for each substrate in ADM1. Four different co-substrates were used, three sludges with different composition and water with carbon-rich source as de-icing fluid (propylene glycol-based). Different scenarios were simulated with different substrates ratios and for two temperature conditions, mesophilic and thermophilic. The simulations with propylene glycol wastewater (PGW) showed a 10% and 11% increase in potential energy production for mesophilic and thermophilic process, respectively, with the organic loading rate (OLR) of propylene glycol containing wastewater (PGW) around 0.47 kgCOD/(m^3d). As for additional sludges, the carbon to nitrogen (C/N) ratio was in focus. Three sludges had different C/N ratios that were lower or almost equal to Vestfjorden Wastewater Company (VEAS) sludge C/N ratio of 9, used as the main feed. The simulations showed an increasing concentration of volatile fatty acids (VFA) in the reactors when the C/N ratio was below 9. For simulation with the lowest C/N ratio of 3.7, the average VFA concentration was at 3.2 kgHAc/m^3. These high VFA concentrations shows that the C/N ratio of 9 the lowest advisable value for stable process. The highest increase in potential energy production was observed when all co-substrates were added, and OLR was increased from 3.6 to 4.5 kgCOD/(m3·day). The increase was 26% for the mesophilic and 47% for the thermophilic processes.

THP literature review showed a possibility of implementing THP in AD modelling by increasing hydrolysis rate and solubilising particulate components. Though more work needed to estimate simulation parameters for different substrates.

Acknowledgement

To my supervisors, Associate Prof. Wenche Hennie Bergland, Associate Prof. Gamunu L. Samarakoon Arachchige and Espen Govasmark from VEAS thank you. You shared your knowledge with me and guided me through this project, and I highly appreciate your time investment. I want to also thank Kine Svensson from CAMBI for finding time for me and sharing her knowledge. My thanks also to my family for their support and patients during the project.

Porsgrunn, 19.05.2021

Veronika Mikelsone

Contents

1 Introduction 17

1.1 Background and motivation for the thesis 17
1.2 VEAS – Vestfjorden Wastewater Company 17
1.3 Aim and objective of the thesis. 17
1.4 Scope of the thesis 18
1.5 Report structure info 18

2 Theory 20

2.1 VEAS process 20
2.2 Anaerobic digestion 21
2.2.1 Process description 21
2.3 Factors of importance for anaerobic digestion 22
2.3.1 Retention time 22
2.3.2 Organic loading rate 22
2.3.3 pH and alkalinity 23
2.3.4 Nutrients and trace metals 23
2.3.5 Carbon to nitrogen (C/N) ratio 23
2.3.6 Inhibition 23
2.3.7 Temperature 24
2.4 Mesophilic and thermophilic digestion 24
2.4.1 Transition from mesophilic to thermophilic process 24
2.5 Anaerobic co-digestion 25
2.5.1 Additional sludge from different treatment plants 25
2.5.2 Anaerobic co-digestion of de-icing fluid from airport 26
2.6 Thermal hydrolysis pre-treatment process 28
2.7 Anaerobic Digestion Model No 1 31

3 Material and methods 33

3.1 Mesophilic and thermophilic (steady-state) process model 33
3.2 Temperature transition (dynamic) models 33
3.2.1 Linear model 33
3.2.2 ADM1_CTM1 33
3.2.3 ADM1_FTnew 34
3.3 Co-substrates implementation 36
3.3.1 Adding different sludge to the model 36
3.3.2 Adding glycol to the model 39
3.4 Energy content estimation 40
3.5 Simulation cases overview 41

4 Results 44

4.1 Validation results of temperature transition models 44
4.1.1 Validation of ADM1_FTnew model 44
4.1.2 Validation of ADM1_CTM1 model 46
4.2 Temperature transition simulation results 48
4.2.1 Laboratory scale experiment 48
4.2.2 VEAS 2016-2017 50
4.3 Mesophilic process simulation results 56
4.3.1 Mesophilic process simulation with propylene glycol 58
4.3.2 Mesophilic process simulation with additional sludge 62
4.3.3 Mesophilic process simulation with propylene glycol and sludges 67

4.4 Thermophilic process simulation results 71
4.4.1 Thermophilic process simulation with propylene glycol 74
4.4.2 Thermophilic process simulation with additional sludges 78
4.4.3 Thermophilic process simulation with propylene glycol and sludges 82
4.5 Methane yield and production 87

5 Discussion 90

5.1 Temperature transition models 90
5.1.1 Performance of ADM1_FTnew model 90
5.1.2 Performance of ADM1_CTM1 model 90
5.2 Effects of co-digestion 91
5.2.1 Propylene glycol as co-substrate 91
5.2.2 C/N ratio in additional sludges 92
5.3 THP 92
5.4 Energy production potential 93

6 Conclusion 94

Nomenclature

Abbreviation	Description
AA	Amino acids
AD	Anaerobic digestion
ADM1	Anaerobic Digestion Model 1
ADM1_CTM1	ADM1 model with CTM1 temperature transition model implemented
ADM1_Ftnew	ADM1 model with Ftnew temperature transition model implemented
BioModel	Multistep dynamic AD model
BMP	Biochemical methane potential
C/N-ratio	Carbon to nitrogen ratio
CM	Cattle manure
COD	Chemical oxygen demand
CSTR	Continuous flow stirred-tank reactor
HAc	Acetic acid
HBu	Butyric acid
HPr	propionic acid
HRT	Hydraulic retention time
Hva	valeric acid
IC	Inorganic carbon
IN	Inorganic nitrogen
LCFA	Long chain fatty acids
MAD	mesophilic anaerobic digestion
MS	Monosaccarids
OLR	Organic loading rate
PG	Propylene glycol
PGW	Propylene glycol containing wastewater
PS	Primary sludge
S0	Sludge 0, from VEAS

S1	Sludge 1, Marker municipality
S2	Sludge 2, Aremark municipality
S3	Sludge 3, Indre Østfold Municipality
sCOD	Soluble oxygen demand
SRT	Solids retention time
STP	Standard Temperature and Pressure
TAD	Thermophilic anaerobic digestion
TAN	Total amonia nitrogen
tCOD	Total chemical oxygen demand
ThOD	Theoretica oxygen demand
THP	Thermo hydrolysis precess
TKN	Total Kjeldahl Nitrogen
TN	Total Nitrogen
TOC	Total organic carbon
TS	Total solids
VEAS	Vestfjorden Wastewater Company(Vestfjorden Avløpsselskap)
VEAS_MS	Simulation of VEAS process with mesophilic temperature
VEAS_TS	Simulation of VEAS process in thermophilic temperature
VFA	Volatile fatty acids
VS	Volatile solids
VSR	Volatile solid reduction
WAS	Waste activated sludge
WWT	wastewater treatment

Symbol	Description	Units
$\mu(T_e)$	Maximum temperature-specific microbial growth rate	[1/d]
μ_{max}	Maximum achiveble microbial growth rate	[1/d]
b	Kinetic parameter calculated in CTM1	
b_{opt}	Optimum value of the kinetic parameter	
F_{Tnew}	Dynamic temperature-dependent maximum growth rate	[1/d]
F_{Tref}	Steady-state temperature-dependent maximum growth rate	[1/d]
$I_{inhibitor,\ process}$	Inhibition function	
Input_K_sludge_i	Input part of flowrate for substrate i	
Input_Q_{in}_dyn	Input dynamic flowrate in AQUASIM	
Input_Q_{in}_sludge_i	Input flowrate for substrate i	
Input_S_i	Inpit variables in AQUASIM for soluble components	
Input_X_i	Inpit variables in AQUASIM for particulate components	
k_{hyd_ch}	First order parameter for hydrolysis of carbohydrates	[1/d]
k_{hyd_li}	First order parameter for hydrolysis of lipids	[1/d]
k_{hyd_pr}	First order parameter for hydrolysis of proteins	[1/d]
k_j	First order parameter for process j	[1/d]
k_m	Monod maximum specific uptake rate	[kgCOD/(kgCOD·d)]
K_s	Half saturation value	[kgCOD_S/m^3]
P	Pressure	bar
P_N	STP preasure	bar
S_{hg}	Constant of change in degrees Celsius	[^oC]
S_i	Soluble component i	[kgCOD/m^3]
T	Temperature	[^oC]
T_a	Temperature microbial groupe adapted to	[^oC]
T_e	Effective or actual temperature	[^oC]
T_{max}	Maximum growth temperature	[^oC]
T_{min}	Minimum temperatures for the microorganism group	[^oC]

Nomenclature

T_N	STP temperature	[^oC]
T_{opt}	Optimum growth temperature	[^oC]
V	Volume	[m^3]
V_N	Normalized volume	[Nm^3]
X_i	Particulate component i	[$kgCOD/m^3$]
α	regression coefficient	[$1/(d \cdot ^oC)$]
ρ_j	Kinetic rate of process j	[$kgCOD\_S/(m^3 \cdot d)$]
σ	Sigma parameter	
τ_a	Microbial group adapttion time constant	[d]

List of Tables

Table 2.1: Some typical value ranges for chemical composition of untreated primary and activated sludge [1]. 26

Table 2.2: Reactions for decomposition of PG to methane, adapted from [22] 27

Table 2.3: Effect of THP on solubilization of particulate material, pH and VFA, ammonium nitrogen in waste activated sludge. 29

Table 3.1: Values for (T_{min}) minimum, (T_{opt}) optimum and (T_{max}) maximum temperatures used in ADM1_CTM1 model for calculation of kinetic parameters in temperature transition. 34

Table 3.2: Parameter values used for the ADM1_FTnew model to simulate temperature transition effect on growth of microorganisms.[34] 36

Table 3.3: The final input parameters for sludge S1 Marker, sludge S2 Aremark, sludge S3 Indre Østfold and sludge S0 VEAS sludge. 38

Table 3.4: Mesophilic digestion parameters added in ADM1 for PG degradation. 40

Table 3.5: Overview of parameters for the simulations done in this work. 41

Table 4.1: Differences between VEAS 2019 data and the simulation. Average values for the same period for both data points and simulation. 58

Table 4.2: Comparison of some average results values from simulations 6.1, 6.2 and 6.3 where PGW to SS ratios are 7.5:192.5 for 6.1, 10.8:189.2 for 6.2 and 14:186 for 6.3 against standard VEAS process simulation. Average values calculated for the same time period for all simulations. 62

Table 4.3: Comparing some average results values from simulations with co-substrate against not altered VEAS process simulation. Average values calculated for the same time period for simulation 5.1, 5.2, 5.3, 5.4 and VEAS process simulation. 66

Table 4.4: Comparing some average results values from simulations with PGW and additional sludges against VEAS process simulation. Average values were calculated for the same period of time for all simulations. 70

Table 4.5: Comparison of average values for mesophilic and thermophilic VEAS simulations together with the relative difference between them. Average values calculated for the same time period for all simulations. 74

Table 4.6: Comparing the relative difference between chosen parameters for some simulations. They were calculated from average values for the same time period in simulations. 78

Table 4.7: Average value for $I_{h2,\ pro}$ (inhibition function) showing inhibition by hydrogen in ADM1 for propionate degraders where 1 is no inhibition 0 is fully inhibited. 78

Table 4.8: Chosen simulations compared by relative difference. Calculation of difference based on the average value taken for the same period for all simulations. 82

Table 4.9: Comparison of relative difference for the chosen simulations. Difference calculated from the average values for the same period for 7.1, 7.3, 10.1 and 10.2. 86

List of Figures

Figure 2.1: VEAS main process flow diagram.[2] 20

Figure 2.2: Schematic representation of AD (AA is amino acids).[5], [6].....22

Figure 2.3: Decomposition pathway of PG in anaerobic conditions; figure was taken from [22]. 27

Figure 2.4: Illustration of Cambi™ batch THP process [29].....29

Figure 2.5: Illustration of the AD steps as implemented in ADM1 with COD flux for the process (monosaccharides (MS); amino acids (AA); long chain fatty acids (LCFA); propionic acid (HPr); butyric acid (HBu); valeric acid (HVa)). [5] 31

Figure 3.1: Illustration of parts of proteins, lipids, carbohydrates and inerts in four sludges used for simulations (1 – Sludge S1 Marker, 2 – Sludge S2 Aremark, 3- Sludge S3 Indre Østfold, 4 – Sludge S0 VEAS sludge).....37

Figure 4.1: Simulated gas production by using ADM1_FTne model(1.1) and reproduced experimental data from [34] research papers (Kovalovzski et al.). 44

Figure 4.2: Simulation results for acetate concentration from ADM1_FTne model(1.1) compared to experimental results from Kovalovszki et al. [34] paper. 45

Figure 4.3: Experimental values reproduced from [34] compared to simulated values by ADM1_FTnew model(1.1). 45

Figure 4.4: Comparing experimental gas flow data points from experimental data [5](Bouškova) and simulated gas flow for the same parameters used in ADM1_CTM1(2.1).....46

Figure 4.5: Comparison of experimental acetate concentration data points from research paper [5] and simulated acetate concentration for the same parameters using ADM1_CTM1(2.1) model.....47

Figure 4.6: Comparison of experimental methane content in biogas data points from research paper [5] and simulated methane content for the same parameters using ADM1_CTM1(2.1) model.....47

Figure 4.7: Comparison of experimental biogas flow data points from research paper [5] and simulated biogas flow for the same parameters using ADM1_FTnew (1.2) and ADM1_CTM1 (2.1) models. 48

Figure 4.8: Comparison of experimental methane content in biogas data points from research paper [5] and simulated methane content for the same parameters using ADM1_FTnew (1.2) and ADM1_CTM1 (2.1) models.....49

Figure 4.9: Comparison of experimental acetate concentration data points from research paper [5] and simulated methane content for the same parameters using ADM1_FTnew (1.2) and ADM1_CTM1 (2.1) models. 49

Figure 4.10: Comparison of VEAS process data points for biogas flow from years 2016-2017 to three models, linear model from previous work[35], ADM1_CTM1 model and ADM1_FTnew model. 50

Figure 4.11: Comparison of VEAS process data points for methane content in biogas flow from years 2016-2017 to three models, linear model from previous work[35], ADM1_CTM1 and ADM1_FTnew models. 51

Figure 4.12: Comparison of VEAS process data points for pH from years 2016-2017 to three models, linear model from previous work[35], ADM1_CTM1 model and ADM1_FTnew model.....51

Figure 4.13: Comparison of VEAS process data points for bicarbonate concentration from years 2016-2017 to three models: linear model from previous work[35], ADM1_CTM1 and ADM1_FTnew models. 52

Figure 4.14: Comparison of VEAS process data points for acetate concentration from years 2016-2017 to three models, linear model from previous work[35], ADM1_CTM1 and ADM1_FTnew models. 53

Figure 4.15: Comparison of VEAS process data points for NH3 and NH4 from years 2016-2017 to three models, linear model from previous work[35], ADM1_CTM1 model and ADM1_FTnew model. 53

Figure 4.16: Comparison of NH3 inhibition of acetate degrading organisms between three models, linear model from previous work[35], ADM1_CTM1 and ADM1_FTnew models. 54

Figure 4.17: Comparing biomass concentration of acetate degraders between three models: linear model from previous work[35], ADM1_CTM1 model and ADM1_FTnew model.....54

Figure 4.18: Comparison of Monod specific growth rate of acetate degraders between three models: linear model from previous work[35], ADM1_CTM1 model and ADM1_FTnew model.....55

Figure 4.19: Biogas production from VEAS 2019 data compared to simulated VEAS 2019 mesophilic process. 56

Figure 4.20: Methane content in biogas from VEAS 2019 process data points against simulation results of the same process. 56

Figure 4.21: pH data points from VEAS 2019 process compared with the simulation of the same VEAS 2019 mesophilic process. 57

Figure 4.22: Acetate concentration data points from VEAS 2019 process compared to the simulated VEAS 2019 process.....57

Figure 4.23: Bicarbonate concentration from VEAS 2019 process data points compared to values obtained from simulation of the same process. 58

Figure 4.24: Comparison of VEAS 2019 biogas flow from both simulation and data points to three VEAS process simulations with PGW, where PGW to SS ratios are 7.5:192.5 for 6.1, 10.8:189.2 for 6.2 and 14:186 for 6.3. 59

Figure 4.25: Comparison of VEAS 2019 methane content from both simulation and data points to three VEAS process simulations with PGW, where PGW to SS ratios are 7.5:192.5 for 6.1, 10.8:189.2 for 6.2 and 14:186 for 6.3. 59

Figure 4.26: Comparison of VEAS 2019 pH values from both simulation and data points to three VEAS process simulations with PGW, where PGW to SS ratios are 7.5:192.5 for 6.1, 10.8:189.2 for 6.2 and 14:186 for 6.3. 60

Figure 4.27: Comparison of VEAS 2019 acetate concentration from both simulation and data points to three VEAS process simulations with PGW, where PGW to SS ratios are 7.5:192.5 for 6.1, 10.8:189.2 for 6.2 and 14:186 for 6.3. 60

Figure 4.28: Comparison of VEAS 2019 bicarbonate concentration from both simulation and data points to three VEAS process simulations with PGW, where PGW to SS ratios are 7.5:192.5 for 6.1, 10.8:189.2 for 6.2 and 14:186 for 6.3. 61

Figure 4.29: Comparison of NH4 concentrations from VEAS process simulation to the three process simulations with PGW as co-substrate, where PGW to SS ratios are 7.5:192.5 for 6.1, 10.8:189.2 for 6.2 and 14:186 for 6.3. 61

Figure 4.30: Comparison of biogas flow from VEAS 2019 process data and VEAS process simulation to four VEAS process simulations with additional sludges. 63

Figure 4.31: Comparison of methane content in biogas from VEAS 2019 process data and VEAS process simulation to four VEAS simulations with additional sludges. 63

Figure 4.32: Comparison of pH values from VEAS 2019 process data and VEAS process simulation to four VEAS simulations with additional sludges. 64

Figure 4.33: Comparison of acetate concentration from VEAS 2019 process data and VEAS process simulation to four VEAS simulations with additional sludges. 65

Figure 4.34: Comparison of inorganic nitrogen concentration from VEAS process simulation to four VEAS simulations with additional sludges. 65

Figure 4.35: Comparison of bicarbonate concentration from VEAS 2019 process data and VEAS process simulation to four VEAS simulations with additional sludges. 66

Figure 4.36: Comparison of biogas flow from VEAS 2019 process data and VEAS process simulation to three VEAS simulations with PGW and additional sludges. 67

Figure 4.37: Comparison of methane content in biogas from VEAS 2019 process data and VEAS process simulation to three VEAS simulations with PGW and additional sludges. 68

Figure 4.38: Comparison of pH values from VEAS 2019 process data and VEAS process simulation to three VEAS simulations with PGW and additional sludges. 68

Figure 4.39: Comparison of biogas flow from VEAS 2019 process data and VEAS process simulation to three VEAS simulations with PGW and additional sludges. 69

Figure 4.40: Comparison of IN concentration from VEAS 2019 process data and VEAS process simulation to three VEAS simulations with PGW and additional sludges. 69

Figure 4.41: Comparison of bicarbonate concentration from VEAS 2019 process data and VEAS process simulation to three VEAS simulations with PGW and additional sludges. 70

Figure 4.42: Biogas production from VEAS 2019 process data and mesophilic simulation compared to VEAS thermophilic simulation. 71

Figure 4.43: Methane content in biogas from VEAS 2019 process data and mesophilic simulation compared to VEAS thermophilic simulation. 72

Figure 4.44: pH value from VEAS 2019 process data and mesophilic simulation compared to VEAS thermophilic simulation. 72

Figure 4.45: Acetate concentration from VEAS 2019 process data and mesophilic simulation compared to VEAS thermophilic simulation. 73

Figure 4.46: Bicarbonate concentration from VEAS 2019 process data and mesophilic simulation compared to VEAS thermophilic simulation. 73

Figure 4.47: IN concentration from VEAS mesophilic simulation compared to VEAS thermophilic simulation. 74

Figure 4.48: Comparison of simulated biogas flow from VEAS mesophilic simulation, mesophilic simulation with PGW (6.3) to VEAS thermophilic simulations and thermophilic simulations with PGW (9). 75

Figure 4.49: Comparison of simulated methane content in biogas from VEAS mesophilic simulation with and without PGW to VEAS thermophilic simulations with and without PGW. 75

Figure 4.50: Comparison of simulated pH from VEAS mesophilic simulation with and without PGW to VEAS thermophilic simulations with and without PGW. 76

Figure 4.51: Comparison of simulated acetate concentration from VEAS mesophilic simulation with and without PGW to VEAS thermophilic simulations with and without PGW. 76

Figure 4.52: Comparison of simulated bicarbonate concentration from VEAS mesophilic simulation with and without PGW to VEAS thermophilic simulations with and without PGW. 77

Figure 4.53:Comparison of simulated IN concentration from VEAS mesophilic simulation with and without PGW to VEAS thermophilic simulations with and without PGW. 77

Figure 4.54: Comparison of simulated biogas flow from VEAS thermophilic simulations with and without additional sludge. 79

Figure 4.55: Comparison of simulated methane content in biogas from VEAS thermophilic simulations with and without additional sludge..... 79

Figure 4.56: Comparison of simulated acetate concentration from VEAS thermophilic simulations with and without additional sludge..... 80

Figure 4.57: Comparison of simulated bicarbonate concentration from VEAS thermophilic simulations with and without additional sludge..... 80

Figure 4.58: Comparison of simulated pH from VEAS thermophilic simulations with and without additional sludge. 81

Figure 4.59: Comparison of simulated biogas flow from VEAS thermophilic simulations with and without additional sludge. 81

Figure 4.60: Comparison of simulated biogas flow from VEAS thermophilic and mesophilic simulations with PWG and additional sludges. 83

Figure 4.61: Comparison of simulated methane content in biogas from VEAS thermophilic and mesophilic simulations with PWG and additional sludges. 83

Figure 4.62: Comparison of simulated acetate concentration from VEAS thermophilic and mesophilic simulations with PWG and additional sludges. 84

Figure 4.63: Comparison of simulated bicarbonate concentration from VEAS thermophilic and mesophilic simulations with added PWG and additional sludges. 84

Figure 4.64: Comparison of simulated IN concentration from VEAS thermophilic and mesophilic simulations with added PWG and additional sludges. 85

Figure 4.65: Comparison of simulated pH from VEAS thermophilic and mesophilic simulations with added PWG and additional sludges. 85

Figure 4.66: Methane yield for VEAS 2019 process and all simulations (blue mesophilic process, orange thermophilic). 87

Figure 4.67: Volume of methane (STP) produced per year by VEAS in 2019 and simulated production for all simulations (blue mesophilic process, orange thermophilic). 88

Figure 4.68: Potential energy production from methane for VEAS 2019 and all simulations (blue mesophilic process, orange thermophilic). 88

Figure 4.69: Difference in simulated potential energy from methane compared to VEAS mesophilic simulation (blue mesophilic process, orange thermophilic). 89

1 Introduction

The introduction chapter contains the description of the background for the master thesis. Defines the scope, aim and objectives that need to be achieved by the end of the project. It also provides an overview of the report structure.

1.1 Background and motivation for the thesis

Anaerobic digestion (AD) is a well-established sludge stabilisation process. It is beneficial due to its ability to process concentrated sludges from wastewater treatment and produce sufficient biogas with enough energy required for plant operation.[1]

AD is a biological process and is influenced by many process parameters. Also, it takes time to recover in case of imbalance. Though significant progress was achieved in understanding the fundamentals and control of the AD process, further research for improvement can be done. One possibility to achieve that is to use mathematical models to simulate the AD process, which can potentially help explore positive and negative effects on AD from, e.g., adding additional substrates and pre-treatments. As well as serve as a tool to evaluate a more efficient process of recovering energy from wastewater. This serves as a motivation for this work to aid in improving the AD process at VEAS by modelling changes they want to explore.

1.2 VEAS – Vestfjorden Wastewater Company

VEAS is a wastewater treatment plant that is owned by Oslo, Asker and Bærum municipalities. Wastewater collected from Oslo, Asker, Bærum, Røyken and Nesodden is treated around the clock and all year round at VEAS wastewater treatment (WWT) plant at Bjerkås in Asker. Equivalent to 750 000 persons of wastewater from owner municipalities is transported via the VEAS tunnel to the treatment plant. In addition to WWT, VEAS produces biogas in 4 biogas reactors that digest sludge from the WWT plant at anaerobic mesophilic conditions. From biogas production, they get methane that is used to produce energy and heat for the plant and heat for the district heating. In 2020 VEAS had an upgrade on biogas plant to produce liquefied methane that can be used as fuel in transportation. Other byproducts from VEAS processes are stabilized and sanitized sludge, VEAS soil for agricultural use, and nitrogen solution for, e.g., fertilizer production [2].

In the future, VEAS is aiming to improve the process of biogas production by 50%. To achieve a 50% increase in production, several changes in the process are assessed. The increase in temperature from mesophilic to thermophilic condition, implementation of pre-treatment technology in the process, and new substrates are all looked into.

1.3 Aim and objective of the thesis.

The work with modelling anaerobic digestion is done extensively in the last few decades for both mesophilic and thermophilic temperatures. Though not much research is done in modelling transitions from one temperature range to another. This thesis aims to investigate microbial adaptation to temperature shift and how it can benefit the analysis of VEAS transition from mesophilic to thermophilic temperatures in the years 2016-2017. The objectives then are

to quantitatively analyse the microbial behaviour to temperature change and then model microbial adaptation to temperature transition. The mathematical model used is Anaerobic Digestion Model No.1 (ADM1), the most common model used for AD modelling. Then simulate VEAS temperature transition with the suggested models and evaluate the possibility of temperature transition optimisation with the simulations.

The second aim of the thesis is to assess the potential effects of additional co-substrates and pre-treatment process on anaerobic digestion. Further, evaluate if the two process modification helps to achieve 50 % increase in biogas production. For the aim to be reached, the following objectives are defined for this thesis. Implement co-substrates addition to VEAS process simulations for both mesophilic and thermophilic conditions. Assess the effect of the Thermal Hydrolysis Process (THP) on the AD.

1.4 Scope of the thesis

The scope of this thesis is to do a literature review and assess mechanisms on how microorganisms in AD adapt to temperature transition from mesophilic to thermophilic temperature. The focus will be on change in kinetic parameters like uptake rates, a yield of biomass and growth rates in the dynamic temperature transition. Further, implement changes needed in Anaerobic Digestion Model No.1 (ADM1) to further simulate and assess VEAS transition from mesophilic to thermophilic process in 2016 - 2017. Study of the effects of supplementary substrate and pre-treatment that VEAS plans to implement will be done using ADM1. Steady-state simulations are to be used in assessing the effects of additional substrates in terms of C/N ratio and gas production. Thermal Hydrolysis Process (THP) pre-treatment will be evaluated only theoretically without implementing in ADM1.

1.5 Report structure info

This report starts with a short introductory chapter that starts with motivation for this master thesis, followed by a short presentation of VEAS. Then aim and objective of the thesis and the definition of the thesis scope.

In the Theory chapter theoretical part of the topic relevant to this report are presented. Topics of interest are AD and factors that influence AD, like retention time, loading rates, pH and alkalinity, nutrients, inhibition factors and temperature. Two different temperature conditions, mesophilic and thermophilic, will be described alongside a short overview of key points from the ADM1 model and co-digestion with the relevant pre-treatment process.

The material and method part presents the overview of simulation cases and how the models used are constructed. Moreover, implementing different co-substrates in ADM1.

The result chapter will present results from simulated cases for temperature transition from mesophilic to thermophilic temperature. Then results of steady-state mesophilic and thermophilic process with implemented modifications and additions to the process.

The discussion chapter presents an evaluation of the simulation result. It is divided into four sub-chapters. The first sub-chapter is discussing the results from the temperature transition models testing. The second and the third assesses mesophilic and thermophilic AD with parameter and process variations. The last one evaluates energy production potential increase by adding co-substrates.

The conclusion chapter will present what the study has determined from the discussion and presented results. As well as conclude if the simulations show that a 50% increase in biogas yield for VEAS is plausible.

2 Theory

2.1 VEAS process

VEAS treats wastewater from the municipalities around Oslofjord, and the main treatment flow diagram is presented in Figure 2.1. VEAS process starts with screening to remove coarse solids and litter, then removal of sand and grit in a sand trap. The removed material from the screen and sand trap is disposed of as waste, then coagulants, Aluminium and Ferric chlorides, are added to the wastewater. After these steps, wastewater is transferred to the primary sedimentation tank and added polymer flocculant. From the sedimentation tank, water is pumped further to biological treatment and then to the Oslofjord. As for settled primary sludge (PS), it is transported to the thickening process, after which the PS is around 7% Total solids (TS).

After thickening, the PS is sent to an equalization tank for pre-heating and then to 4 bioreactors. The reactors are continuous flow stirred-tank reactors (CSTR) with 6000 m^3 volume each and operate at mesophilic temperature (37^{o}C). The active volume of each reactor in 2019 was approximately 5000m^3, and average OLR and hydraulic retention time (HRT) of 2.25 kgVS/m^3· d and 25.9 days, respectively [3]. The feeding of the reactors is semi-continuous, meaning that the effluent is withdrawn from the reactor before the substrate is added. The substrate is added to each reactor in a cycle of 180 minutes for 45minutes per reactor.

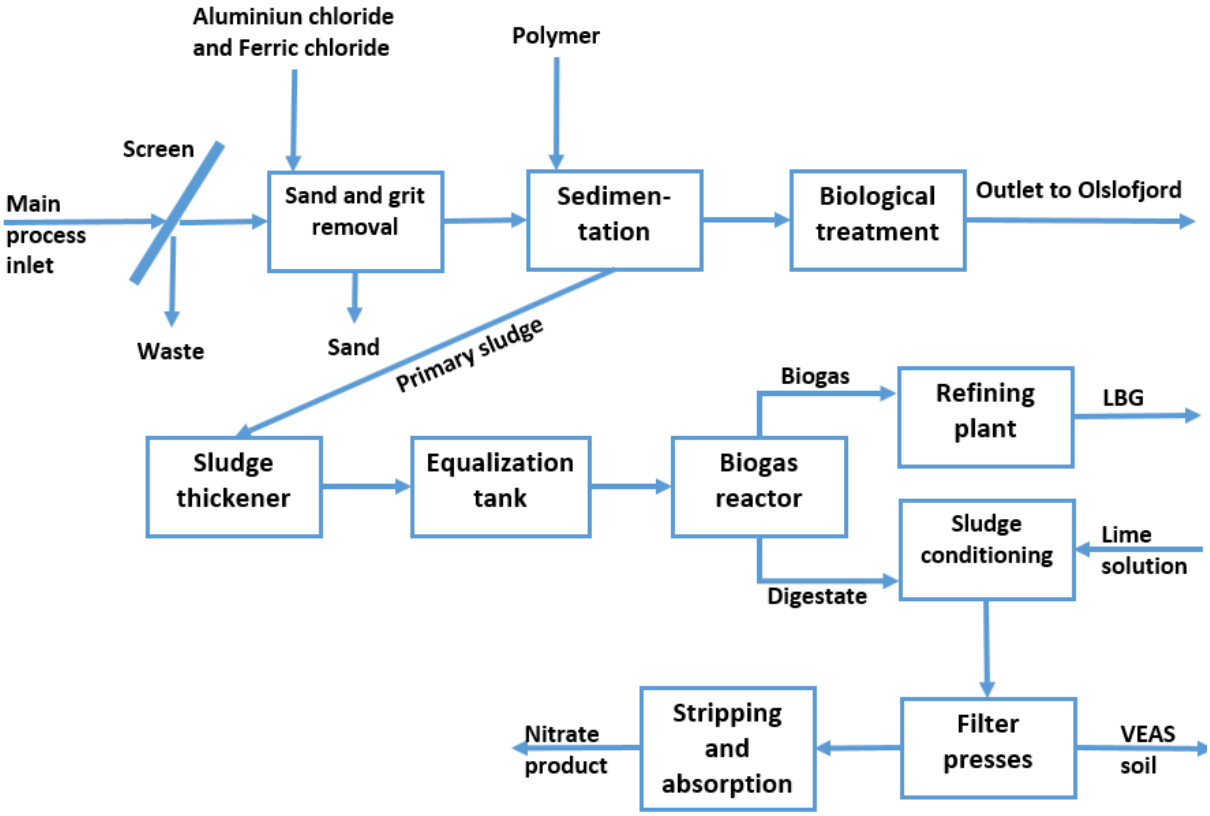

Figure 2.1: VEAS main process flow diagram.[2]

The produced biogas from the reactors is sent to the refining plant to produce liquid biogas (LBG) after it can be used as fuel. Digestate is added lime solution in the conditioning step,

then transported to dewatering process. In the dewatering process, a VEAS soil is produced together with ammonia-rich water. The ammonia-rich water is then transported to the stripping tower to strip it for ammonia, which can then be used to produce fertilizer.

2.2 Anaerobic digestion

AD is a biological process of stabilising primary and secondary sludge in the absence of molecular oxygen. Here, biodegradable material is converted to methane, carbon dioxide, microbial biomass mainly and some other products. The main advantage of AD treatment compared to aerobic treatment is energy production in the form of biogas [4]. The most common temperature ranges that AD can be operated at is mesophilic (30 – 35^{o}C). Another temperature range of interest for this thesis is thermophilic (50 – 57^{o}C), which also had an interest increase in the last years.[1]

2.2.1 Process description

Processes of converting biodegradable material into biogas can be separated in two main types. The first type of processes is biochemical, which includes intracellular and extracellular processes. The second type is physico-chemical, which are not biological processes and include gas-liquid transfer, precipitation and ion association/dissociation.[5]

Extracellular processes have two steps which are disintegration and hydrolysis. Then intracellular processes include three steps which are acidogenesis or fermentation, acetogenesis and methanogenesis [5]. All steps are shown in Figure 2.2.

In the disintegration and hydrolysis steps, complex organic material is broken down and converted to soluble substrates. Composite particulate materials are broken down in disintegration step into mainly complex polymers. Hydrolysis is a step at which complex polymers, with the help of enzymes produced by different microorganisms, convert to monomers and oligomers. Different enzymes are needed to break down lipids, carbohydrates, and fats. Lipids are broken down into long chain fatty acids (LCFA), proteins to amino acids and carbohydrates to monosaccharides.[4], [5]

The first intracellular step is acidogenesis which is a microbial process, and here, volatile fatty acid (VFA), CO_2 and hydrogen are produced. Sugars and amino acids ferment into acetate, propionate, butyrate, CO_2 and hydrogen and LCFA ferment into acetate, CO_2 and hydrogen. In this process, there is no need for an additional electron acceptor or donor as substrates serve as both.[4]

The second intracellular step is acetogenesis which is further bacterial fermentation to produce acetate, CO_2 and hydrogen from propionate, butyrate and valerate. [4]

The third intracellular step is methanogenesis which is carried out by Archaea organisms. There are two groups of these methanogenic organisms: aceticlastic methanogens and hydrogenotrophic methanogens. Aceticlastic methanogens split acetate into methane and CO_2 when hydrogenotrophic methanogens use hydrogen and CO_2 as electron donor and electron acceptor, respectively.[4]

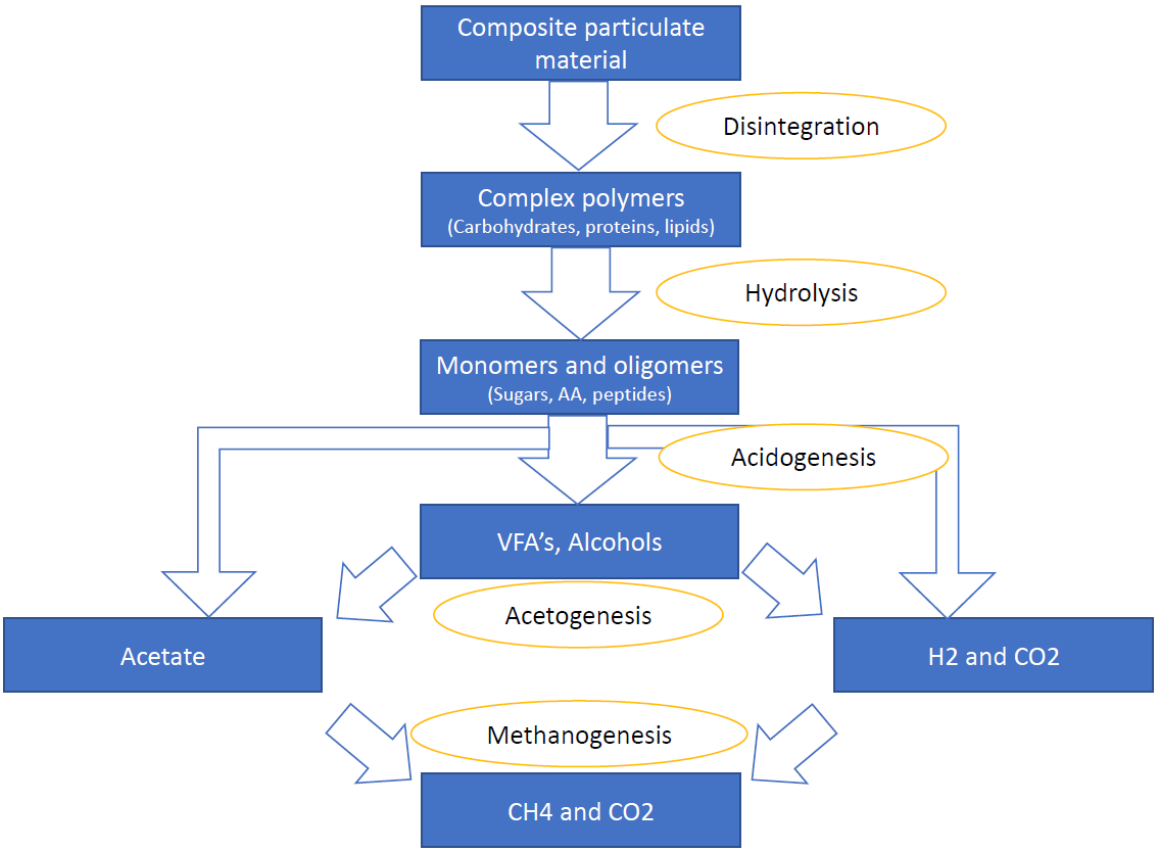

Figure 2.2: Schematic representation of AD (AA is amino acids).[5], [6]

2.3 Factors of importance for anaerobic digestion

Factors for anaerobic digestion that are of importance for this work are presented in this chapter. This includes factors like solids and hydraulic retention time, temperature, alkalinity, pH, inhibition, and nutrients are presented.

2.3.1 Retention time

Sufficient solids retention time (SRT) and HRT are important for the substantial destruction of volatile solids in a well-mixed reactor. This is what sizing of AD reactor is based on. SRT is the time that the solids are held in an AD process, where HRT is the time the liquid is held in an AD process.[1] In a CSTR reactor, SRT is the same as HRT due to continuous flow in the reactor. The usual HRT in the reactor is 15 -30 days.[1]

2.3.2 Organic loading rate

The OLR is a measurement of the organic substrate mass rate added per volume unit of an AD reactor. When it comes to AD and volumetric OLR, it is usually higher than in aerobic processes. This difference leads to smaller reactor volumes and more compact treatment facilities compared to aerobic processes. For example, the OLR for an anaerobic process may be between 3.2 and 32 kgCOD/m3·d, as for aerobic processes between 0.5 and 3.2 kgCOD/m^3·d. [1] For a CSTR, the usual OLR is 1-4 kgCOD/m^3·d [7].

2.3.3 pH and alkalinity

The pH has a significant influence on the growth and survival of microorganisms in the AD process. Relatively narrow pH ranges are optimal for particular microorganisms to grow optimally. The majority of bacteria cannot sustain a pH level exceeding 9.5 and dropping below 4, but the optimum level lies between 6.5 and 7.5. Stable methanogenic activity is between 6.8 and 7.8 reactor pH values [4], though some archaea can grow at extremely low pH.[1]

The pH can be maintained by controlling the influent alkalinity of the reactor. In AD a 30-35% of produced biogas is CO_2, and alkalinity is needed to offset the effect of carbonic acid and other acids on the pH. To maintain pH at a neutral level, alkalinity concentration between 3000 to 5000 mg/L as $CaCO_3$ is usually needed. In the sludge AD process, the breakdown of proteins and amino acids produce NH3. The NH3 then combines with CO2 and H2O to produce alkalinity as NH4(HCO3).[4] A monitoring parameter can be used to observe the health of the AD process, a ratio between VFA and alkalinity. Values between 0.05 and 0.25 should be maintained for a stable process[1].

2.3.4 Nutrients and trace metals

AD requires less nitrogen and phosphorus for biomass growth, and this is due to that process produces less sludge. However, some substrates may lack the nutrients needed, for example, industrial wastewater, which may need nutrient addition.[4]

The other thing necessary for the growth of methanogenic microorganisms is the presence of trace metals. The suggested amounts of iron, nickel, cobalt and zinc for a mesophilic process are 0.2, 0.0063, 0.017 and 0.049 g/kgCOD removed, respectively, and for a thermophilic process: 0.45, 0.049, 0.054 and 0.24 g/kgCOD removed when using glucose as substrate[8]. Though, the amounts can vary for different substrates.

2.3.5 Carbon to nitrogen (C/N) ratio

Both carbon and nitrogen are needed for microorganisms to grow, and this makes the C/N ratio an important parameter in AD. If the substrate has too low C/N ratio, ammonia nitrogen concentration may increase, thus increasing the risk of inhibiting the microorganisms. On the other hand, too high C/N ratio can cause a lack of nitrogen for cellular growth and deactivate methanogens.[9] Most processes operate efficiently when C/N ratio is from 20 – 30, though it may be waste specific and range from 9 to 30 [10], [11], [7].

2.3.6 Inhibition

Different substances can inhibit the AD process. Substance like free ammonia is inhibitory to aceticlastic methanogens, though hydrogenotrophic methanogens appear to be less sensitive. Ammonia is a week acid that dissociates in water to then form ammonium. The ammonia concentration is strongly dependent on pH and temperature in the reactor. With higher temperatures and constant pH, ammonia dissociates more in ammonium; furthermore, with increasing pH, ammonia concentration increase. The concentrations of ammonia that are suggested for the normal AD process are between 50 mg/L and 200 mg/L [12], [13]. Ammonia nitrogen concentrations between 1500 mg/L and 3000 mg/L are considered moderately inhibitory and can cause problems in the process, though reactor can be acclimatised to higher ammonia values [1], [12], [7].

Inhibition of methanogenesis can also occur due to high acetate concentrations in the reactor even when pH is maintained above 7 with sufficient alkalinity. The acetate concentration higher than 3000 g/m^3 is inhibitory for the methanogens.[4]

2.3.7 Temperature

Temperature is an important parameter in the efficient AD process. The temperature has a big influence on microbial consortia in the reactor and the kinetic of the process itself. The kinetic parameters that are influenced by temperature include the specific growth rate of microorganisms, the half-saturation constant, the growth yield, and decay rate. The AD is usually operated in three temperature ranges psychrophilic (4 - 15^{o}C), mesophilic (20 - 40^{o}C) and thermophilic (45 - 70^{o}C). These temperature ranges have an optimum temperature for the microorganisms between 35 - 38^{o}C for mesophilic and thermophilic around 55^{o}C. Below the temperature optimum, the reaction rate for the AD process is increasing, above it - decreasing.[1], [5], [7]

Changes in temperature strongly affect microorganisms in an AD reactor. For stable process, changes in temperature less than 0.5^{o}C are recommended.[1] Temperature also influences the gas-transfer rate, which changes dissolved gas concentration in the reactor.

2.4 Mesophilic and thermophilic digestion

This part of the report will present theoretical background for two AD operating temperature ranges - mesophilic and thermophilic.

A mesophilic AD process is more common to use for biogas production than a thermophilic AD process. The temperature range for mesophilic AD is between 20 to 40^{o}C with optimal temperature approximately at 35^{o}C. Thermophilic AD has an operating temperature range from 45 to 70^{o}C, with the optimal temperature at around 55^{o}C [5]. Some works show that with the same OLR and retention time, the methane yield and degradability for mesophilic and thermophilic AD processes don't have a significant difference [14], [15]. Though, due to temperature increase, the reaction rate doubles with every 10^{o}C until an optimum temperature is reached. This fact makes thermophilic digestion a faster process than mesophilic [1], [16]. The increase in reaction rate can decrease HRT, thus reduce reactor volume requirements. On the other hand, the thermophilic process is more unstable and more prawn to foaming and inhibition by ammonia. The higher temperature in the reactor leads to higher ammonia content, and digestate from a thermophilic process holds more ammonia than mesophilic process. This may lead to more ammonia in dewatering side-stream [1], [17].

2.4.1 Transition from mesophilic to thermophilic process

Multiple works show a successful transition from mesophilic to thermophilic temperatures, both with abrupt temperature increase and stepwise transition. In [18] a 3^{o}C/day transition from 36^{o}C to 53.3^{o}C temperature was assessed. Temperature increase resulted in a fluctuation of VFA and daily gas production. However, steady-state was achieved within 35 days after the start of temperature increase.

A successful transition was also shown by [14] assessing two different strategies, one-step transition and multi-step transition. The multi-step transition had a temperature increase as followed 35^o – 43^o – 50^o – 55^{o}C. The work concluded that both strategies were equally effective

and recovered efficiency after 20 days in terms of methane yield. Nevertheless, higher VFA concentrations and elevated propionate to acetate ration were detected during temperature transition. It was also noted in [14] that in the multi-step strategy, temperature between 43°C and 50°C was critical for methanogenic activity. Here it was experienced the most drop in gas production.

Another work, [19], selected a strategy with a very slow temperature increase of 0.38°C/day and long periods of time maintaining at temperature 43°C and 45°C without feeding. Then slowly increase to 55°C and slowly started feeding. The reactor showed unstable function in temperature 43°C and 45°C. In the end, the work suggested to slowly increase the temperature in the reactor to 43°C with maximum increments of 2.5°C with some days in between for stabilising of the reactor. Then fast increase to 50°C without feed and then same slow increase as before until 55°C with feeding.

A study presented in [20] compared two cases with rapid temperature transition in one-step and slow in multi-steps, 37° – 42° – 47° – 51° – 55°C. The study concluded that although the one-step change was more unstable in terms of methane production and VFA, it reached stable operation after 30 days. Though for multiple-step it took 70 days to transition and reach steady operation. It was also noticed in the work that at 42° to 47°C temperature it was strong disturbances in the reactor work.

2.5 Anaerobic co-digestion

Anaerobic co-digestion is when two or more different type of organic waste are combined in an anaerobic digestion reactor. A co-digestion is beneficial to implement when the reactor has extra capacity to process additional waste, thus increasing biogas production and available energy for the facility or other community uses. Co-digestion is also beneficial when processing substrates that are lacking nutrients, alkalinity and/or have C/N imbalance to sustain stable digestion. In case of nutrients or imbalance in the process, the addition of co-substrates that have the laking components may be a good solution. Also, some technical, economical and environmental factors, like increasing use of digester capacity, reducing greenhouse gas emission and avoid creation of additional treatment capacities.[1]

In sewage sludge AD, the alkalinity and nutrient deficiency is usually not an issue due to the presence of phosphorus and degradation of organic nitrogen in both PS and waste activated sludge (WAS). Though sludge may be low in carbon compared to nitrogen, thus C/N ratio might be unbalanced to have efficient digestion [1], [11]. Many different feedstocks that are high in carbon content may be used for this purpose, such as plant waste and fruit waste, energy crops and stillage.[7] Another interesting substrate for the anaerobic co-digestion may be wastewater containing glycol. One of the sources of glycol containing wastewater can be airports as most of the aircraft de-icing fluids are ethylene glycol and propylene glycol-based [21], [22]. De-icing fluid as a co-substrate will be described in sub-chapter 2.5.2.

2.5.1 Additional sludge from different treatment plants

Sludge has quite varying characteristics that depend on the age of the sludge, the type of process it has been through and the origin of the sludge. Some typical values for sludge's chemical composition are provided in Table 2.1. To treat the sludge most efficiently and then reuse the end products, one must consider the characteristics and composition of the sludge. For example, chemical constituents of the treated sludge are important when thinking about the

disposal of the end products and dewatered liquid. To have better control of AD process parameters of the sludge, like pH, alkalinity and content of organic acid, is of importance. If land application or incineration of digestate is considered, then it is important to think about content of heavy metals, pesticides and hydrocarbons, and also a risk of pathogen contamination.[1]

Table 2.1: Some typical value ranges for chemical composition of untreated primary and activated sludge [1].

Item	Untreated primary sludge	Untreated activated sludge
TS [%]	1-6	0.4-1.2
VS [% of TS]	60-85	60-85
Grease and fats [% of TS]	5-8	5-12
Proteins [% of TS]	20-30	32-41
Nitrogen [N, % of TS]	1.5-4	2.4-5
pH	5-8	6.5-8
Alkalinity [mg$CaCO_3$/L]	500-1500	580-1100
VFA [mgHAc/L]	200-2000	1100-1700

2.5.2 Anaerobic co-digestion of de-icing fluid from airport

De-icing fluids are used at airports to remove ice and snow from aircrafts. The majority of de-icing fluids are either ethylene glycol (EG) or propylene glycol (PG) based. Other components that can be in the de-icing fluid are corrosion inhibitors, wetting agents, surfactants and thickeners, amongst other chemicals. The theoretical oxygen demand (ThOD) of EG and PG are 1400 kg/m^3 and 1680 kg/m^3, respectively [21]. It was shown by [23] that PG based de-icing fluid can efficiently co-digest with wastewater sludge. In this co-digestion, sludge is providing alkalinity, nitrogen and trace metals and de-icing fluid supplies organics. It is also shown by [16] and [18] that EG under anaerobic conditions decomposition to ethanol and acetate, then ethanol converts to acetate and hydrogen. PG first transformed to equal molar parts of n-propanol and propionate, then n-propanol is transformed to propionate and hydrogen [22]. VEAS has an opportunity to receive wastewater with de-icing fluid based on PG, and this work will focus on the PG degradation pathway shown in Figure 2.3.

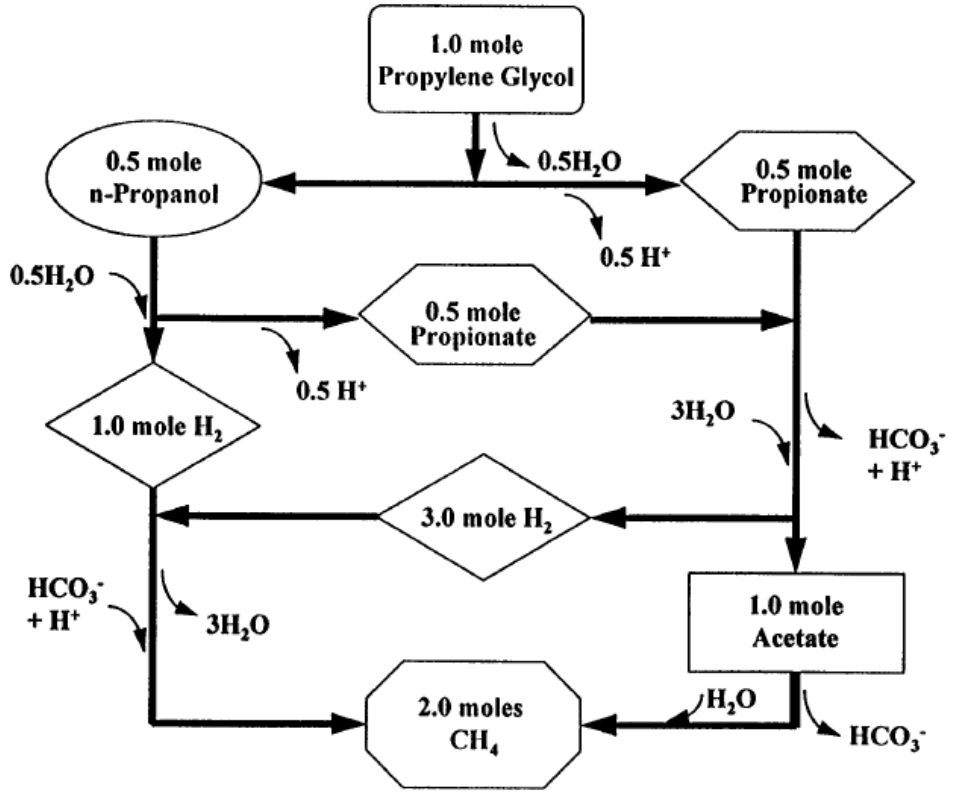

Figure 2.3: Decomposition pathway of PG in anaerobic conditions; figure was taken from [22].

The degradation pathway in Figure 2.3 was proposed then confirmed by an experiment in [22]. The work showed that glycol converts to propionate and n-propanol within 2 days in a serum bottle. After that followed a decrease in n-propanol and corresponding increase in propionate for about 13 days when propionate reached peak value. This was then followed by a decrease of propanol and corresponding increase in methane. The chemical reactions for this degradation pathway were adapted from [22] and presented in Table 2.2. Reactions 1 and 2 show the degradation during first 2 days and then 13 days of the experiment, then reaction 3 is just a combination of 1 and 2. Reactions 4, 5 and 6 are propionate degradation to acetate, then conversion of acetate and hydrogen to methane. Reaction 7 is a combination of reactions 1, 2, 4, 5 and 6.

Table 2.2: Reactions for decomposition of PG to methane, adapted from [22]

Reaction No.	Chemical equation	$\Delta G^{o\prime}$ [kJ/mol]
1	Propylene Glycol →Propionate + n-Propanol	− 24.4
$CH_3CH(OH)CH_2OH \rightarrow 0.5\ CH_3CH_2COO^- + 0.5\ H^+ + 0.5\ CH_3CH_2CH_2OH + 0.5\ H_2O$		
2	n-Propanol → Propionate	+ 2.9
$H_3CH_2CH_2OH + H_2O \rightarrow CH_3CH_2COO^- + H^+ + 2\ H_2$		

3	Propylene Glycol → Propionate (1+2)	- 22.9
$CH_3CH(OH)CH_2OH \rightarrow CH_3CH_2COO^- + H^+ + H_2$		
4	Propionate → Acetate	+ 18.3
$CH_3CH_2COO^- + 3\ H_2O \rightarrow CH_3COO^- + H^+ + HCO_3^- + 3\ H_2$		
5	Acetate → Methane	- 7.4
$CH_3COO^- + H_2O \rightarrow HCO_3^- + CH_4$		
6	Hydrogen → Methane	- 32.4
$4\ H_2 + H^+ + HCO_3^- \rightarrow CH_4 + 3H_2O$		
7	Propylene Glycol → Methane (1+2+4+6+7)	- 44.5
$CH_3CH(OH)CH_2OH + H_2O \rightarrow 2\ CH_4 + H^+ + HCO_3^-$		

2.6 Thermal hydrolysis pre-treatment process

Many different anaerobic digestion pre-treatment technologies have been developed and are used to increase the solids loading, increase in volatile solids reduction (VSR), increase biogas production and destruction of pathogens. One such technology is a Thermal Hydrolysis Process (THP). THP is a thermal treatment process where sludge is treated by steam at high pressure and temperature in a pre-treatment chamber. Temperatures are usually in the range of 150 - 200^{o}C, and the pressure is in the range of 6 to 25 bars [1], [25]. The effect of THP on sludge is increased solubilisation and destruction of cells. These two effects make organic materials more available for digestion.[25] The other benefits of THP pre-treatment are increased dewaterability of digestate and increase of product quality when it comes to odour.[1] It is also have been shown that gas production is increased after THP pre-treatment [26], [27].

There are several THP technologies applied on an industrial scale; some of them are Cambi™, Biothelys, Exelys, Turbotec and CTH, as well as others [28].

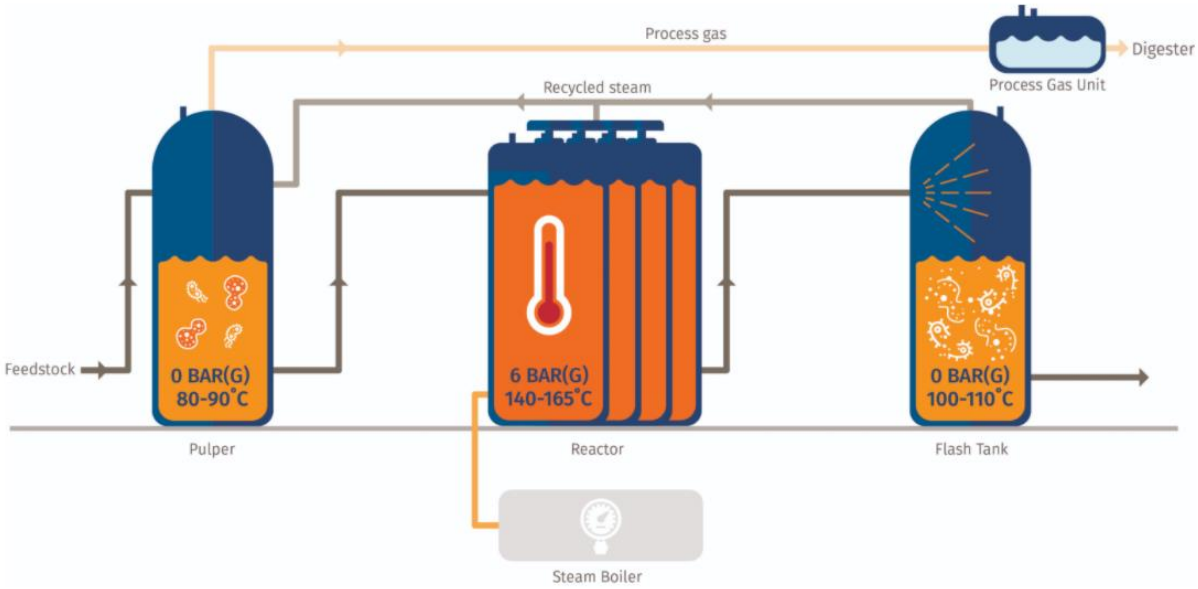

Figure 2.4: Illustration of Cambi™ batch THP process [29].

VEAS is planning on integrating THP pre-treatment supplied by Cambi™, and the process is batch-based, and the focus further will be batch THP. In Figure 2.4, an illustration of batch THP is provided. The first step in the process is to continuously feed sludge from primary and secondary treatment to a pulper. The sludge needs to be thickened to a 16-18% dry solid content. In the pulper, by using recovered steam, the sludge is pre-heated to 100^{o}C and homogenised. The next step is to feed pre-heated sludge into reactors. The sludge is feed in sequence to have separated batches in each reactor. A typical number of reactors in the Cambi™ process is between 2 and 5. After the reactor is filed, the temperature is rased to 160-180^{o}C by steam, and pressure is at about 6 bars. The duration of a THP process is usually 20 to 30 minutes for each batch. This is done to guarantee the eradication of pathogens in the sludge. The third step in the process starts when treated sludge from the reactors is pumped into a flash tank. The sludge is exposed to the atmospheric pressure inside the flush tank. This pressure drop is causing significant cell destruction of organic matter. The steam from the pressure release is then recycled into the pulper. After leaving the flash tank, the sludge is cooled down to temperatures of AD by use of heat exchangers and feed into the AD reactor.[29] Though the effects of the THP on AD are well known, how much it is affecting the solubilisation and physical properties of sludge is not widely studied. Table 2.3 presents some results from several works on solubilization of particulate material, pH, VFA, NH4-N and hydrolysis rate in WAS.

Table 2.3: Effect of THP on solubilization of particulate material, pH and VFA, ammonium nitrogen in waste activated sludge.

Sources	[30]	[31]	[32]	[25]
TS	-	3.3-1.48	7	-
Temperature [^{o}C]	165	165	165	180
Duration [min]	30	30	30	60

COD solubilization [%]	18	42.75	25.48	-
Hydrolysis rate increase [%]	-	-	-	30.8
Solubilization of protein [%]	40	20-30	-	-
Solubilization of carbohydrates [%]	15	30	-	-
Solubilization lipids [%]	n.d.	n.s.	-	-
Total lipid concentration [%]	-	100	-	-
VFA concentration [%]	-	400	105	-
NH4-N [%]	-	-	115	-
pH [%]	-	-	-11.5	-

n.d. – Not determined; n.s. – Not solubilized.

2.7 Anaerobic Digestion Model No 1

The Anaerobic Digestion Model No. 1 (ADM1) is a structured model developed by the International Water Association (IWA) Task Group for Mathematical Modelling of Anaerobic Digestion Process. The ADM1 includes steps like disintegration, hydrolysis, acidogenesis, acetogenesis and methanogenesis. As it was mentioned in chapter 2.2, AD consists of reaction series that can be divided into two main types, biochemical reactions and physico-chemical reactions. These types of reactions are included in ADM1, except for precipitation. [5]

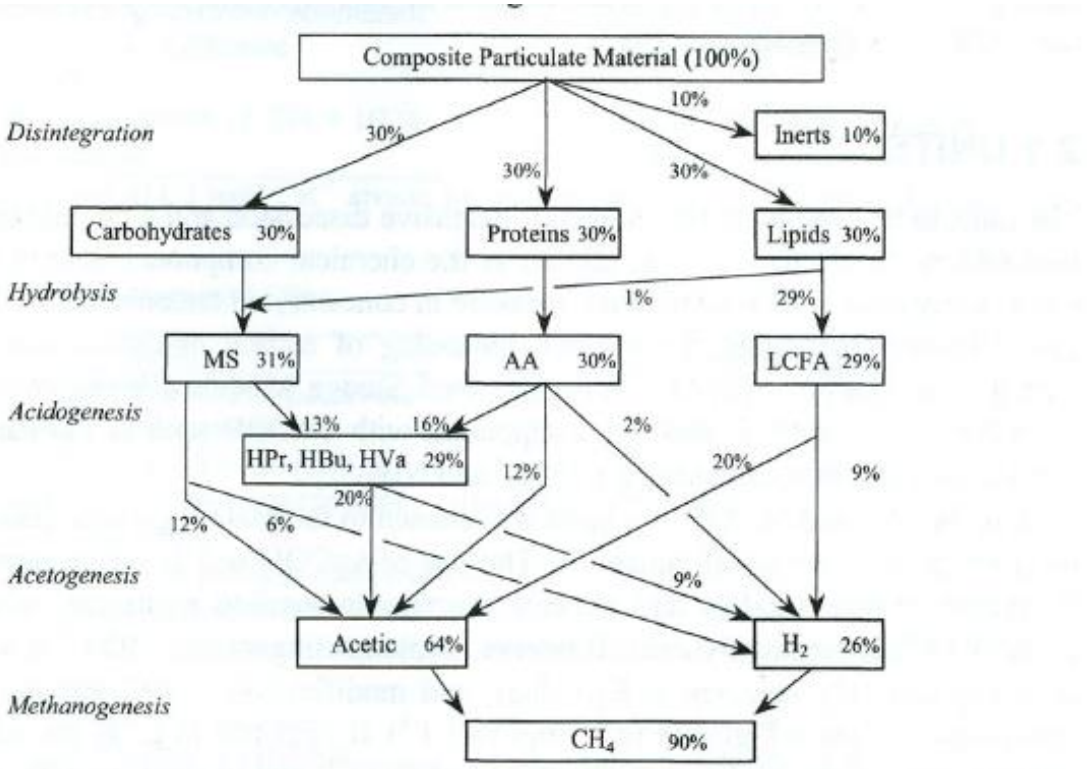

Figure 2.5: Illustration of the AD steps as implemented in ADM1 with COD flux for the process (monosaccharides (MS); amino acids (AA); long chain fatty acids (LCFA); propionic acid (HPr); butyric acid (HBu); valeric acid (HVa)). [5]

The ADM1 model consists of three biological steps or cellular steps and two extracellular steps. The two extracellular steps are disintegration and hydrolysis, see Figure 2.5. In the disintegration step, complex particulate and inactive biomass is modelled to convert into 10% inerts (soluble and particulate), 30% fats(lipids), 30 % proteins, and 30% carbohydrates on COD bases. This step is intended to including lysis, non-enzymatic decay, phase separation and physical breakdown. Then in the hydrolysis step, carbohydrates and proteins convert to monosaccharides (MS) and amino acids (AA), respectively. Fats convert to mostly long chain fatty acids (LCFA) and a small amount to MS. Extracellular steps are modeled as first order kinetic rate in ADM1, the equation (2.1) where ρ_j is kinetic rate of process j [kgCOD_S/(m^3·d)], k_j first order parameter for process j [1/d] and X_i is particulate component I [kgCOD/m^3].[5]

$$\rho_j = k_j \cdot X_i \quad [5] \tag{2.1}$$

The three cellular steps are acidogenesis, acetogenesis and methanogenesis and the kinetics of these steps described by three expressions, growth, uptake and decay. The most important rate equation is for uptake of substrate, and it is based on Monod-type kinetics. Equation (2.2) the equation for uptake where ρ_j is kinetic rate of process j [kgCOD_S/(m^3·d)], k_m is Monod maximum specific uptake rate [kgCOD_S/(kgCOD_X·d)], K_s is half-saturation value [kgCOD_S/m^3], X_i is particulate component i [kgCOD/m^3] and S_i is soluble component I [kgCOD/m^3]. The decay of biomass is modelled as first order expression. The Acidogenesis step is modelled to convert some of MS and AA to propionate butyrate and valerate. Then acetogenic step is converting the rest of MA, VFA, LCFA and AA to 64% acetate and 26% hydrogen. As a last cellular step, acetate and hydrogen are converted to methane by modelling aceticlastic methanogenesis and hydrogenotrophic methanogenesis. [5]

$$\rho_j = \frac{k_m \cdot S_i}{K_s + S_i} X_i \tag{2.2}$$

[5]

The inhibition from pH for all organism groups is used in the model. Inhibition from hydrogen is implemented for all acetogenic group and inhibition by free ammonia for aceticlastic methanogens. Also, a function to regulate uptake for IN is implemented, which is done to limit growth when there is a deficiency in nitrogen.[5]

From physico - chemical processes, only ion association/dissociation and liquid-gas transfer are modelled in ADM1. These two processes were important to implement, so biological inhibition factor, like pH, free acid and base and dissolved gas concentrations could be expressed.[5]

3 Material and methods

All models in this work are using ADM1 as a base model and AQUASIM 2.1f as a working environment. Python was used to solve a differential equation and print out some values for ADM1_FTnew simulation in a list. The code for python is provided as supplementary material together with the AQUASIM files.

3.1 Mesophilic and thermophilic (steady-state) process model

Mesophilic and thermophilic process models without temperature transition were modelled with parameters suggested by the IWA Task Group for both mesophilic and thermophilic simulations. The table with parameters is presented in Appendix B. The changes to the model were made only regarding co-substrates. No other changes for temperature transition are required since mesophilic and thermophilic conditions were simulated in steady-state in terms of temperature. The flow rate of sludge into the reactor was chosen to be the same as in VEAS 2019 process data instead of an average constant value. This choice was made to have an opportunity to compare the simulation results and VEAS process data. The mixing of co-substrates was done as a volumetric ratio in flow rate as like it was several parts in total flowrate representing each co-substrate. More description of the modelling of co-substrate presented in the 3.3 chapter.

3.2 Temperature transition (dynamic) models

ADM1 model is designed to simulate AD with constant temperature, and temperature dependency is not implemented. It was decided to use two research works, [33] and [34], as a basis for the two temperature transition models in this work.

3.2.1 Linear model

The Linear model is a modified ADM1 model taken from the work done previously in a group project [35]. In the Linear model, parameter values suggested by the IWA Task Group (Appendix B) for the mesophilic and thermophilic processes were linearly interpolated when temperature was set to change. A T_corr variable was added to the model that was used as a modifying parameter. The variable corrects the temperature and calculates interpolated values for the k_m, Y, K_s and K_I parameters in AQUASIM according to temperature change.

3.2.2 ADM1_CTM1

The research [33] was used as a basis to modify the first ADM1 model for dynamic temperature transition. In the research, the Cardinal Temperature Model 1 (CTM1) was used to model temperatures between 15 and 45^{o}C. According to the research, the CTM1 model was better suited for this temperature range than the Arrhenius model. Equation (3.1) shows the CTM1 model where b is the parameter calculated, b_{opt} is the optimum value of the kinetic parameter of interest, T_{min}, T_{opt} and T_{max} are the minimum, optimum and maximum temperatures for the organisms, respectively [^{o}C].

$$b = b_{opt}\frac{(T - T_{max})(T - T_{min})^2}{(T_{opt} - T_{min})[(T_{opt} - T_{min}) \cdot (T - T_{opt}) - (T_{opt} - T_{max}) \cdot (T_{opt} + T_{min} - 2T)]} \quad (3.1)$$

[33]

In this work, the decision was to implement two sets of equations (3.1) to calculate parameters of interest for mesophilic and thermophilic conditions separately. With this way of implementation, the change in microbial community is represented when the reactor goes from mesophilic to thermophilic conditions. The AQUASIM will follow equations set to calculate mesophilic parameters until temperature 44.5^{o}C; after that, it will shift to the equation set with thermophilic parameters. A temperature of 44.5^{o}C was chosen due to some mathematical difficulties in AQUASIM. Nonetheless, this temperature is corresponding to a range between 43^{o}C and 50^{o}C, which was reported as mots unstable period in transition between mesophilic and thermophilic process [14], [19], [20]. To transition from one equation set to another in AQUASIM, an "if" function was used.

The optimum kinetic values, needed for calculation in the modified ADM1_CTM1 model for mesophilic and thermophilic temperatures, were taken as they were suggested by the IWA Task Grope (Appendix B). The sets of new equations implemented into the ADM1_CTM1 calculate first order parameter for hydrolysis of carbohydrates (k_{hyd_ch}), proteins (k_{hyd_pr}) and lipids (k_{hyd_li}), uptake rate (k_m) and yield of biomass (Y) for acetogenic, acidogenic and methanogenic groups. The T_{min}, T_{opt} and T_{max} were divided into three parameter groups for each of the temperature ranges, mesophilic and thermophilic.

Table 3.1: Values for (T_{min}) minimum, (T_{opt}) optimum and (T_{max}) maximum temperatures used in ADM1_CTM1 model for calculation of kinetic parameters in temperature transition.

Parameter group	Mesophilic			Thermophilic		
	T_{min} [^{o}C]	T_{opt} [^{o}C]	T_{max} [^{o}C]	T_{min} [^{o}C]	T_{opt} [^{o}C]	T_{max} [^{o}C]
Hydrolysis ($k_{hyd,ch}$, $k_{hyd,pr}$, $k_{hyd,li}$)	4.2	40.3	45.5	41	55	70
Acidogenesis/ Acetogenesis ($k_{m,i}$, Y_i)	29	37	45.2	41	55	70
Methanogenesis ($k_{m,i}$, Y_i)	11	34	46.3	41	55	70

3.2.3 ADM1_FTnew

To modify the second ADM1 model for temperature transition simulation, research [34] was used as a source for the temperature response model. Equations (3.2) - (3.7) were implemented into the new temperature transition model, ADM1_FTnew. The T_e is effective or actual temperature, T_a is the temperature microbial group adapted to, T_{opt} and T_{max} are optimum and maximum growth temperatures, respectively. F_{Tref} is a steady-state temperature-dependent

maximum growth rate with an optimum temperature point. F_{Tnew} is the dynamic temperature-dependent maximum growth rate, and it consists of two parts $F_{SS,}$ the long-term temperature adaptation and F_{DYN}, the dynamic term of temperature adaptation. F_{SS} term is dependent on parameters like μ_{max}, T_{opt}, T_{max}, T_a and regression coefficient (α). T_a is calculated as shown in equation (3.5) though Python was used to calculate and print the values needed to a list. Then the list variable was created in AQUASIM for the T_a values. Python was used for this step because it was problematic to implement differential equation in ADM1 and AQUASIM, and this solution was quicker to implement. Parameter sigma (σ) controls the extent of growth disturbance that is caused by the deviation between T_e and T_a, and is dependent on constant $S_{hg.}$ [34]

Since the mathematical equations (3.2) and (3.3) calculating growth rate for the changing temperature, k_m needed to be changed to formula variable and value was calculated by dividing $F_{Tref,\ i}$ or $F_{Tnew,\ i}$ by Y_i. The complete list with implemented or changed variables in ADM1_FTnew is presented in Appendix G.

$$\mu_i(T_e) = F_{Tref,i}(T_e) = \begin{cases} \mu_{max,i} - \alpha_i \times (T_{opt,i} - T_e), & T_e < T_{opt,i} \\ \mu_{max,i} \times \dfrac{T_{max,i} - T_e}{T_{max,i} - T_{opt,i}}, & T_e > T_{opt,i} \end{cases} \quad (3.2)[34]$$

$$\mu_i(T_e, T_{a,i}) = F_{Tnew,i}(T_e, T_{a,i}) = F_{SS,i}(T_{a,i}) \times F_{DYN,i}(T_e, T_{a,i}) \quad (3.3)[34]$$

$$F_{SS,i}(T_{a,i}) = \begin{cases} \mu_{max,i} - \alpha_i \times (T_{opt,i} - T_{a,i}), & T_{a,i} < T_{opt,i} \\ \mu_{max,i} \times \dfrac{T_{max,i} - T_{a,i}}{T_{max,i} - T_{opt,i}}, & T_{a,i} > T_{opt,i} \end{cases} \quad (3.4)[34]$$

$$\dot{T}_{a,i}(t) = \frac{T_e(t) - T_{a,i}(t)}{\tau_{a,i}} \quad (3.5)[34]$$

$$F_{DYN,i}(T_e, T_{a,i}) = e^{\frac{(T_e - T_{a,i})^2}{2 \times \sigma_i^2}} \quad (3.6)[34]$$

$$\sigma_i = \left(-\frac{S_{hg,i}^2}{2 \times lin0.5} \right)^{0.5} \quad (3.7)[34]$$

BioModel from the research work [34] has some differences from ADM1. Not all parameter values were used in modified ADM1 that were presented in the research. It was decided to only use parameters that are relevant for ADM1. For example, carbohydrate degraders and lipid degraders were not implemented in ADM1 because it has a hydrolysis step to convert carbohydrates and lipids. Though the values for μ_{max} in ADM1_FTnew were taken as provided in the research work. The values of μ_{max} in the research work differ from the values that can be calculated from IWA Task Group suggested parameters. But due to the changes that needed to

be implemented in ADM1_FTnew it was decided to take the μ_{max} values from the research paper, see Table 3.2. The parameters for the disintegration, hydrolysis, hydrogen degraders and sugar degraders are left as they were modelled in the Linear model [35]; see sub-chapter 3.2.1.

Table 3.2: Parameter values used for the ADM1_FTnew model to simulate temperature transition effect on growth of microorganisms.[34]

i	Group name	μ_{max} [1/d]	α [1/(d·°C)]	T_{opt} [°C]	T_{max} [°C]	τ_a [d]	S_{hg} [°C]
n.u.	Carbohydrate degraders	5.088	0.0936	55	65	n.d.	n.d.
n.u.	Lipid degraders	0.528	0.00984	55	65	n.d.	n.d.
1	Amino acids degraders	6.384	0.1176	55	65	n.d.	n.d.
2	LCFA degraders	0.552	0.01008	55	65	n.d.	n.d.
3	Propionate degraders	0.48	0.00888	53	65	n.d.	n.d.
4	Butyrate and valerate degraders	0.684	0.01248	60	70	n.d.	n.d.
5	Acetate degraders	0.624	0.01128	55	65	10	3

n.d. – Not defined; n.u. – Not used.

3.3 Co-substrates implementation

Implementation of co-substrates into the model was done by creating new variables in AQUASIM for each substrate input value for particulates components (Input_X_i), and soluble components (Input_S_i). Also, there were added inflow variable for each substrate (Input_K_sludge_i) which represented part of the co-substrate in the total inflow rate. Then it was multiplied with the total inflow rate (Input_Q_{in}_dyn) to calculate the inflow rate for the specific co-substrate (Input_Q_{in}_sludge_i). This Input_Q_{in}_sludge_i was then implemented into the reactor input compartment in AQUASIM for each component to calculate the total concentration of input components.

3.3.1 Adding different sludge to the model

Three sludges, S1, S2 and S3, from three different WWT plants in municipalities Aremark, Marker and Indre Østfold, respectively, were collected and then analysed by ALS Laboratory Group. The analysis report is provided in Appendix F, and component values used for simulation together with input values for simulations for all sludges are provided in Appendix A.

After studying the analysed values and preparing values for simulation input, a total COD (tCOD), protein content, carbohydrates, and particulate inert content (X_I) needed to be calculated from the components. Protein content was estimated by subtracting total ammonia nitrogen (TAN) from total nitrogen (TN) and then multiplying with 6.25 (g protein/g organic

N) factor [36]. Since the total Kjeldahl nitrogen (TKN) was not measured, an assumption that TN contains insignificant amounts of nitrate and nitrite had to be made. The tCOD was measured in the analyses report, but the sum of the COD for the sludge components was much higher than the measured value. For S1, S2 and S3, the calculated tCOD was 16, 11 and 19 times higher than the measured, respectively. Thus, it was decided to calculate COD of TOC for sludges S1, S2 and S3 and use the value as tCOD. The COD of TOC for S1 was 59.4 gCOD/L ,for S2 60.7 gCOD/L and S3 60.7 gCOD/L at 7.3% TS for all sludges. All measured particulate and soluble components included in the tCOD were adjusted to match the new tCOD value. This procedure will make sludges less similar to the composition of the analysis report, but it was the simplest way at the moment to make sludges applicable in simulations.

Due to lack of biochemical methane potential (BMP) test, an alternative way to estimate X_I needed. It was decided to take an average value of 14.5% X_I fraction of tCOD calculated from reported COD fractions in primary domestic wastewater from different countries, data presented in [37].

After deciding on tCOD, X_I and calculating proteins, carbohydrate content was estimated. It was done by calculating particulate COD (pCOD) for all three sludges. Then part of carbohydrates was calculated by using equation (3.8) for each sludge individually. This way, sludges get a very different composition compared to each other in terms of protein, lipid, and carbohydrate content, see Figure 3.1.

$$Carbohydrates(\%COD) = pCOD - (Proteins(\%COD) + Lipids(\%COD) + X_I(\%COD)) \quad (3.8)$$

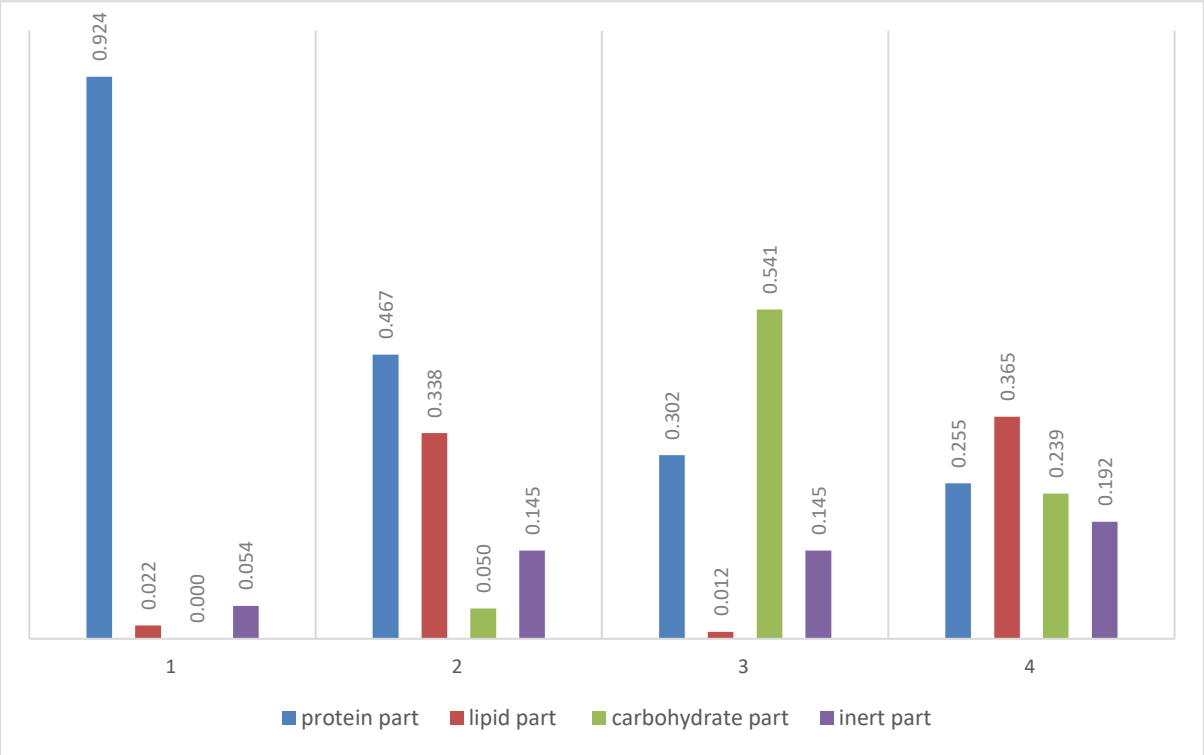

Figure 3.1: Illustration of parts of proteins, lipids, carbohydrates and inerts in four sludges used for simulations (1 – Sludge S1 Marker, 2 – Sludge S2 Aremark, 3- Sludge S3 Indre Østfold, 4 – Sludge S0 VEAS sludge)

Further in this work, it was assumed that soluble inerts and composite content in S1, S2 and S3 are zero, same as it was done previously in a group project for S0. The final input parameters are presented in Table 3.3 for all sludges used in simulations with TS adjusted to 7.3%.

Table 3.3: The final input parameters for sludge S1 Marker, sludge S2 Aremark, sludge S3 Indre Østfold and sludge S0 VEAS sludge.

Input variables	Description	S0	S1	S2	S3	Units
tCOD (g/L)	Total COD	90.73	59.373	60.736	60.736	gCOD/L
sCOD (g/L)	Soluble COD	9.46	1.514	1.909	0.128	gCOD/L
Input_X_li	Lipids	9.90	1.2787	19.8943	0.702	gCOD/L
Input_X_ch	Carbohydrates	19.1	0**	2.9266**	32.816**	gCOD/L
Input_X_pr	Proteins	20.4	53.453	27.4764	18.302	gCOD/L
Input_S_su	Monosaccharides	0.019	-***	-***	-***	gCOD/L
Input_S_ac	Acetate	3.44	0.7465	1.0169	0.058	gCOD/L
Input_S_pro	Propionate	1.78	0.7674	0.8891	0.07	gCOD/L
Input_S_bu	Butyrate	4.33	-***	-***	-***	gCOD/L
Input_S_va	Valerte	0.44	-***	-***	-***	gCOD/L
Input_S_I*	Soluble inerts	0	0	0	0	gCOD/L
Input_X_I	Particulate inerts	11.2	3.1279	8.53	8.788	gCOD/L
Input_S_aa	Amino acids	0	-***	-***	-***	gCOD/L
Input_S_fa	LCFA	0	-***	-***	-***	gCOD/L
Input_S_IN	Inorganic nitrogen	0.0523	0.0722	0.0466	0.00029	Mol N/L
Input_S_IC	Inorganic carbon	0.18*	0.1393	0.1874	0.0.072	Mol C/L
Input_X_c*	Composite	0	0	0	0	gCOD/L

*Assumed values; ** Calculated as a part of particulate COD; *** below the detection limit in the analysis report (Appendix F).

The calculations of the C/N ratio of substrate mixtures were done by using equation (3.9) and the fact that all sludges were adjusted to have the same %TS. In the equation, S_n represents cubic meters per day of substrate n, OC_n organic carbon content for substrate n, and TKN_n is nitrogen part for the substrate n. The different simulation scenarios were planned to have the same OLR but different total C/N ratio in the co-digestions; for the values, see Table 3.5.

$$\frac{C}{N}(mix) = S_1\frac{OC_1}{TKN_1} + \ldots + S_n\frac{OC_n}{TKN_n} \tag{3.9}$$

3.3.2 Adding glycol to the model

To model the effect of PGW in this work, some assumptions and simplifications were needed to be made. Information about the de-icing fluid at Sandefjord Lufthavn Torp (SLH) and collected quantities are provided by Espen Govasmark at VEAS. The following is known. Products for de-icing of aircraft Clariant Safewing type I and type II fluids, which are both propylene glycol (PG) based with different concentrations of it. The other products that are used on the de-icing platform are Aviform S-solid (Sodium formate) and/or Aviform L50 (Potassium formate) for ground de-icing. Water mixed with de-icing fluid, snow, ice, and rainwater are all collected in tanks from the de-icing and runway areas. The tanks are emptied with trucks with a 30 m^3 capacity. The usual amount of the water and de-icing fluid mixture per week is 300 to 400 m^3 in periods from November to May. In days with a lot of rainfall, the de-icing fluid concentrations in the water mix can be around 1-5%, with usual concentrations lower than 10% and times as high as 30%.

This work did not have the composition analysis for the water, and de-icing fluid mixture from SLH and following simplifications were made. As PG is the main component of interest, it was decided to model it as a solution of only water and 10% PG and assumed to be supplied to the AD in three different quantities for three different scenarios. The first scenario is that PG is supplied one truck once a day – 30 m^3/day or 7.5 m^3/day per reactor. The second scenario is that it is supplied 300 m^3/week or around 10 m^3/day per reactor, and the third is 400 m^3/week or 14 m^3/day per reactor. After this assumption and simplification, the PG degradation pathway was implemented in ADM1 with some simplifications. The pathway for PG degradation was presented in chapter 2.5.2 and showed that PG degrades first to propionate and n-propanol in equal molar amounts. Then n-propanol is degrading to propionate and hydrogen. The simplification made in this work was combining the two disintegration steps into one, as shown in reaction 3 in Table 2.2 or equation (3.7).

$$\begin{gathered}\text{Propylene Glycol} \rightarrow \text{Propionate} + \text{Hydrogen} \\ CH_3CH(OH)CH_2OH \rightarrow CH_3CH_2COO^- + H^+ + H_2\end{gathered} \tag{3.10 [22]}$$

The additional parameters in ADM1 then needed only for PG degradation, and they are presented in Table 3.4 for mesophilic optimum temperature. For thermophilic temperature, it was assumed that parameters k_m, K_S, Y and K_I, can be linearly interpolated to 55°C with the

same slope as for the same parameters for valerate and butyrate. Values for K_I and Y was assumed the same as for valerate and butyrate due to lack of data on PG degraders. Parameter k_m for mesophilic temperature was calculated from μ of 0.28 1/d taken from [38]. K_S, half-saturation constant, models the concentration influence on the substrate degradation rate. The suggested values for different organisms in ADM1 are from 0.1 to 0.5 kgCOD_S/m^3. [39] There is not enough information on PG degrading organisms, and the value for K_S was assumed to be the lowest suggested in ADM1 of 0.1 kgCOD_S/m^3. Also, a new input parameter for PG was added, shown in Table 3.4.

Table 3.4: Mesophilic digestion parameters added in ADM1 for PG degradation.

Parameters	Description	Value	Source
C_lac [mole/gCOD]	carbon content of PG	0.28*	-
f_h2_pg	yield of hydrogen from PG degradation	0.13*	-
f_pro_pg	yield of propionate from PG degradation	0.87*	-
kdec_xpg	decay rate for PG degrading organisms	0.02**	-
km_pg	maximum specific uptake rate for PG degraders	4.7*	[38]
Ks_pg	half saturation constant for PG degradation	0.1**	[39]
pKa_pg	-log10Ka PG at 298K	14.8	[40]
Y_pg [kgCOD/kgCOD]	yield of biomass on uptake of PG	0.06**	-
X_pg (initial) [kgCOD/m^3]	Initial amount of PG degraders in the reactor compartment	0.35**	-
Input parameters for PG			
input_S_pg_cos_2 [gCOD/L]	Propylene glycol	168*	-

*Calculated value; **Assumed value.

3.4 Energy content estimation

One of the objectives of this work is to evaluate the potential increase of the energy production in VEAS AD process by 50%. To do the evaluation, the energy content of methane was estimated. The energy content of methane at standard temperature and pressure (STP)

conditions is 38 846 kJ/m^3 [1] or 10.79 kWh/m^3. Also, the assumption about the methane temperature needed to be made, and it was assumed that methane has ether mesophilic (37^{o}C) or thermophilic (55^{o}C) temperature. The volume of the methane from the simulation results needed to be normalised to STP with Equation (3.11). Where P_N is STP pressure (1 bar), T_N is STP temperature (273.15 K), and V_N is a normalized volume at STP conditions (Nm^3/day), and P, T and V are the pressure, temperature, and volume at simulated process conditions, respectively. The pressure at simulated process conditions was taken from the simulated data.

$$V_N = \frac{T_N \cdot P \cdot V}{T \cdot P_N} \tag{3.11}$$

3.5 Simulation cases overview

Table 3.5 Presents all the simulation cases done in this work with results presented in chapter 4. The table also has information about what substrate was used in the simulation, the ratio of the substrates in case of co-digestion, OLR, HRT, days of the simulation, temperature, and C/N ratio for simulations with additional sludges. Every simulation has its own number, which will be used further in the text as a reference to according simulation in Table 3.5.

Table 3.5: Overview of parameters for the simulations done in this work.

No.	C/N total	Substrates	Substrate ratio (v:v)	%TS total	OLR [kgCOD/m3/day]	HRT	Simulation length [day]	T [^{o}C]	Source
Validation of temperature transition ADM1_FTnew model with Kovalovszki (No.1.1) and Boušková (No.1.2) experiments.									
1.1	-	CM (catle manure)	One substrate	3.66	1.8 kgVS/(m3*days)	14	1-49	37^{o}C	[34], [41]
							50-60	55^{o}C	
							61-112	37^{o}C	
1.2	-	PS:WAS	40:60	4.6	1.9	20	-6 - 0	37^{o}C	[20]
							1-10	42^{o}C	
							11-34	47^{o}C	
							35-41	51^{o}C	
							42-70	55^{o}C	
Validation of temperature transition ADM1_CTM1 model with Boušková experiment									
2	-	PS:WAS	40:60	4.6	1.9	20	-6 - 0	37^{o}C	[20]

							1-10	42°C	
							11-34	47°C	
							35-41	51°C	
							42-70	55°C	
Temperature transition for VEAS 2016-2017 process simulations with ADM1_FTnew (No. 4) and ADM1_CTM1 (No. 3) models									
3, 4	-	S0	One substrate	7.29	3.6	25	730	VEAS data	
Additional sludges in mesophilic VEAS process S1 (Marker), S2 (Aremark), S3 (Østfold)									
5.1	3.7	S0:S1:S2:S3	140:60:0:0	7.29	3.27	25	365	37°C	-
5.2	8.3	S0:S1:S2:S3	140:0:60:0	7.29	3.27	25	365	37°C	-
5.3	9.8	S0:S1:S2:S3	140:0:0:60	7.29	3.27	25	365	37°C	-
5.4	6.1	S0:S1:S2:S3	140:20:20:20	7.29	3.27	25	365	37°C	-
Propylene glycol wastewater (PGW) as a carbon source in the mesophilic VEAS process									
6.1	-	PGW:S0	7.5:192.5	-	3.7	25	365	37°C	-
6.2	-	PGW:S0	10.8:189.2	-	3.8	25	365	37°C	-
6.3	-	PGW:S0	14:186	-	3.8	25	365	37°C	-
Additional sludges and propylene glycol in mesophilic VEAS process									
7.1	-	S0:S1:S2:S3:PGW	162:8:8:8:14	-	3.7	25	365	37°C	-

7.2	-	S0:S1:S2:S3:PGW	150:12:12:12:14	-	3.6	25	365	37^{o}C	-
7.3	-	S0:S1:S2:S3:PGW	200:14:14:14:14	-	4.5	19.5	365	37^{o}C	-
Additional sludges in thermophilic VEAS process S1 (Marker), S2 (Aremark), S3 (Østfold)									
8.1	3.7	S0:S1:S2:S3	140:60:0:0	7.29	3.27	25	365	55^{o}C	-
8.2	8.3	S0:S1:S2:S3	140:0:60:0	7.29	3.27	25	365	55^{o}C	-
8.3	9.8	S0:S1:S2:S3	140:0:0:60	7.29	3.27	25	365	55^{o}C	-
8.4	6.1	S0:S1:S2:S3	140:20:20:20	7.29	3.27	25	365	55^{o}C	-
Propylene glycol (PGW) as a carbon source in the thermophilic VEAS process									
9	-	PGW:S0	14:186	-	3.8	25	365	55^{o}C	-
Additional sludges and propylene glycol in thermophilic VEAS process									
10.1	-	S0:S1:S2:S3:PGW	162:8:8:8:14	-	3.7	25	365	55^{o}C	-
10.2	-	S0:S1:S2:S3:PGW	200:14:14:14:14	-	4.5	19.5	365	55^{o}C	-

4 Results

4.1 Validation results of temperature transition models

In this subchapter, simulation results of two experimental studies,[20], [34]. These experiments are used to validate the two temperature transition models tested in this thesis, ADM1_CTM1 and ADM1_FTnew. First, the results from the ADM1_FTnew model will be compared to experimental results from the research work [34]. The simulation of gas production, acetate concentration and pH will be presented. Then simulation results for models ADM1_FTnew and ADM1_CTM1 will be compared to experimental results from [20] research paper.

4.1.1 Validation of ADM1_FTnew model

The results from simulation 1.1 (Table 3.5) are presented in this sub-chapter. As can be seen from Figure 4.1, the simulated gas production has a similar fall as the experimental data (Kovalovzski) between day 50 and 60 when the temperature is increased from 37 to 55°C. After day 60, when the temperature was set back to 37°C, the gas production slowly rose again for the simulation and experimental data in a similar pattern.

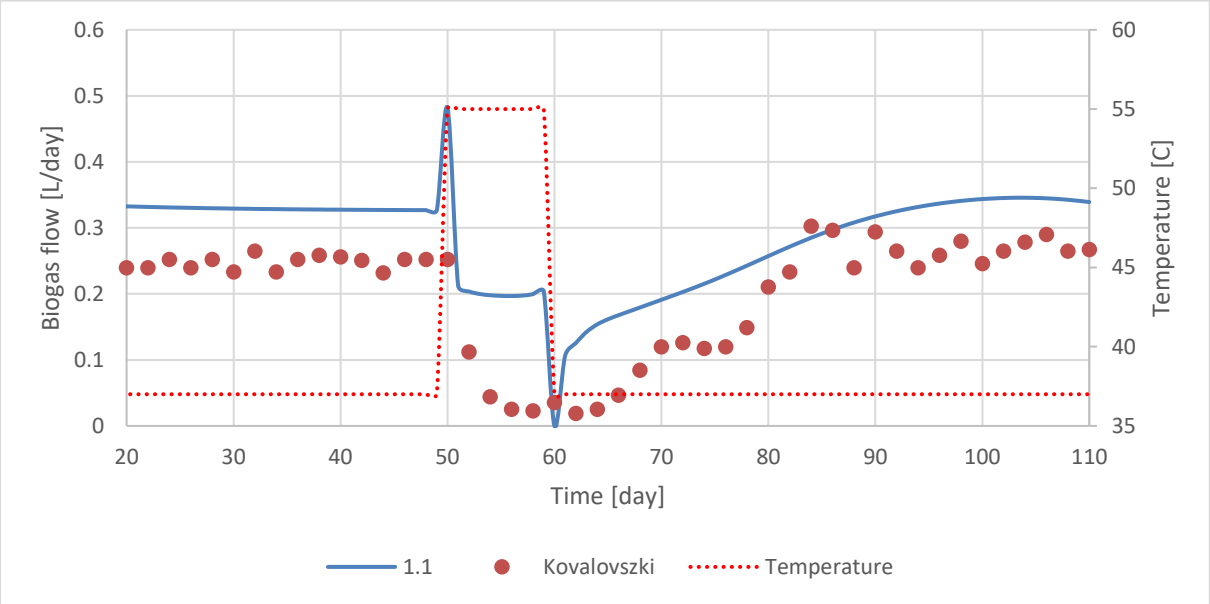

Figure 4.1: Simulated gas production by using ADM1_FTne model(1.1) and reproduced experimental data from [34] research papers (Kovalovzski et al.).

Acetate concentrations for both experiment and simulation are presented in Figure 4.2. After the temperature increase on day 50, the simulation shows similar behaviour as the experimental results. However, the simulated acetate concentration peaks at a higher value and takes longer time to drop down again after the temperature is returned to 37°C after day 60.

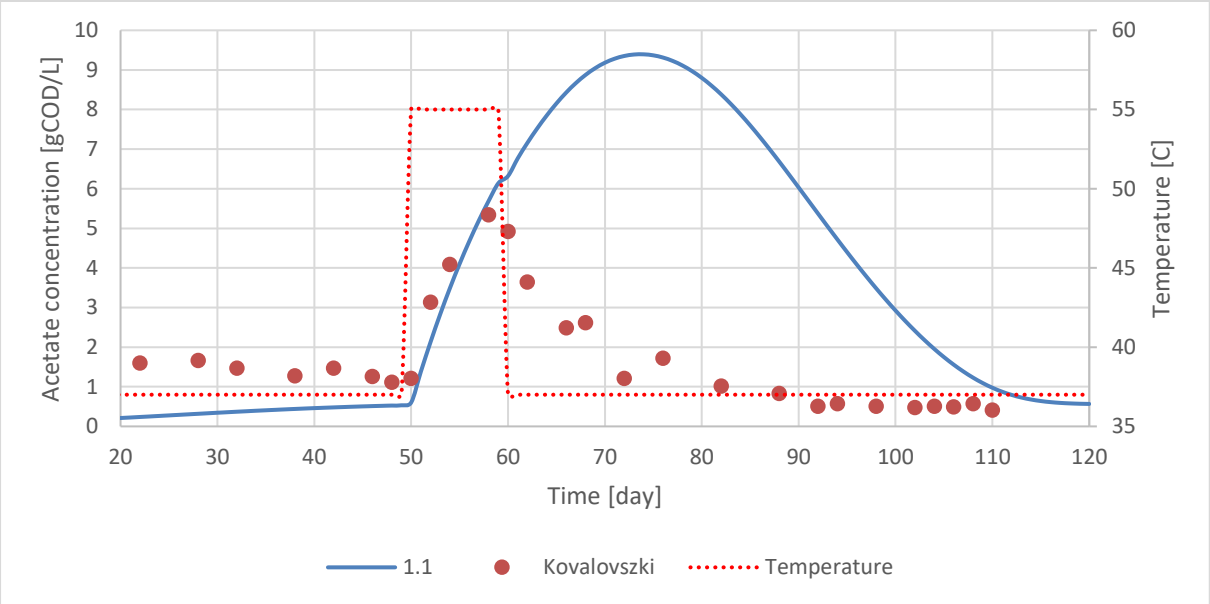

Figure 4.2: Simulation results for acetate concentration from ADM1_FTne model(1.1) compared to experimental results from Kovalovszki et al. [34] paper.

Between day 50 and 60, the simulated pH has a somewhat similar pattern as the experimental values, see Figure 4.3. However, the drop after day 60 is more for the simulation, which can correspond with a higher simulated value for acetate concentration from Figure 4.2. The pH does recover to the same values as experimental data points in the end.

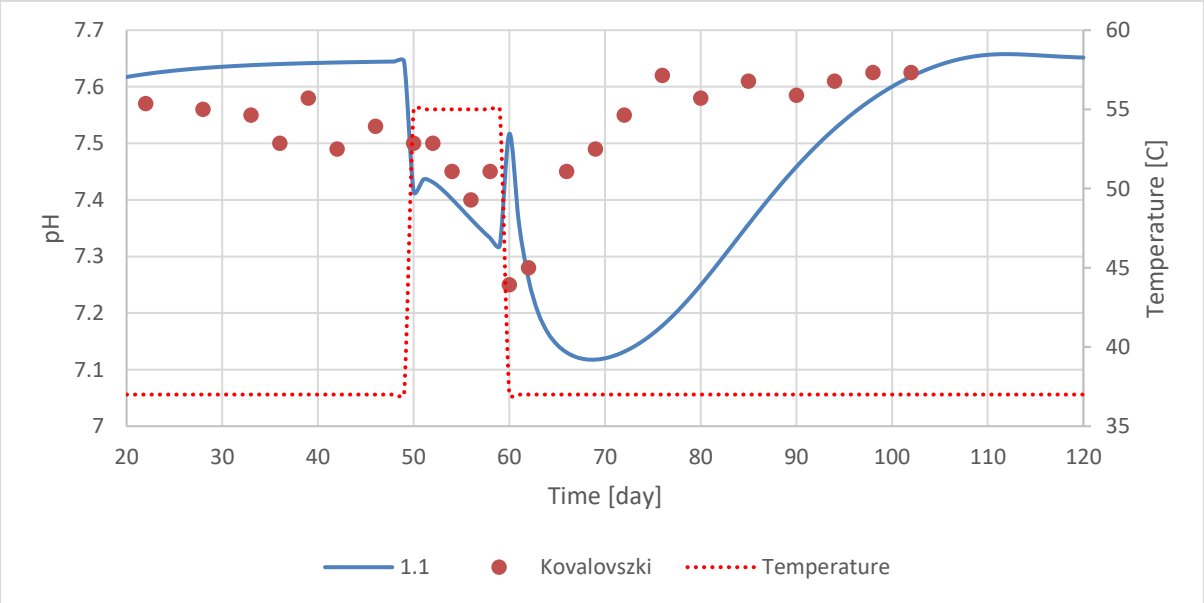

Figure 4.3: Experimental values reproduced from [34] compared to simulated values by ADM1_FTnew model(1.1).

4.1.2 Validation of ADM1_CTM1 model

The results from simulation 2.1 (Table 3.5) are compared to experimental results from [20] and presented in this chapter. The simulation has a stepwise temperature transition from mesophilic to thermophilic temperatures. The red dotted line in the figures represent temperature change.

Biogas flow result for the simulation and experimental data is shown in Figure 4.4. It can be observed that simulation has peaks in gas production at day 0, 10, 35 and 43 when the temperature is changed. Where for the experimental data, there are drops in gas production after days 0 and 10. Then on day 20, the gas production starts to increase rapidly and drops again at around day 30, which is not the case for the simulation.

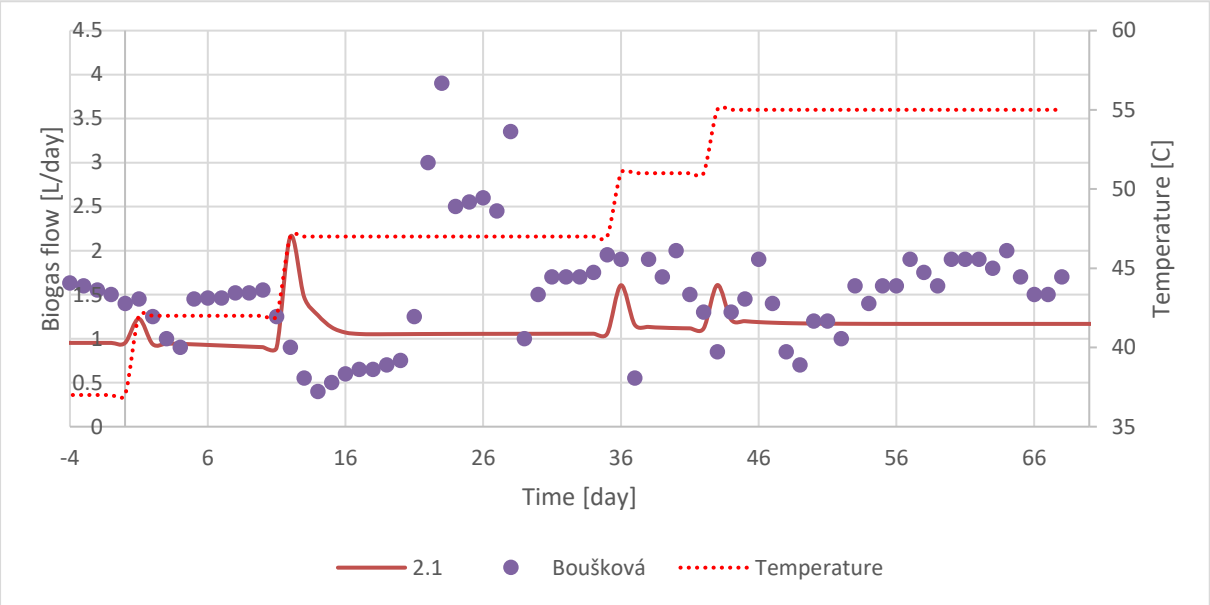

Figure 4.4: Comparing experimental gas flow data points from experimental data [5](Bouškova) and simulated gas flow for the same parameters used in ADM1_CTM1(2.1).

When it comes to simulated and experimental acetate concentration in Figure 4.5, the model starts to respond to temperature change sooner than experimental data. This sooner increase may correlate with a sooner peak in gas production at day 11 for simulation in Figure 4.4. The simulated acetate concentration underpredicts the peak value at day 11 compared to the experimental data peak at day 19.

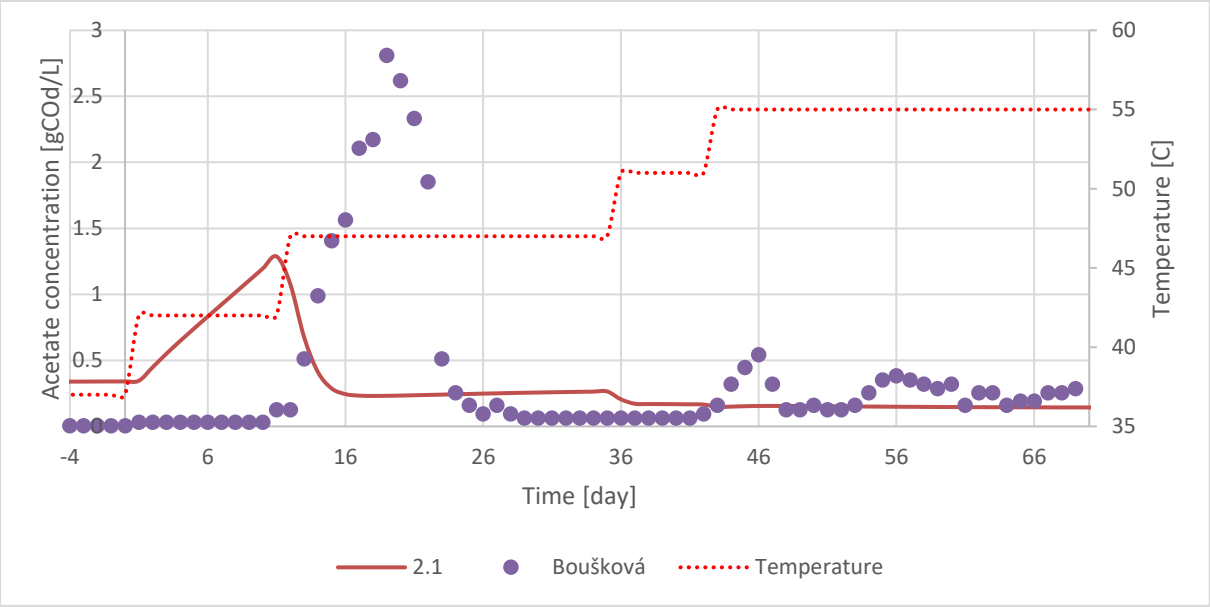

Figure 4.5: Comparison of experimental acetate concentration data points from research paper [5] and simulated acetate concentration for the same parameters using ADM1_CTM1(2.1) model.

From methane content in Figure 4.6 it can be observed that the model is reacting dynamically on days when it is step-change in temperature. Even though the model shows somewhat similar pater to experimental data points after day 36, it does not show the same dynamical behaviour between days 10 and 36. This might be because the model is calculating new rate values only when it has a change in temperature.

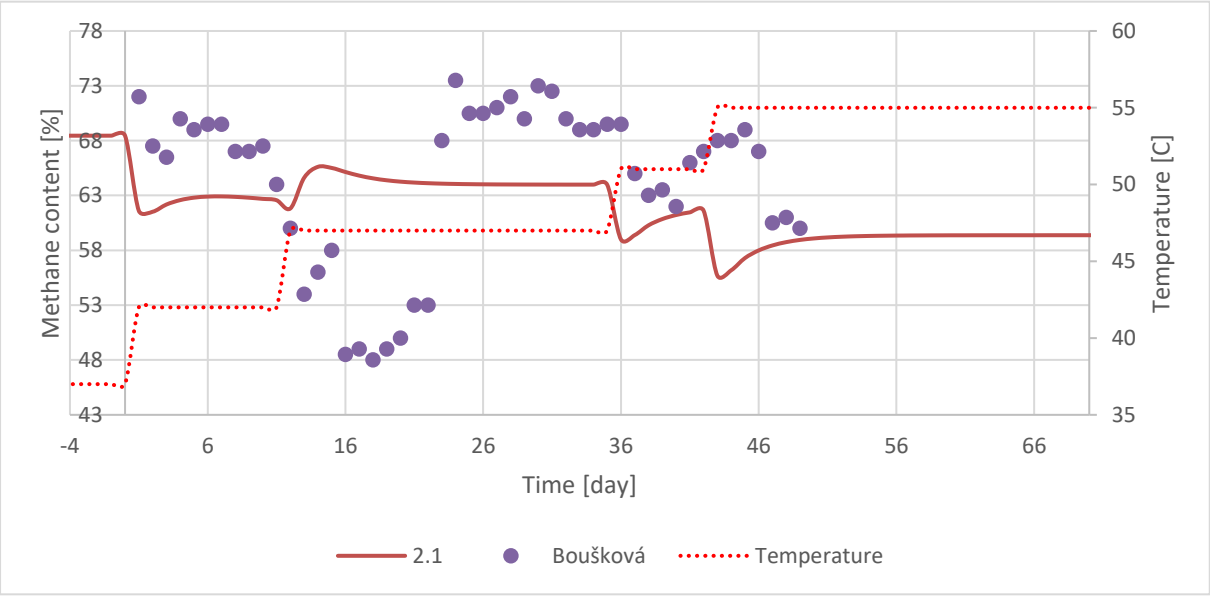

Figure 4.6: Comparison of experimental methane content in biogas data points from research paper [5] and simulated methane content for the same parameters using ADM1_CTM1(2.1) model.

4.2 Temperature transition simulation results

Simulation results for both ADM1_CTM1 and ADM1_FTnew modified models for temperature transition are presented in this chapter. Two simulation cases were taken to test and compare these two models against each other, simulation cases number 3 and 4 described in Table 3.5. Both models were used to simulate the two cases and then compared to each other.

4.2.1 Laboratory scale experiment

One case of a laboratory experiment was chosen as a simulation case to compare two modified ADM1 models for temperature transition. The case is the one with stepwise temperature transition, [20], to see the response of models to temperature change.

Biogas flow presented in Figure 4.7. The ADM1_FTnew (1.2) simulation results fit well with experimental data compared to ADM1_CTM1(2.1), especially between days 10 to 30. However, the ADM1_FTnew model does not have the same peak as experimental data have between days 20 to 30.

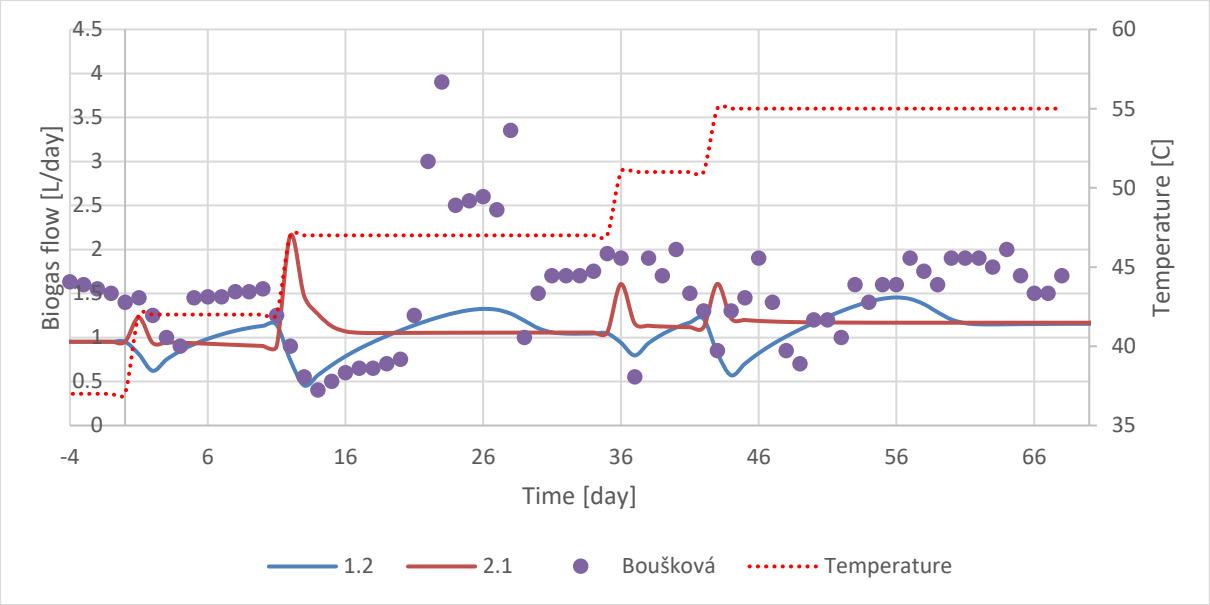

Figure 4.7: Comparison of experimental biogas flow data points from research paper [5] and simulated biogas flow for the same parameters using ADM1_FTnew (1.2) and ADM1_CTM1 (2.1) models.

From methane content results in Figure 4.8, one can observe that the model ADM1_FTnew (1.2) behaves very similar to experimental data between days 10 to 30. Then the ADM1_CTM1 (2.1) model dos not show the same behaviour in the same period. Though both models show response when the temperature is changed, the ADM1_FTnew (1.2) model shows a more dynamic response when the temperature is not changed.

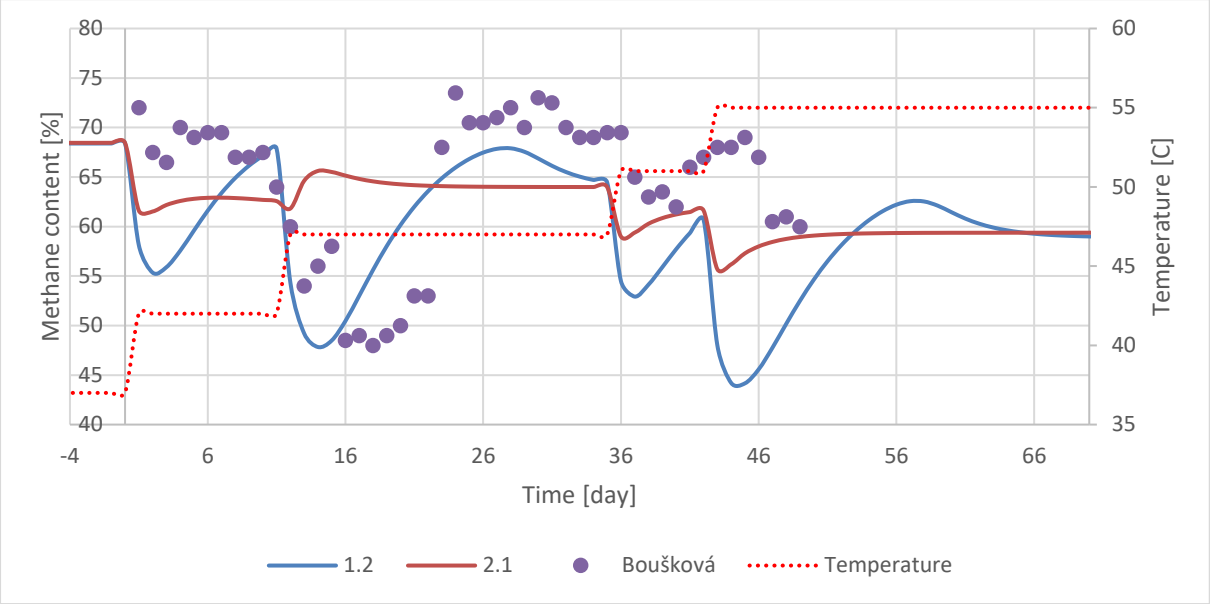

Figure 4.8: Comparison of experimental methane content in biogas data points from research paper [5] and simulated methane content for the same parameters using ADM1_FTnew (1.2) and ADM1_CTM1 (2.1) models.

When it comes to simulation results for acetate compared to the experimental data in Figure 4.9, both models seem to have some similarities and differences. Both models predict acetate peaks in temperature change, and ADM1_FTnew is very close to experimental values between days 10 and 30. Nevertheless, it also has another spike in acetate concentration when the temperature was increased on days 1 to 9. The model also spikes higher than experimental data between days 40 and 60.

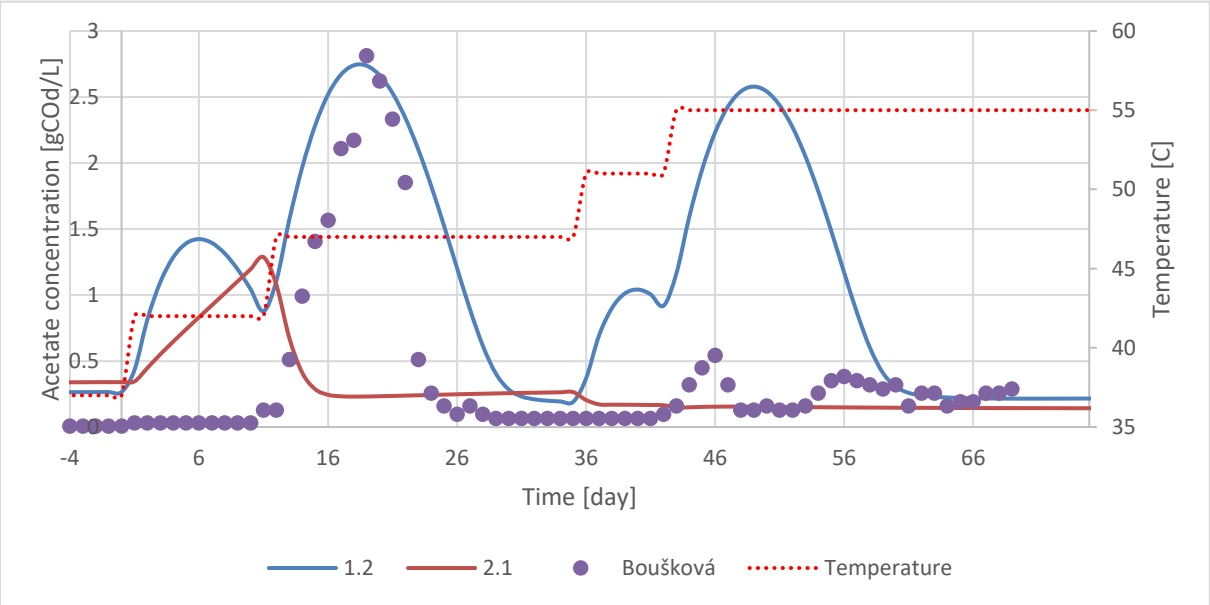

Figure 4.9: Comparison of experimental acetate concentration data points from research paper [5] and simulated methane content for the same parameters using ADM1_FTnew (1.2) and ADM1_CTM1 (2.1) models.

4.2.2 VEAS 2016-2017

Simulation results for VEAS 2016-2017 (VEAS_1617) temperature transition are presented in this chapter. Model from the last semesters' group project with temperature transition modelled as a linear interpolation (Linear model) is compared to ADM1_CTM1 and ADM1_FTnew models. VEAS stopped feeding the reactor between days 19 to 62 and 473 to 514. This stop is reflected in two biogas flow drops which all three models in Figure 4.10 also predict. When the temperature is steady, the models are similar in trend and quite close to the VEAS process data points.

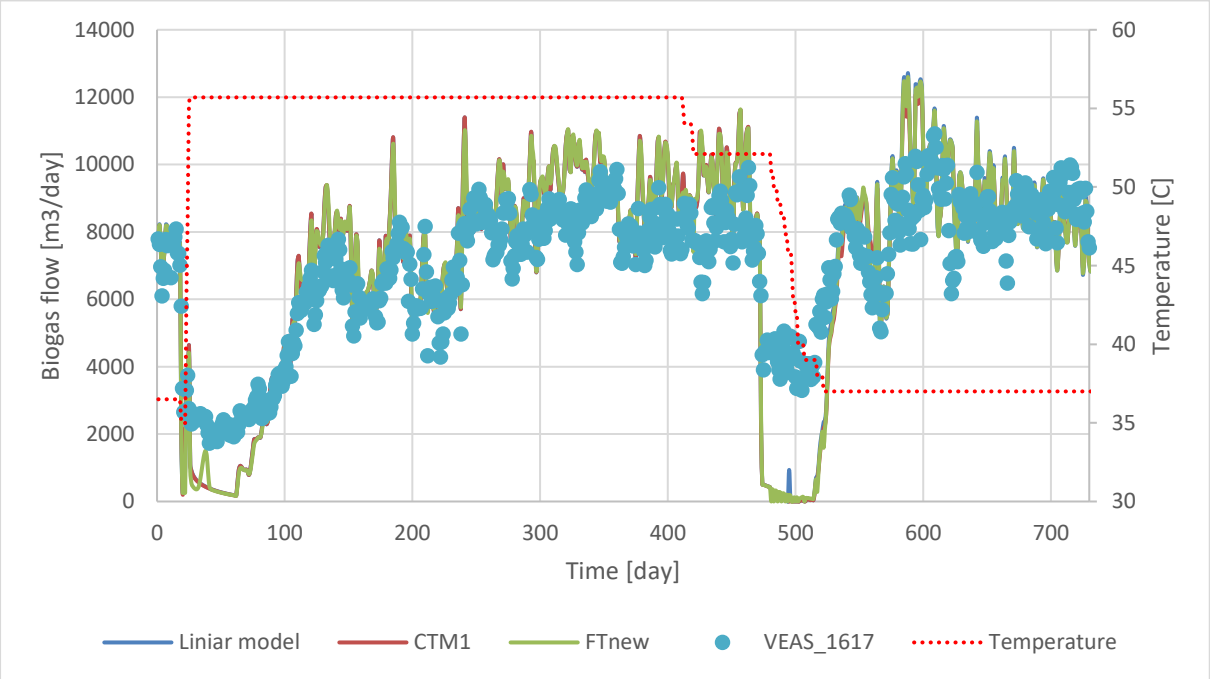

Figure 4.10: Comparison of VEAS process data points for biogas flow from years 2016-2017 to three models, linear model from previous work[35], ADM1_CTM1 model and ADM1_FTnew model.

From Figure 4.11, the simulated methane content in the biogas reactor is lower than VEAS data points. Both Linear and FTnew models overlap each other most of the time. However, the CTM1 model has a bit higher values in constant temperature periods. When the temperature changes during days 411 to 522, all three models show a spike in methane content. Here, the model response to the temperature change is later than the process data. However, in the earlier case (Figure 4.8), the ADM1_CTM1 model responds quicker than the experimental case and ADM1_FTnew close to the experimental case.

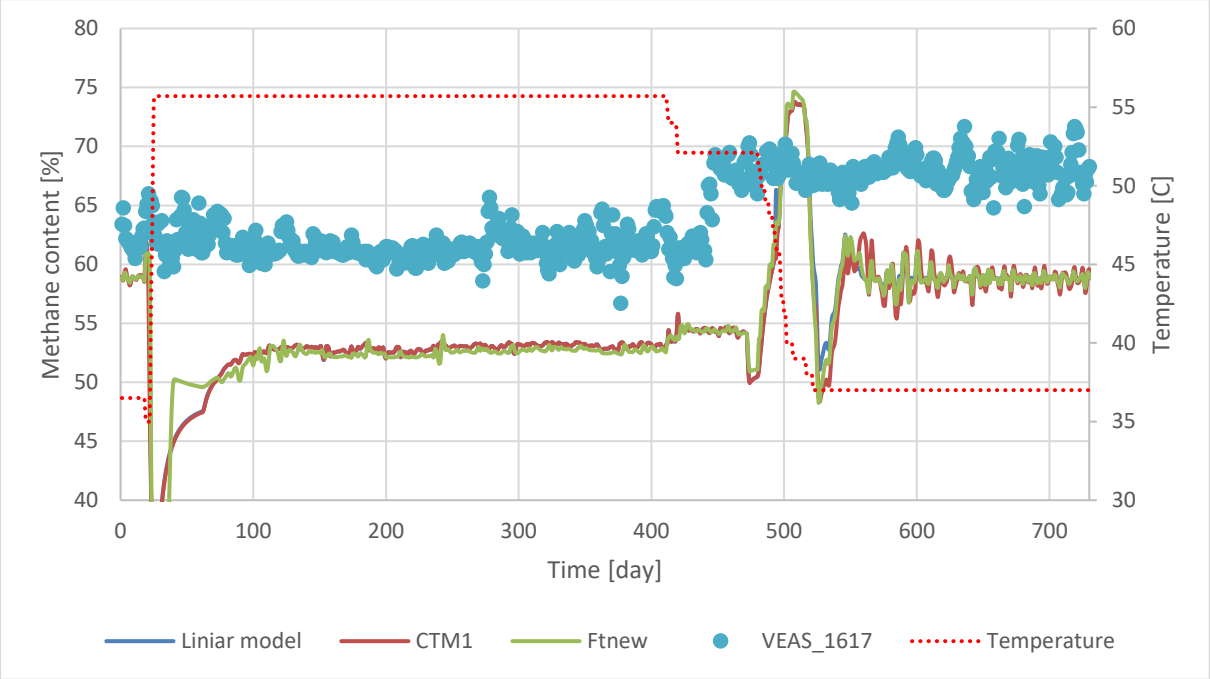

Figure 4.11: Comparison of VEAS process data points for methane content in biogas flow from years 2016-2017 to three models, linear model from previous work[35], ADM1_CTM1 and ADM1_FTnew models.

When studying the results from Figure 4.12, all three models predict pH alike. The most significant difference between the result for the three models can be seen between the days 500 and 600 after the temperature is dropped back to mesophil. It seems that CTM1 has the lowest drop in the pH value then followed by FTnew and linear model at the end. Overall, all three models underestimate pH value at 55°C compared to VEAS data points but have a good match when the temperature drops back to 37°C.

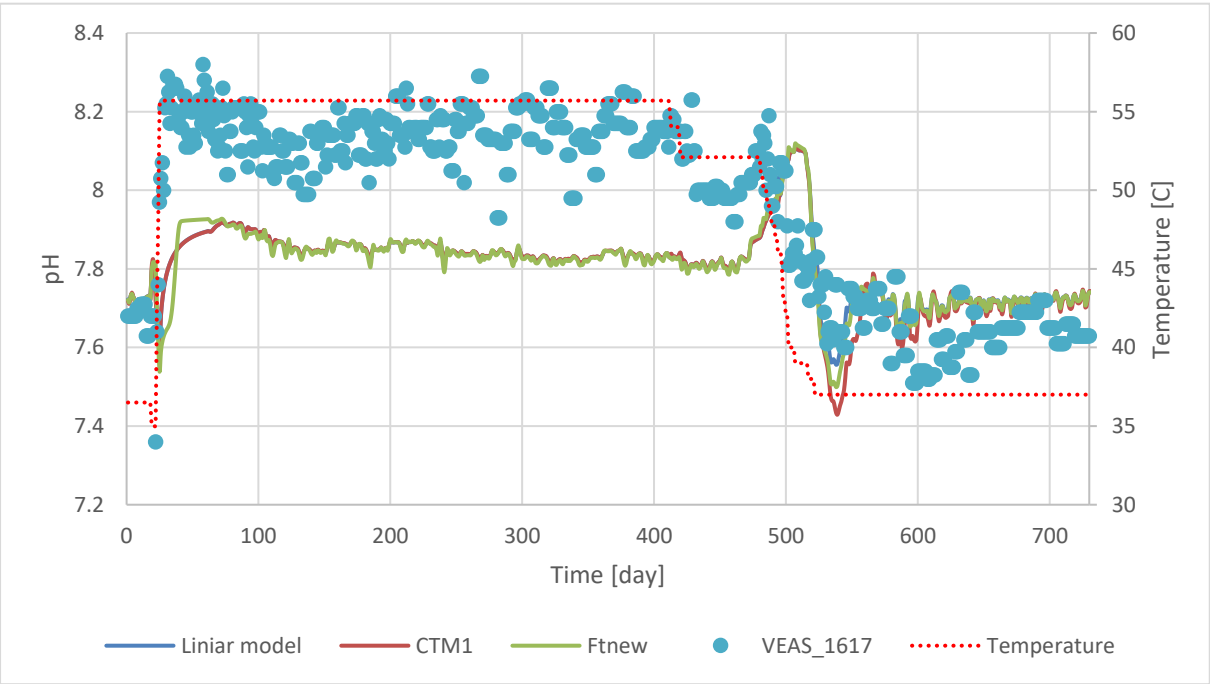

Figure 4.12: Comparison of VEAS process data points for pH from years 2016-2017 to three models, linear model from previous work[35], ADM1_CTM1 model and ADM1_FTnew model.

In Figure 4.13, simulation results for bicarbonate concentrations are presented together with VEAS data points for the same process. All three simulations are overestimating the concentration. However, the response for the temperature change is somewhat the same, with a slight increase after day 22 and an increase followed by a spike downwards after day 450. Linear and FTnew models seem to show the same results except for the drop on day 540. There the lowest drop is for model CTM1 followed by FTnew and linear model in the end. CTM1 model shows a bit higher concentration while it is 55°C in the reactor, and lower than the other two models when the temperature is at 37°C.

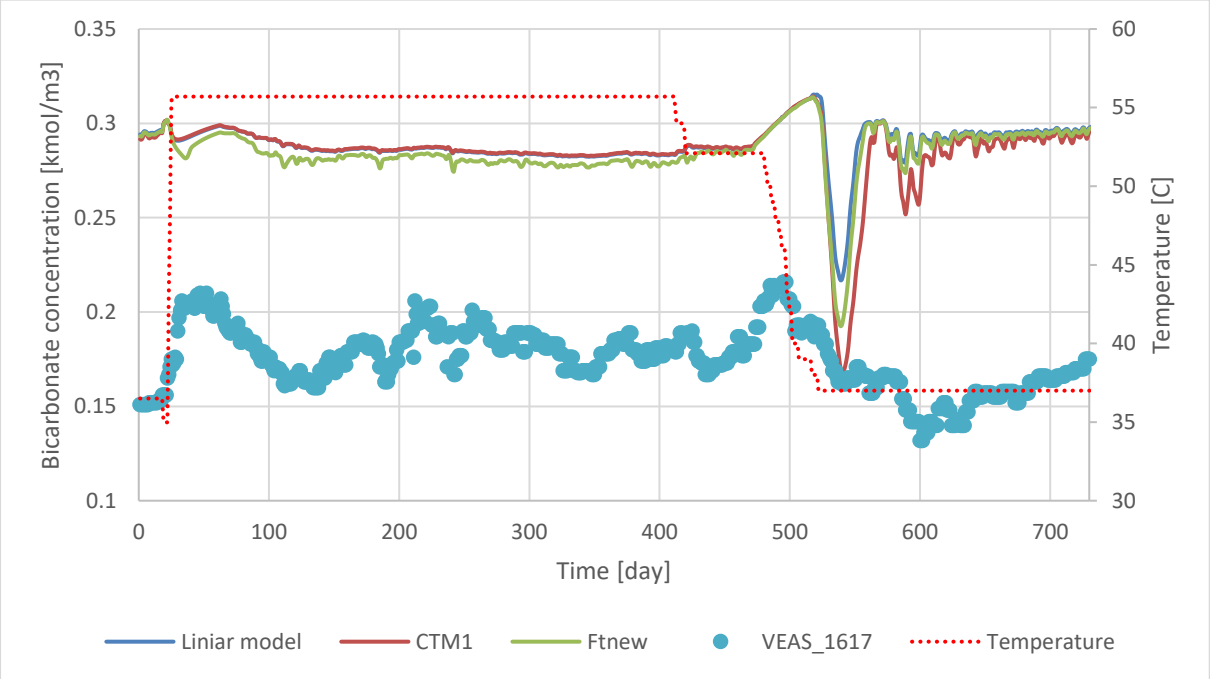

Figure 4.13: Comparison of VEAS process data points for bicarbonate concentration from years 2016-2017 to three models: linear model from previous work[35], ADM1_CTM1 and ADM1_FTnew models.

As it can be observed in Figure 4.14, acetate concentration is higher in the VEAS process than simulated results. When the temperature is changed to 55°C after day 22, there is a peak in FTnew model results, similar to VEAS data points. The model is then continuing to have a slightly higher acetate concentration compared to the two other models. However, it has not the highest peak value after day 500 when the temperature is changed back to 37°C. The highest value is from the CTM1 model, but also, there are no such peaks in VEAS data points.

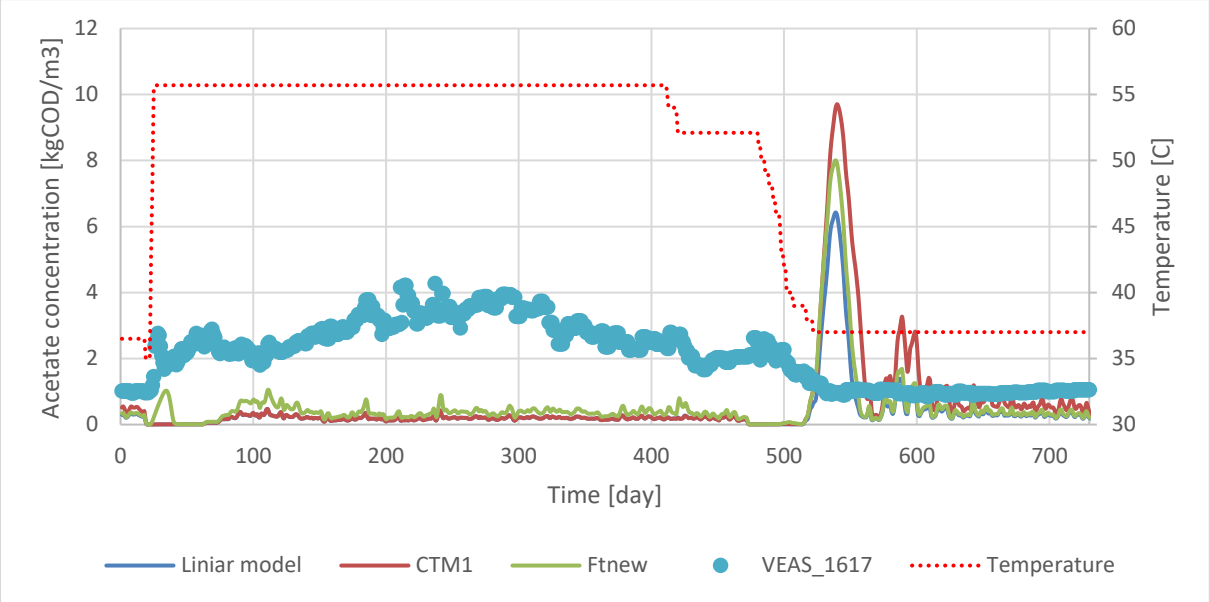

Figure 4.14: Comparison of VEAS process data points for acetate concentration from years 2016-2017 to three models, linear model from previous work[35], ADM1_CTM1 and ADM1_FTnew models.

Figure 4.15 shows the simulated concentration of inorganic nitrogen compared to VEAS process data points. All three models show very similar concentration and behaviour. Since VEAS data points are available only for the period from day 495 to 681, and only that period can be compared to simulations. VEAS data points seem to have more fluctuation in that period than simulated values and show lower concentrations.

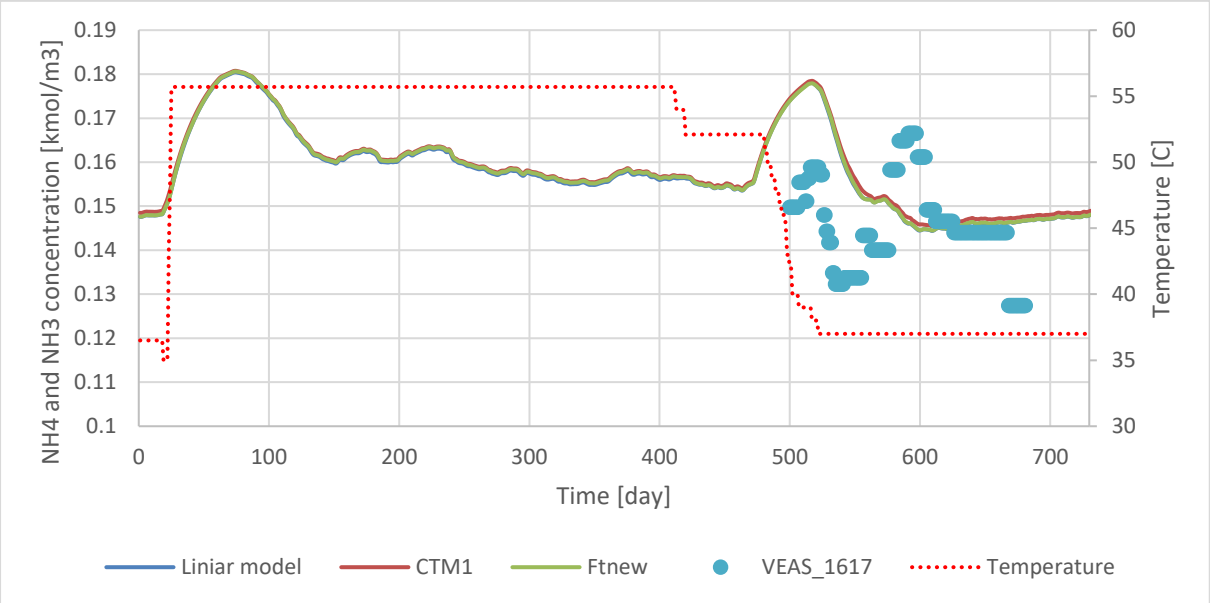

Figure 4.15: Comparison of VEAS process data points for NH3 and NH4 from years 2016-2017 to three models, linear model from previous work[35], ADM1_CTM1 model and ADM1_FTnew model.

After looking at Figure 4.16, one can see that the three models have the same result in parts that have a constant temperature. Nevertheless, the FTnew model peaks highest when the temperature is changed after day 22. The other two models are somewhat close. After temperature returns to 37°C, at day 540, all models have a peak with CTM1 peaking highest then followed by FTnew and the linear model having the lowest peak.

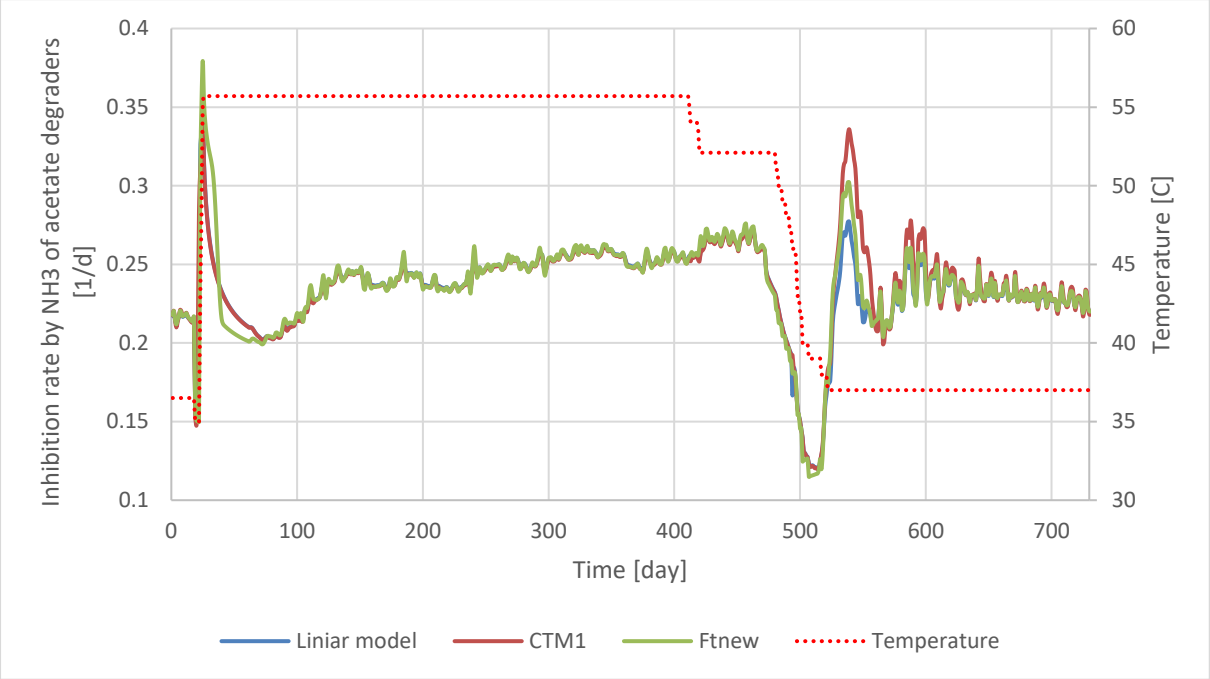

Figure 4.16: Comparison of NH3 inhibition of acetate degrading organisms between three models, linear model from previous work[35], ADM1_CTM1 and ADM1_FTnew models.

In Figure 4.17, results for biomass concentration of acetate degraders simulation are presented. Since acetate degraders had a more dynamic model than the rest of the organisms in ADM1_FTnew, it would be interesting to compare the there dynamics to ADM1_CTM1 and Linear models. Results are fairly similar for all three models, up until day 422 when the temperature was gradually changed back to 37°C. Then the CTM1 model showed slightly lower values than the other two models that showed a similar result.

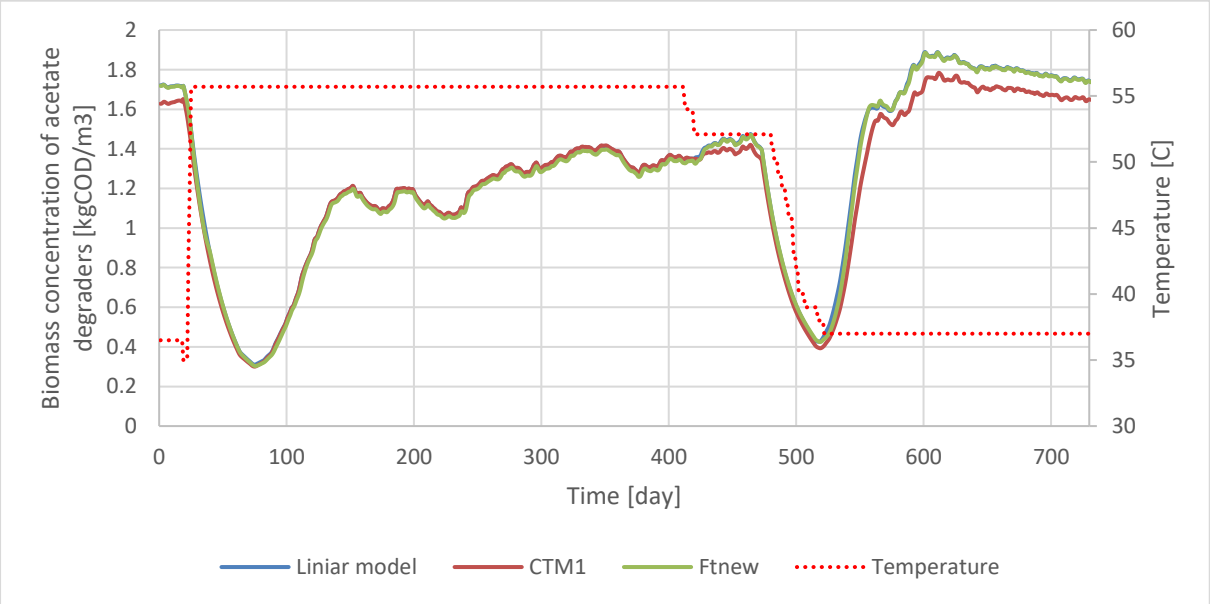

Figure 4.17: Comparing biomass concentration of acetate degraders between three models: linear model from previous work[35], ADM1_CTM1 model and ADM1_FTnew model.

When studying Figure 4.18, one can notice that the growth rate of acetate degraders for all three models differ from each other. The FTnew predicts a lower growth rate than the other

two models even in the first 20 days before the first temperature change. FTnew is recovering faster after days 64 and 513 when reactor feed was started again, even though dynamics look similar for all models. Then after day 540, the Linear model has the highest values for the growth rate, closely followed by CTM1 and with FTnew having the lowest values.

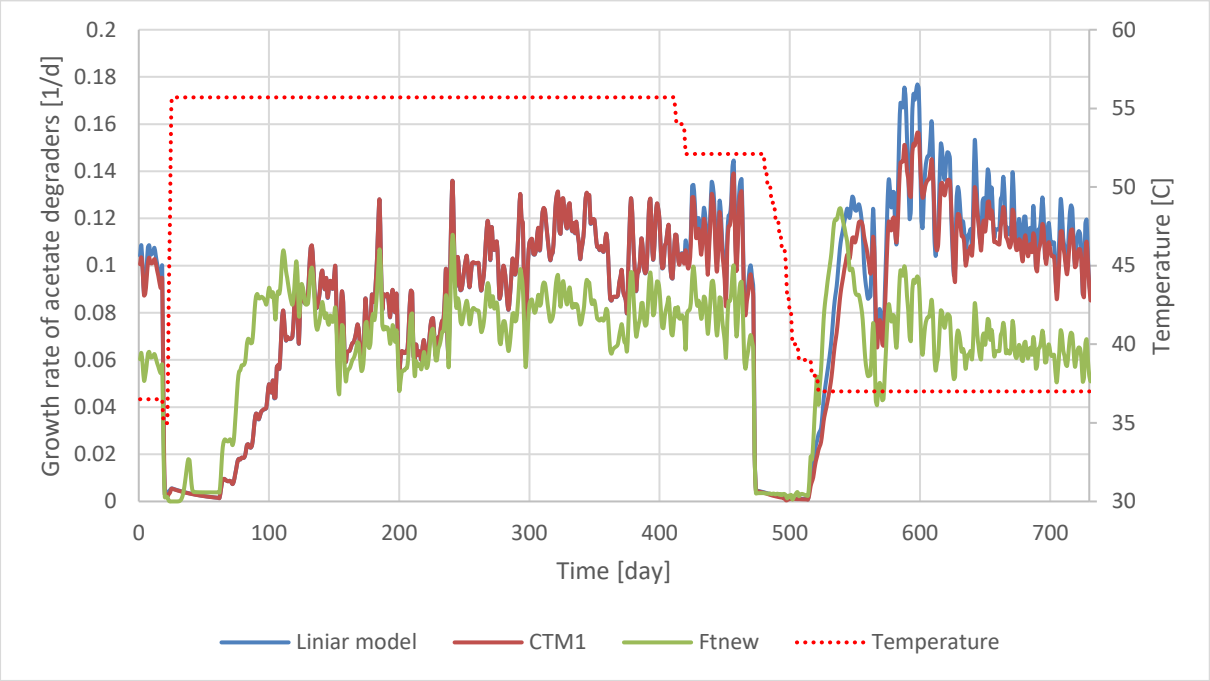

Figure 4.18: Comparison of Monod specific growth rate of acetate degraders between three models: linear model from previous work[35], ADM1_CTM1 model and ADM1_FTnew model.

4.3 Mesophilic process simulation results

Results from simulations with numbers 5.1-5.4, 6.1-6.3 and 7.1-7.3 from Table 3.5 will be presented in this chapter. Also, VEAS process data points from 2019 will be compared to VEAS 2019 process simulation without any change as well.

Figure 4.19 compares biogas flow from VEAS 2019 process data to the simulated biogas flow for the same process. From the graph, it is observed a good match of simulated values compared to the data points.

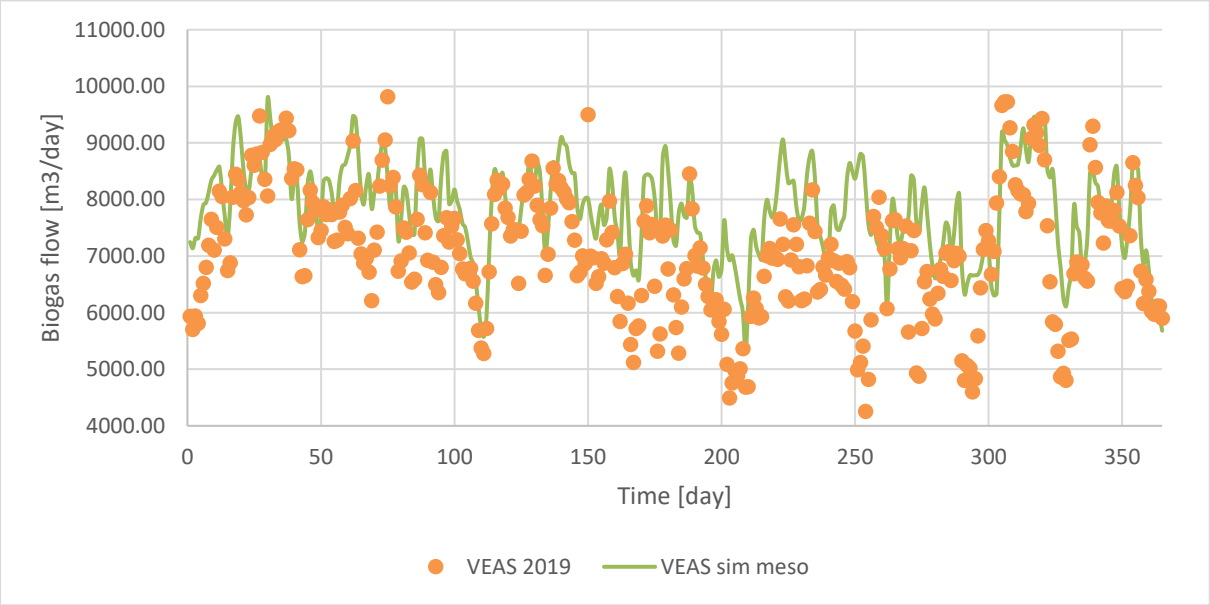

Figure 4.19: Biogas production from VEAS 2019 data compared to simulated VEAS 2019 mesophilic process.

Simulated methane content in Figure 4.20 shows a good match with the VEAS process data point and biogas flow in Figure 4.19.

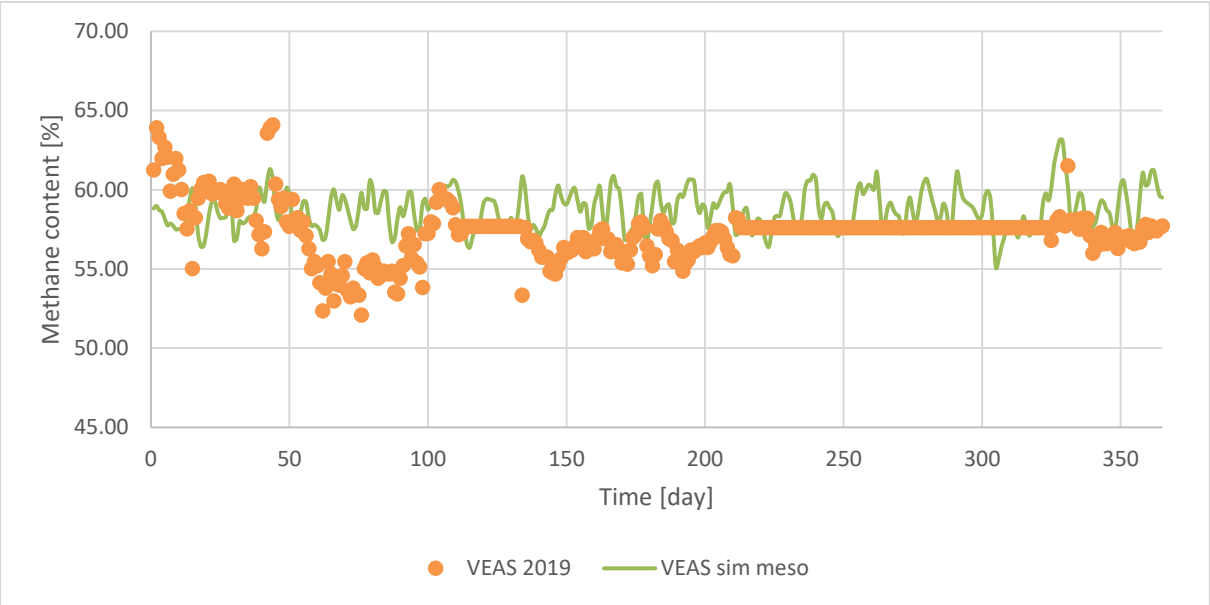

Figure 4.20: Methane content in biogas from VEAS 2019 process data points against simulation results of the same process.

For pH in Figure 4.21, VEAS process data points are more spread than the simulation is predicting, but both the simulation and VEAS data points are in the same range.

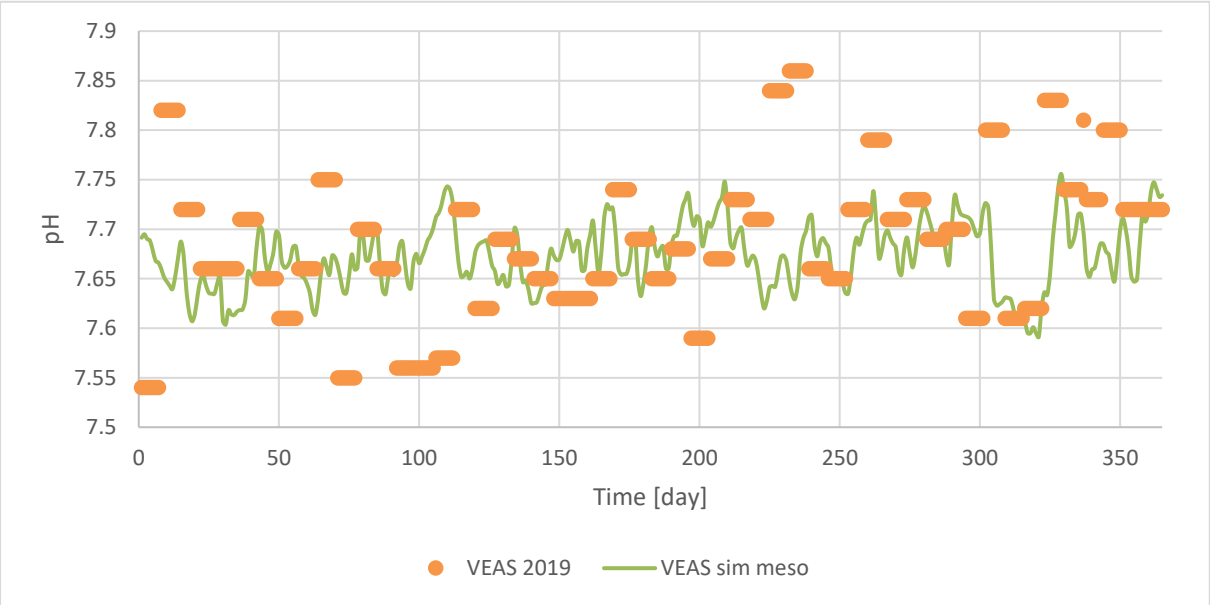

Figure 4.21: pH data points from VEAS 2019 process compared with the simulation of the same VEAS 2019 mesophilic process.

The difference in the simulated acetate concentration and VEAS process data points can be seen in Figure 4.22. The simulation has more fluctuation and predicts lower concentrations of acetate in the reactor than it is measured in the VEAS 2019 process. On the other hand, bicarbonate concentration is overestimated by the simulation, see Figure 4.23. The simulation overestimation or underestimation of different parameters are summarized in Table 4.1.

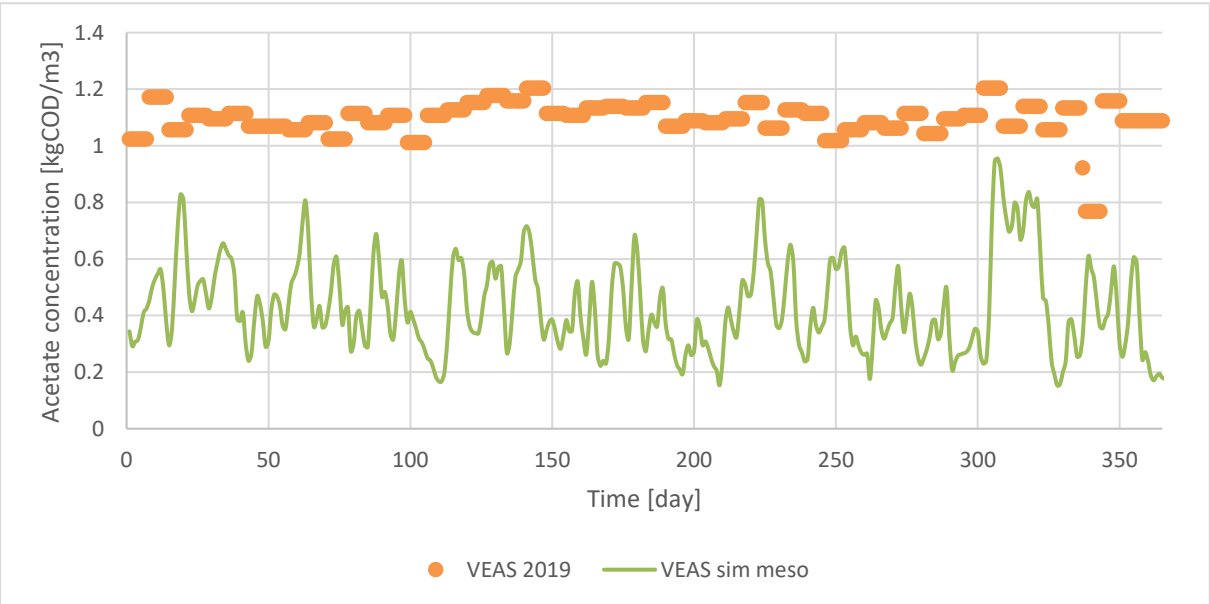

Figure 4.22: Acetate concentration data points from VEAS 2019 process compared to the simulated VEAS 2019 process.

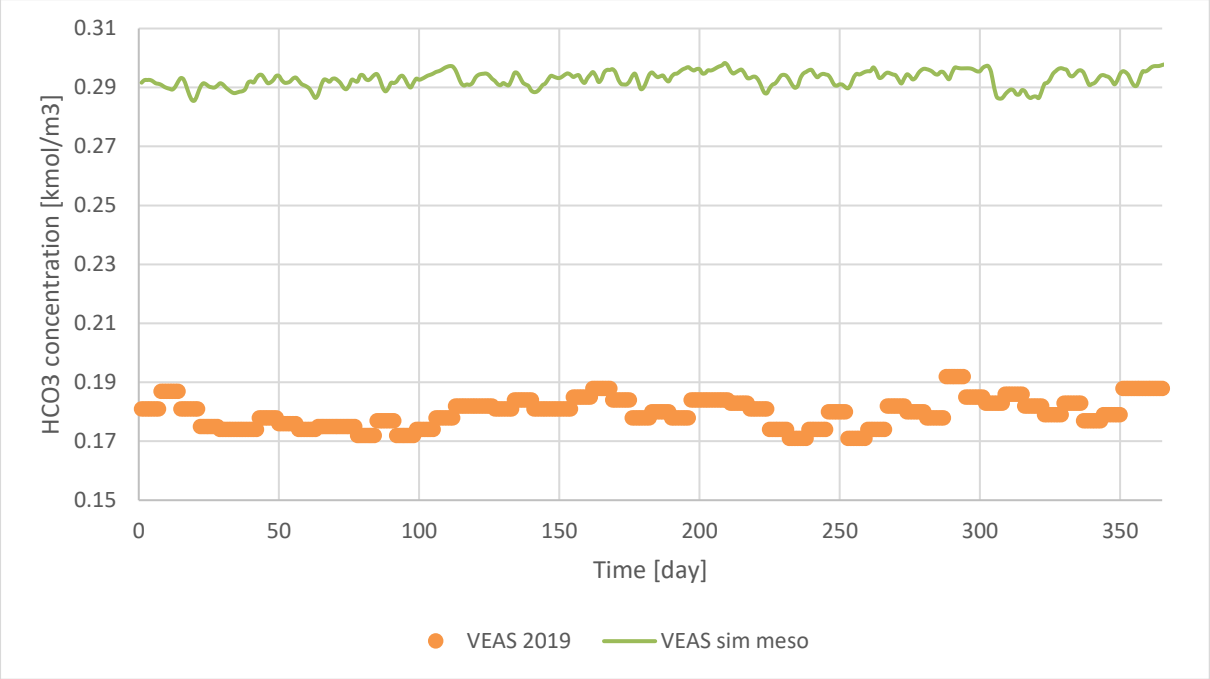

Figure 4.23: Bicarbonate concentration from VEAS 2019 process data points compared to values obtained from simulation of the same process.

As shown in Table 4.1, the average values of simulation and VEAS 2019 data points for the same period show some differences. Methane content and pH are relatively similar, as it was also seen in Figure 4.20 and Figure 4.21. However, the average biogas flow from the simulation is increased by 28%. The noticeable difference was also in a 61% decrease in average simulated acetate concentration and an increase by 63% in average simulated bicarbonate concentration.

Table 4.1: Differences between VEAS 2019 data and the simulation. Average values for the same period for both data points and simulation.

Results compared	VEAS 2019 data	VEAS 2019 simulation	Relative difference
Biogas flow rate (STP)	6251 [m3/day]	8016 [m3/day]	28%
Methane content	57.3%	58.8%	2.5%
pH	7.69	7.67	-0.2%
Acetate concentration	1.1 [kgCOD/m3]	0.42 [kgCOD/m3]	-61%
HCO3	0.18 [kmol/m3]	0.29 [kmol/m3]	63%

4.3.1 Mesophilic process simulation with propylene glycol

The results from three VEAS mesophilic process simulations with PGW as co-substrate are looked at in this sub-chapter. These three simulations were presented in Table 3.5 by number 6.1, 6.2 and 6.3, with PGW to SS ratios 7.5:192.5, 10.8:189.2 and 14:186, respectively. The

results from the simulations are compared to VEAS data points and simulated results of mesophilic not changed process.

From Figure 4.24, it is seen that by adding PGW to the process, biogas flow is increasing compared to VEAS mesophilic process, both data and simulation. Biogas flow is also slightly increasing when the PGW volume is increasing.

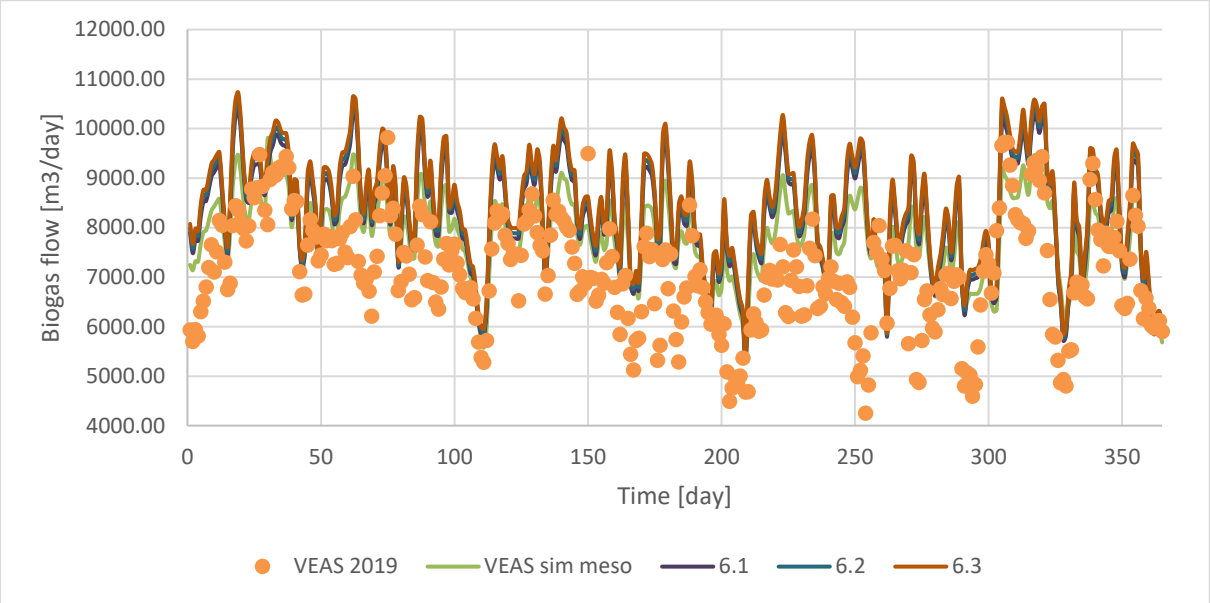

Figure 4.24: Comparison of VEAS 2019 biogas flow from both simulation and data points to three VEAS process simulations with PGW, where PGW to SS ratios are 7.5:192.5 for 6.1, 10.8:189.2 for 6.2 and 14:186 for 6.3.

Methane content seems to be less fluctuating than simulation without co-substrate; see Figure 4.25. All Simulation have quite a close match.

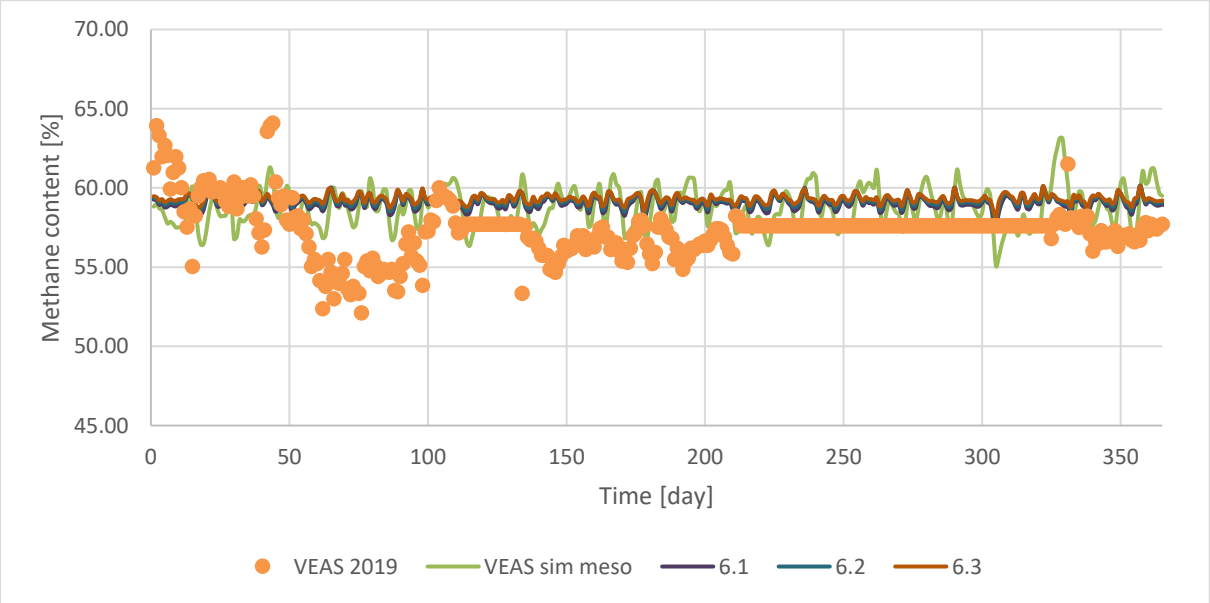

Figure 4.25: Comparison of VEAS 2019 methane content from both simulation and data points to three VEAS process simulations with PGW, where PGW to SS ratios are 7.5:192.5 for 6.1, 10.8:189.2 for 6.2 and 14:186 for 6.3.

As it can be seen in Figure 4.26, pH differs slightly between simulations with PGW and VEAS process simulation. It seems that the pH value fluctuates less when PGW is added and slightly goes down with increasing PGW content.

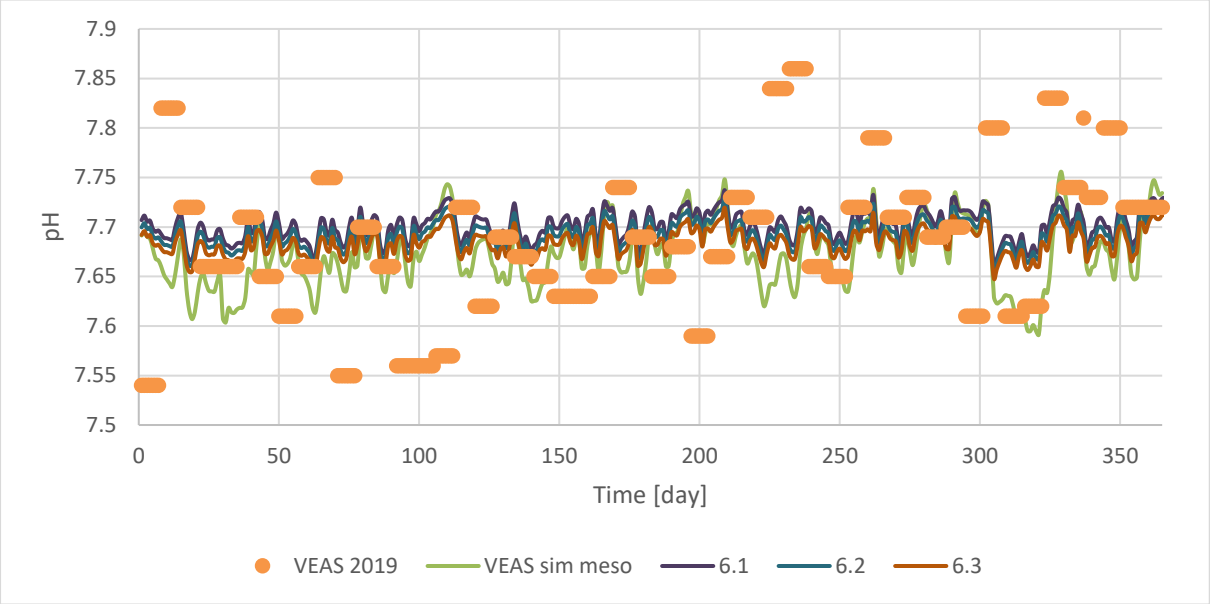

Figure 4.26: Comparison of VEAS 2019 pH values from both simulation and data points to three VEAS process simulations with PGW, where PGW to SS ratios are 7.5:192.5 for 6.1, 10.8:189.2 for 6.2 and 14:186 for 6.3.

From Figure 4.27, it is seen that acetate concentration is decreasing with increasing PGW content in the inflow. However, the three simulations predict only slightly lower acetate concentration compared to the VEAS process simulation.

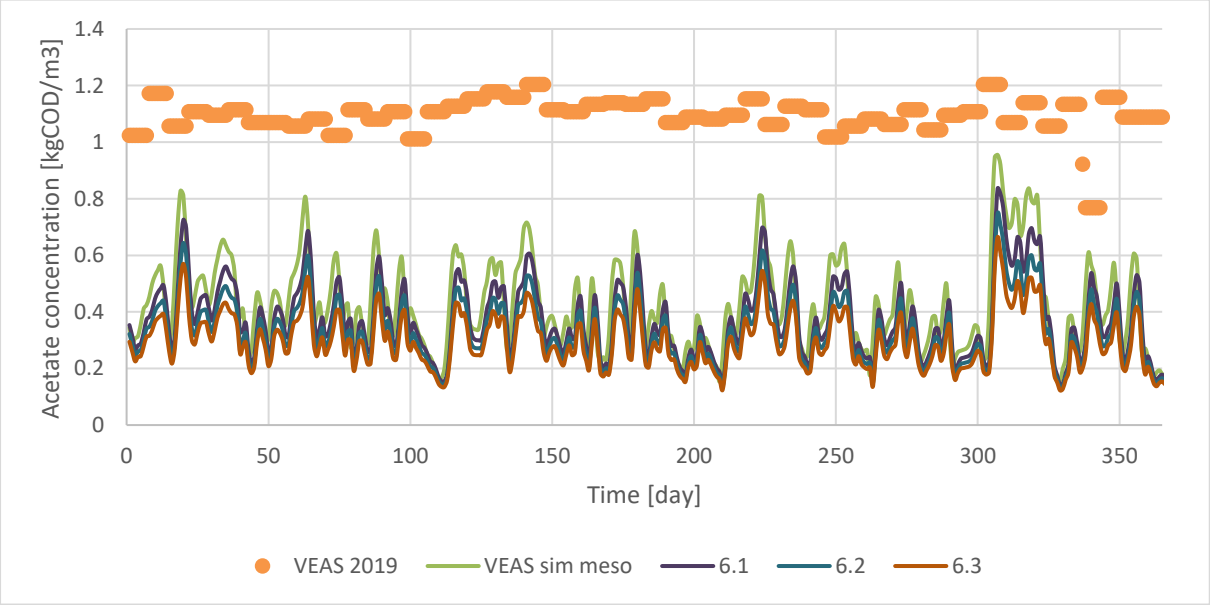

Figure 4.27: Comparison of VEAS 2019 acetate concentration from both simulation and data points to three VEAS process simulations with PGW, where PGW to SS ratios are 7.5:192.5 for 6.1, 10.8:189.2 for 6.2 and 14:186 for 6.3.

For the bicarbonate concentration in Figure 4.28, one can see that concentration decreases when the inflow volume of PGW increases. All three simulations also have lower bicarbonate

concentration compared to the VEAS process simulation. Though not as low as the data points from VEAS 2019 process.

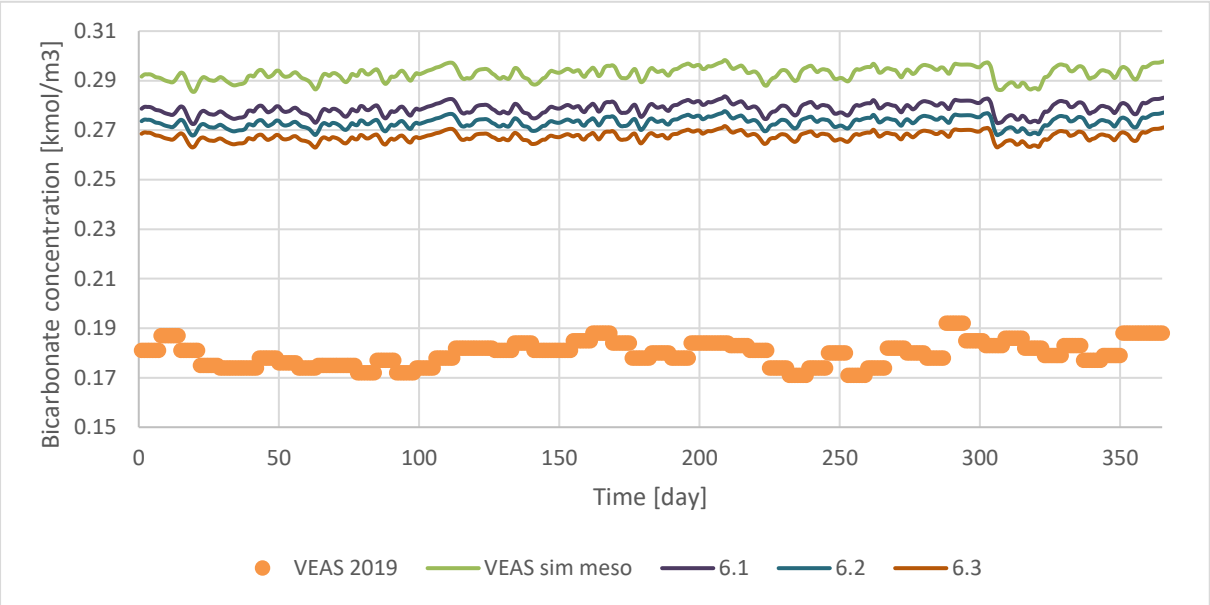

Figure 4.28: Comparison of VEAS 2019 bicarbonate concentration from both simulation and data points to three VEAS process simulations with PGW, where PGW to SS ratios are 7.5:192.5 for 6.1, 10.8:189.2 for 6.2 and 14:186 for 6.3.

Since VEAS did not measure inorganic nitrogen content in their process, Figure 4.29 shows the results from simulations only. The VEAS process simulation is compared to the three VEAS simulations with PGW as co-substrate. It is observed that with increasing PGW part, the NH4 concentrations decrease.

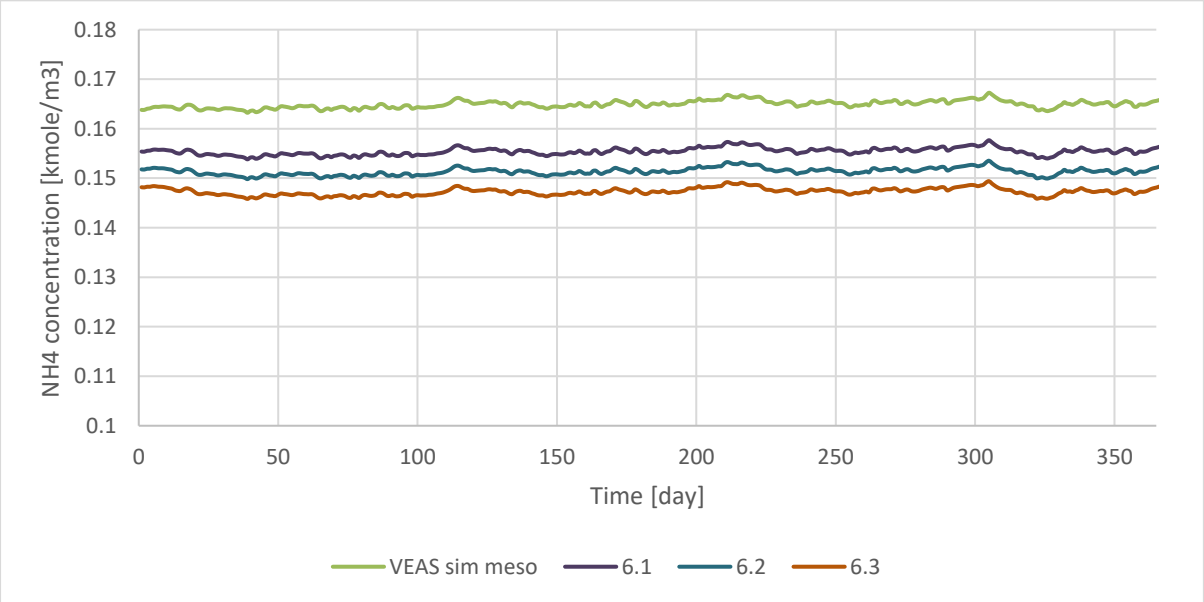

Figure 4.29: Comparison of NH4 concentrations from VEAS process simulation to the three process simulations with PGW as co-substrate, where PGW to SS ratios are 7.5:192.5 for 6.1, 10.8:189.2 for 6.2 and 14:186 for 6.3.

The relative difference calculated from average simulation result values was compared between simulations with PGW and VEAS simulation in Table 4.2. After studying the table, one can

see that average pH values and methane content in biogas do not change more than 1% when comparing simulations 6.1, 6.2 and 6.3 to VEAS simulation. When it comes to acetate, bicarbonate and NH4 concentrations, the average values are dropping with the increasing ratio of PGW in feed. Though it seems like the average flow of biogas is increasing when more PGW is added.

Table 4.2: Comparison of some average results values from simulations 6.1, 6.2 and 6.3 where PGW to SS ratios are 7.5:192.5 for 6.1, 10.8:189.2 for 6.2 and 14:186 for 6.3 against standard VEAS process simulation. Average values calculated for the same time period for all simulations.

	Relative differences					
Results compared	pH [%]	Acetate [%]	HCO3 [%]	NH4 [%]	Methane content [%]	Biogas flow [%]
VEAS sim meso to 6.1	0.37	-12.93	-4.84	-5.79	0.47	6.01
VEAS sim meso to 6.2	0.26	-22.30	-6.75	-8.26	0.71	7.64
VEAS sim meso to 6.3	0.15	-30.29	-8.68	-10.74	0.95	9.25

4.3.2 Mesophilic process simulation with additional sludge

This chapter presents simulation results of the VEAS process with three additional substrates compared to VEAS 2019 data points and VEAS process simulation results. Four simulations with additional sludges were done during the thesis work. The simulations are 5.1, 5.2, 5.3, 5.4, parameters of which were summarised in Table 3.5. Sludge ratios for the simulations are S0:S1:S2:S3 at values 140:60:0:0 for 5.1, 140:0:60:0 for 5.2, 140:0:0:60 for 5.3 and 140:20:20:20 for 5.4

Figure 4.30 shows some minor changes when additional sludges are added to the VEAS process simulations. It seems like all four simulations with additional sludges drop in gas flow compared with VEAS process simulation with no additional sludges added. The one that has the lowest gas flow in the graph seems to be simulation 5.1, with sludge ratio S0:S1:S2:S3 at 140:60:0:0. Simulations 5.2, 5.3 and 5.4 seems to be somewhat in between VEAS simulation and simulation 5.1.

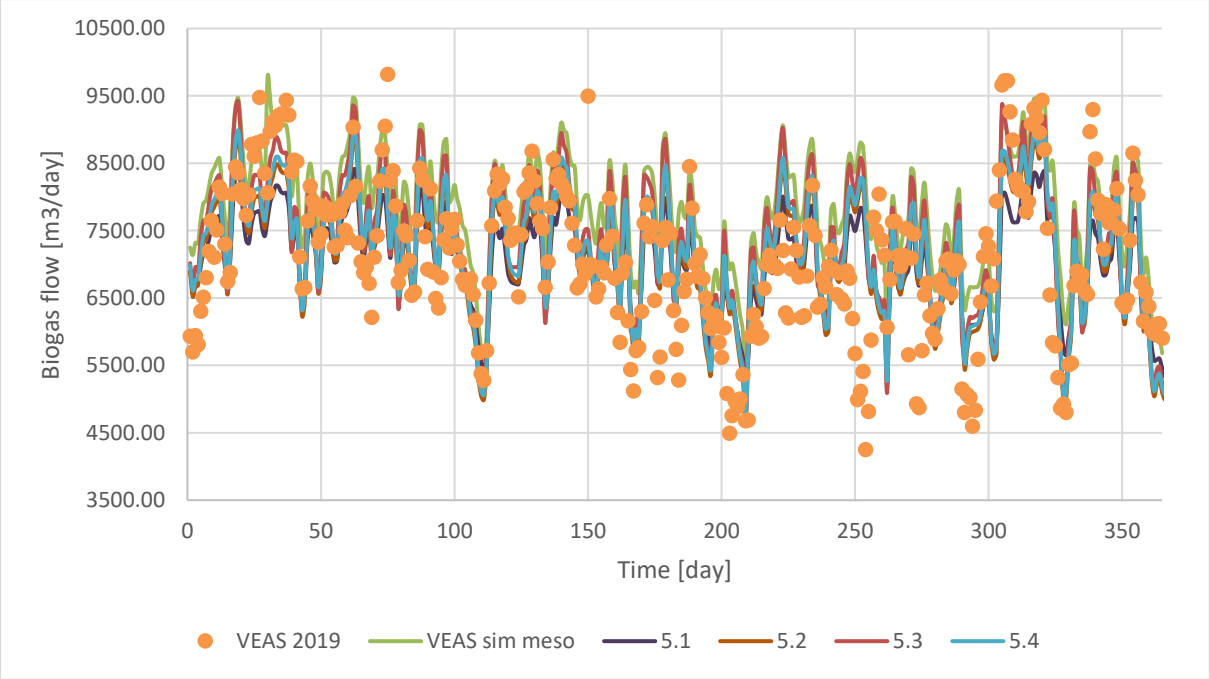

Figure 4.30: Comparison of biogas flow from VEAS 2019 process data and VEAS process simulation to four VEAS process simulations with additional sludges.

When comparing methane content in biogas from VEAS co-digestion simulations in Figure 4.31, one can observe that VEAS simulation and 5.1, 5.2 and 5.4 are quite similar in behaviour and range. Simulation 5.3, on the other hand, does not show that much fluctuation and seems to have lower methane content values than other simulations. It seems to have very close methane content values to VEAS data points in a stable period (day 220 to 320).

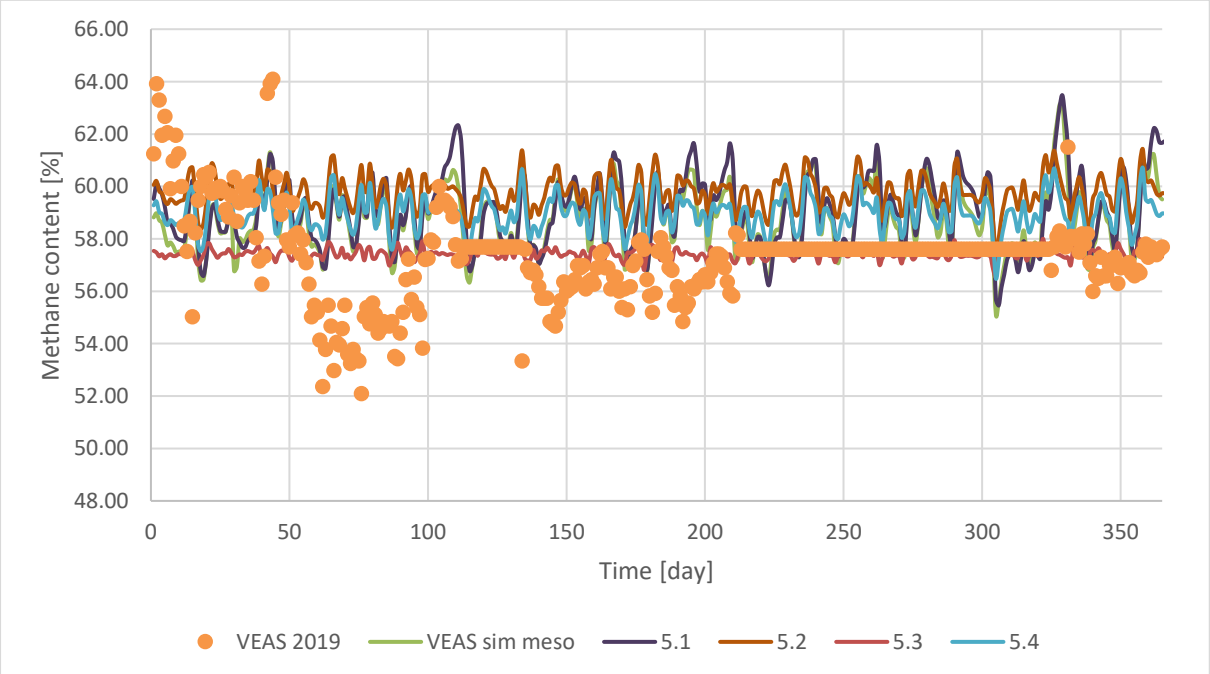

Figure 4.31: Comparison of methane content in biogas from VEAS 2019 process data and VEAS process simulation to four VEAS simulations with additional sludges.

From Figure 4.32, the simulated pH value for all simulations are very similar and in range for VEAS 2019 process data.

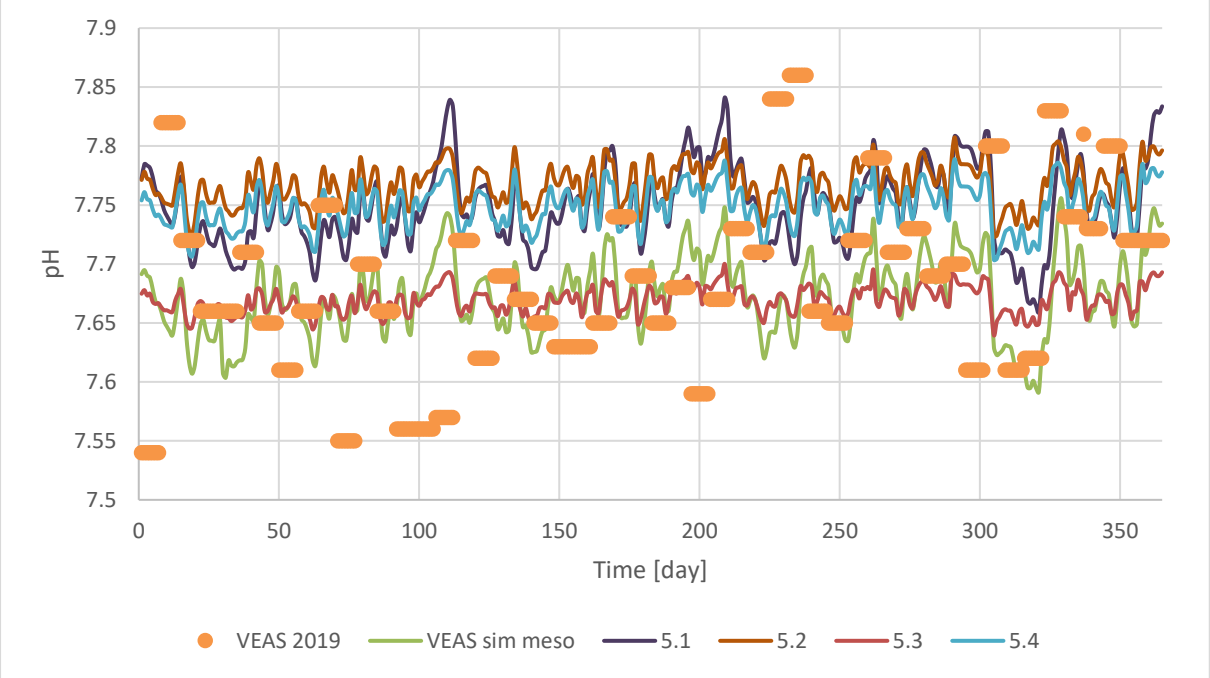

Figure 4.32: Comparison of pH values from VEAS 2019 process data and VEAS process simulation to four VEAS simulations with additional sludges.

When simulation results for acetate concentrations are compared in Figure 4.33, one can see interesting results. The 5.1 simulation has very high acetate concentrations compared to the other simulations and VEAS data points. Then the simulations 5.2 and 5.4 seem to overlap each other and show acetate concentration peaks reaching over 1 kgCOD/m^3. Simulation 5.3 has the lowest acetate concentration, even lower than VEAS process simulation.

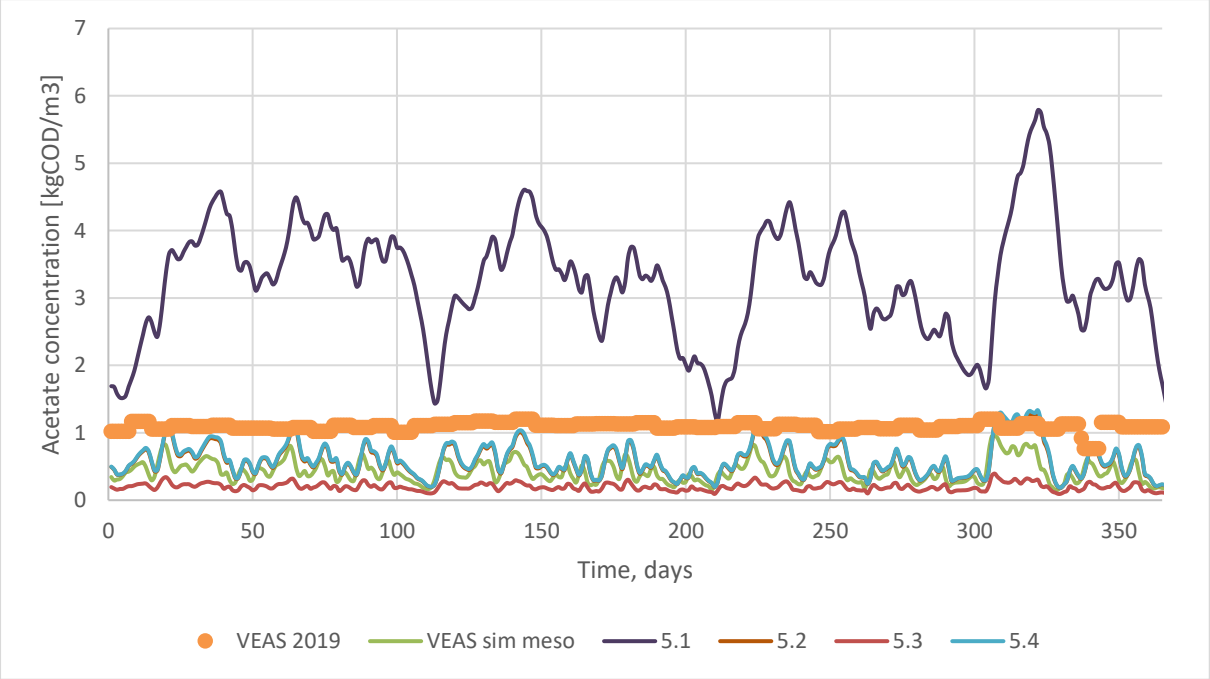

Figure 4.33: Comparison of acetate concentration from VEAS 2019 process data and VEAS process simulation to four VEAS simulations with additional sludges.

As it was mentioned before, VEAS did not measure the IN concentrations in the process. Thus Figure 4.34 shows the simulation result of the VEAS process with additional sludges compared to the VEAS process simulation. It is seen that the 5.1 simulation has much higher IN concentrations than the VEAS simulation. As for the simulations 5.2, 5.3 and 5.4, they are showing a decrease in IN compared to the VEAS simulation. With 5.3 having the lowest values, 5.4 closest to the VEAS simulation and 5.2 slightly lower than 5.4.

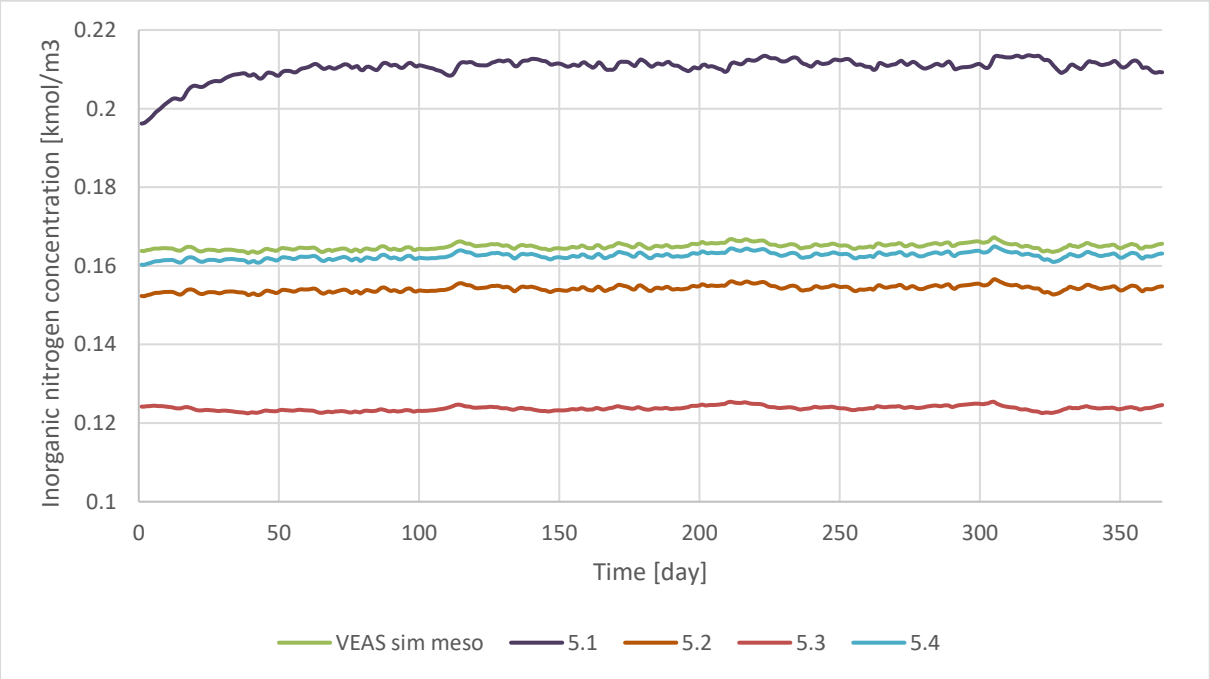

Figure 4.34: Comparison of inorganic nitrogen concentration from VEAS process simulation to four VEAS simulations with additional sludges.

Figure 4.35 compares simulated bicarbonate concentrations from simulations with additional sludges to VEAS 2019 process data and VEAS simulation. It appears that simulation 5.1 has somewhat higher concentrations than VEAS simulation, in addition to more fluctuation. Simulations 5.2 and 5.4 have similar fluctuations as the VEAS simulation but slightly higher concentration. As for 5.3, the simulation is showing the lowest concentrations of five simulations.

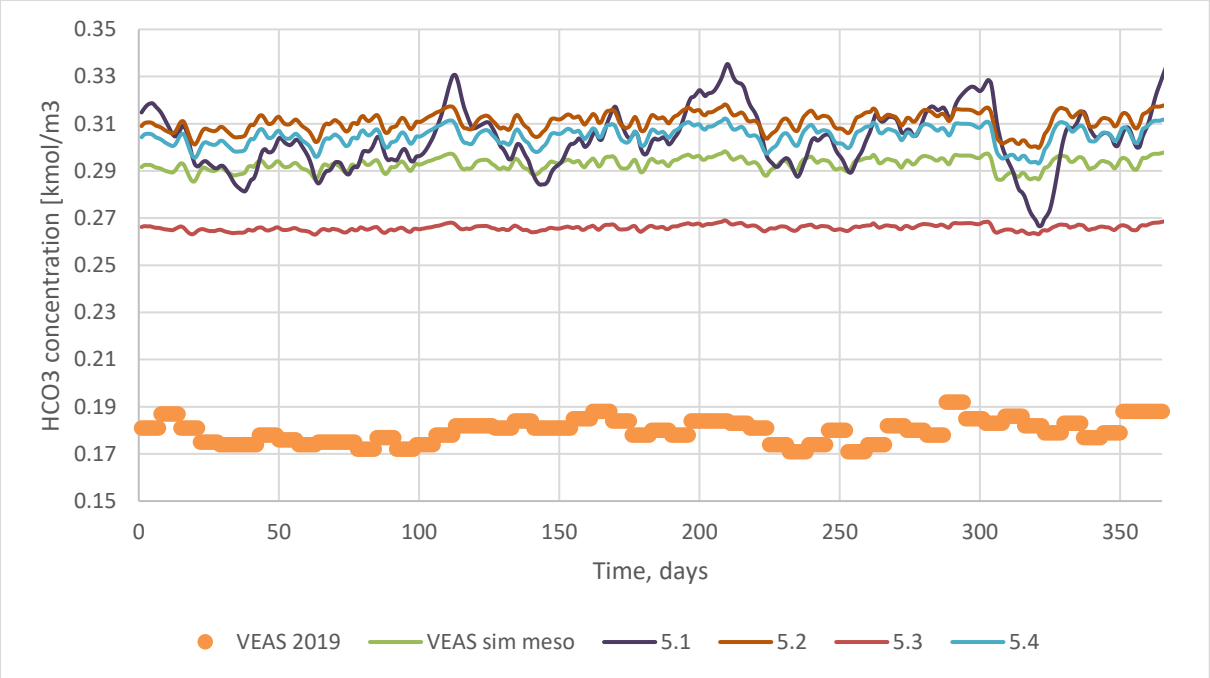

Figure 4.35: Comparison of bicarbonate concentration from VEAS 2019 process data and VEAS process simulation to four VEAS simulations with additional sludges.

The average values of parameters simulated in this chapter for the different sludges are compared to the VEAS process simulation. The results are presented in Table 4.3. After looking at the table, one can see that pH and methane content changes are quite small. Though acetate varies significantly for all simulations, there was a 659% increase in simulation 5.1 compared to the VEAS simulation. One can also observe that average biogas flow decreases for all simulations with additional sludges compared to VEAS simulations.

Table 4.3: Comparing some average results values from simulations with co-substrate against not altered VEAS process simulation. Average values calculated for the same time period for simulation 5.1, 5.2, 5.3, 5.4 and VEAS process simulation.

	Relative differences					
Results compared	pH [%]	Acetate [%]	HCO3 [%]	NH4 [%]	Methane content [%]	Biogas flow [%]
VEAS sim meso to 5.1	1.01	659.19	3.73	27.94	0.56	-11.52
VEAS sim meso to 5.2	1.24	37.16	6.13	-6.46	1.72	-10.17

VEAS sim meso to 5.3	-0.04	-53.31	-9.23	-25.00	-2.27	-6.53
VEAS sim meso to 5.4	0.99	41.02	4.06	-1.41	0.38	-8.74

4.3.3 Mesophilic process simulation with propylene glycol and sludges

This part of the report presents results from three simulations with different combinations of PGW and additional sludges, simulations 7.1, 7.2, 7.3 in Table 3.5 . As well as compares them with VEAS 2019 data points and VEAS simulation.

From Figure 4.36, it can be observed an increase in biogas flow for simulations 7.2 and especially 7.3. However, it looks like 7.1 has a slight decrease in biogas flow compared to the VEAS process.

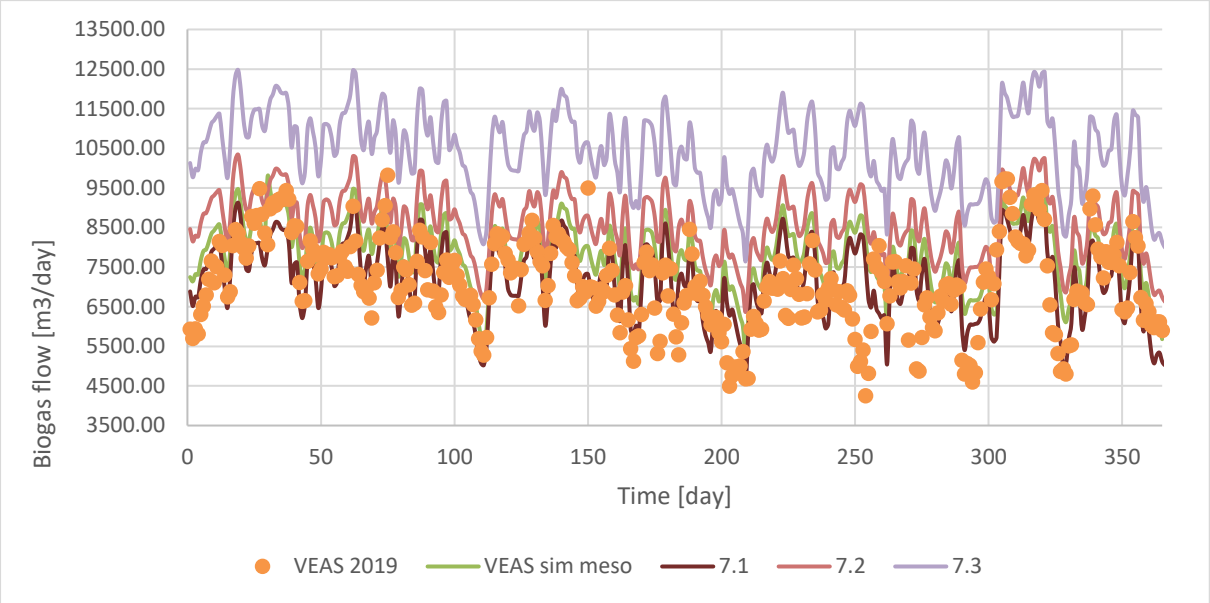

Figure 4.36: Comparison of biogas flow from VEAS 2019 process data and VEAS process simulation to three VEAS simulations with PGW and additional sludges.

When it comes to the simulation results of methane content in Figure 4.37, it is seen that the 7.1 simulation is close to the VEAS simulation, though not as oscillating. Then the simulation 7.2 and 7.3 are almost overlapping each other in results, and they show lower values than the VEAS process simulation.

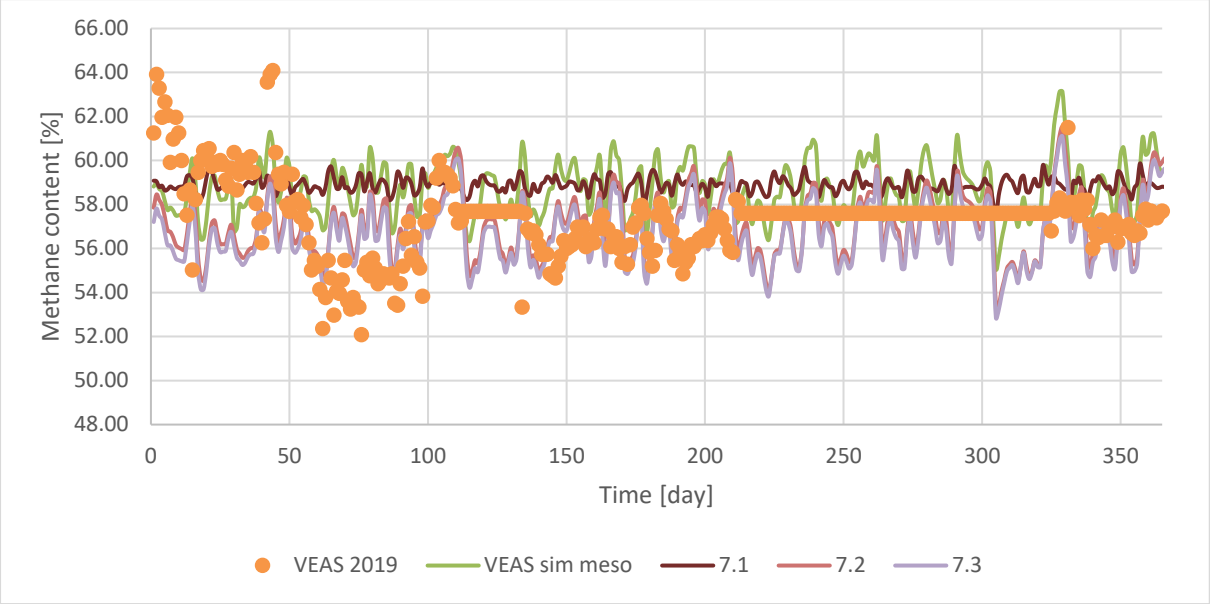

Figure 4.37: Comparison of methane content in biogas from VEAS 2019 process data and VEAS process simulation to three VEAS simulations with PGW and additional sludges.

The pH values in Figure 4.38 go slightly up for simulations 7.1 and 7.2 when comparing to the VEAS process simulation. Simulation 7.3, on the other hand, is showing a slight decrease in pH.

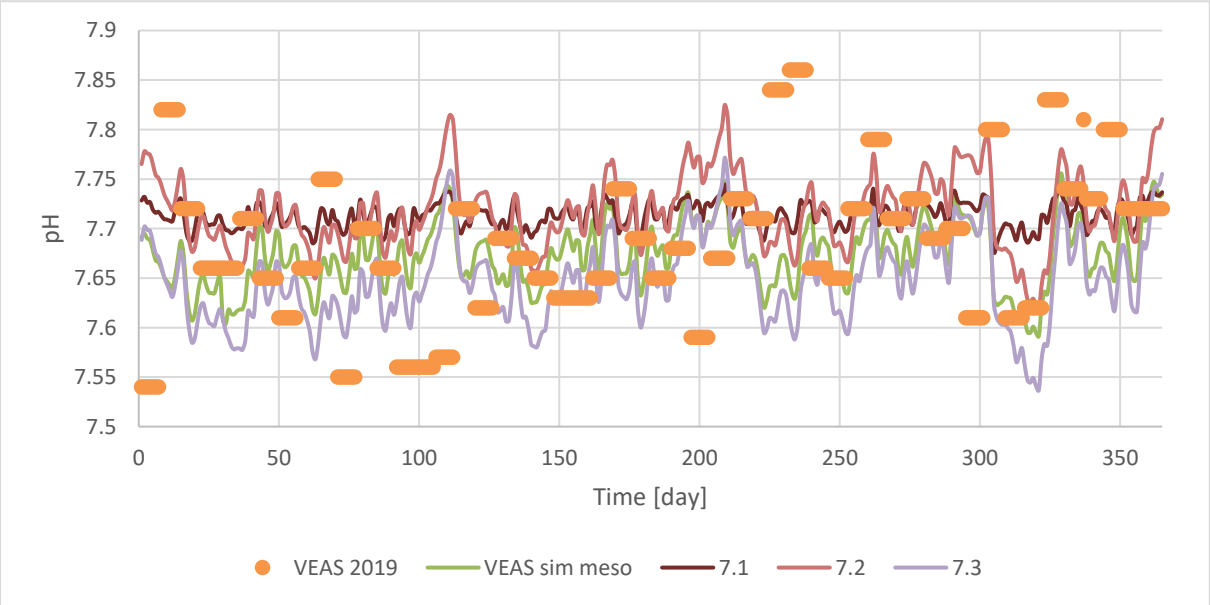

Figure 4.38: Comparison of pH values from VEAS 2019 process data and VEAS process simulation to three VEAS simulations with PGW and additional sludges.

By looking at Figure 4.39, it seems like simulations 7.2 and 7.3 have very high acetate concentrations. The values are way above the VEAS data points value, with some peaks rising above 10 kgCOD/m^3. In contrast, simulation 7.1 is sightly below VEAS simulation values and are not rising higher than 1 kgCOD/m^3.

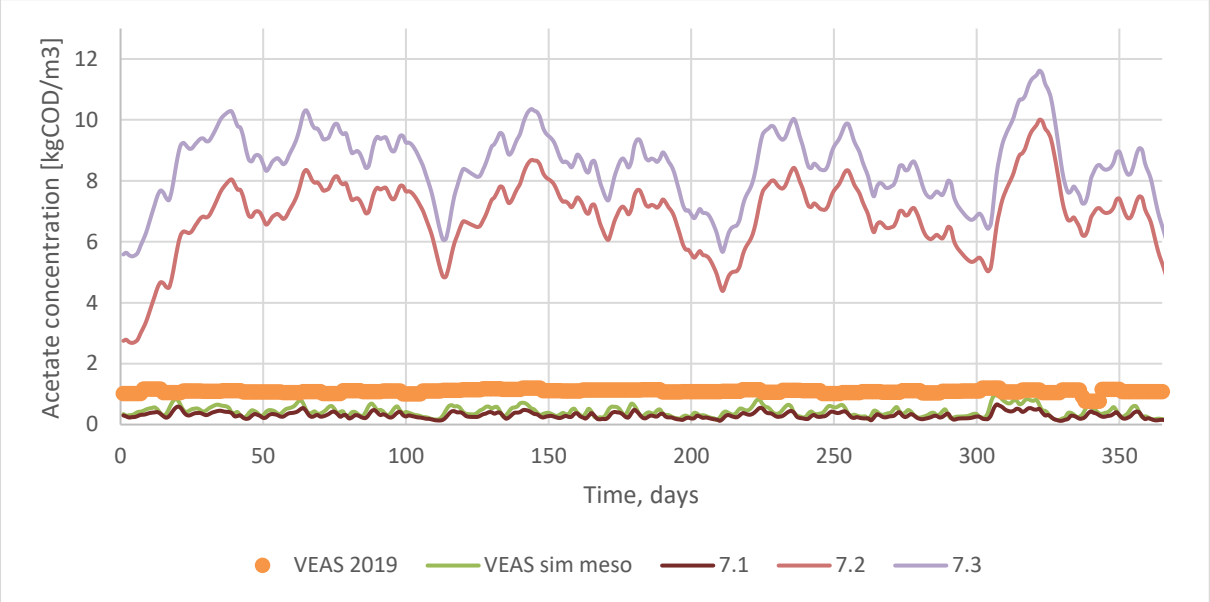

Figure 4.39: Comparison of biogas flow from VEAS 2019 process data and VEAS process simulation to three VEAS simulations with PGW and additional sludges.

The simulated values of IN concentration in Figure 4.40 shows that simulation 7.2 and 7.3 have higher concentrations than the VEAS process simulation values. Simulation 7.1, on the other hand, has IN concentration around 0.14 kmol/m^3 and below VEAS simulation values.

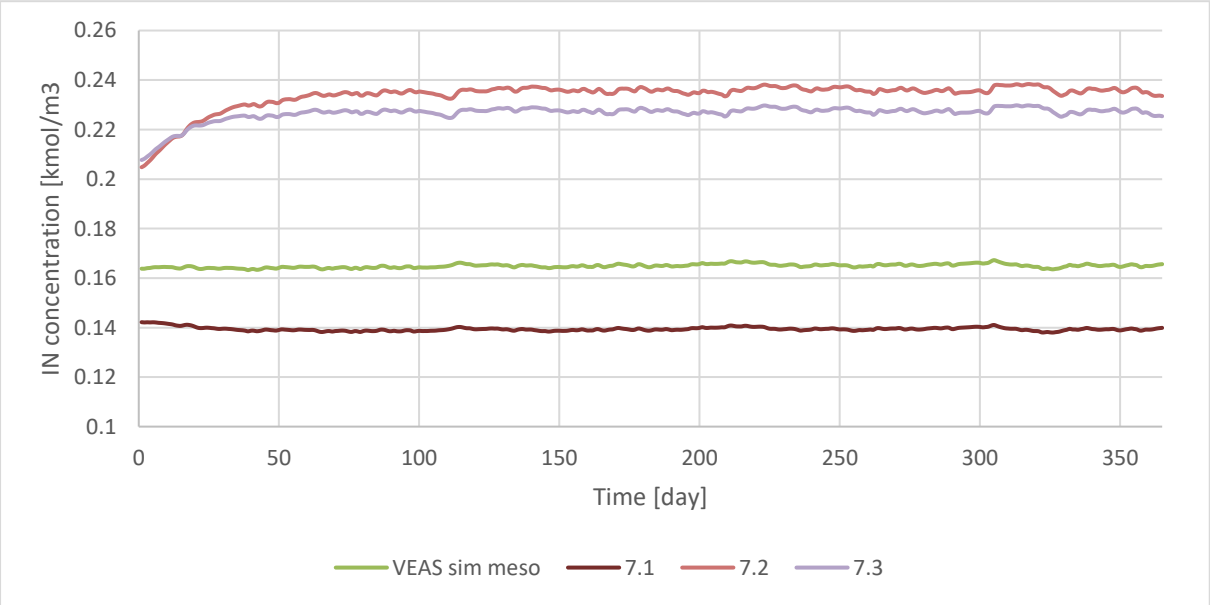

Figure 4.40: Comparison of IN concentration from VEAS 2019 process data and VEAS process simulation to three VEAS simulations with PGW and additional sludges.

When comparing simulated and measured bicarbonate concentration in Figure 4.41, simulation 7.1 has a slightly lower concentration than the VEAS process simulation. Simulations 7.2 and 7.3 have more fluctuating pater than VEAS process simulation, and in addition, 7.2 seems to have the highest values of all simulations. When 7.3, on the other hand, somewhere similar to 7.1 simulation values.

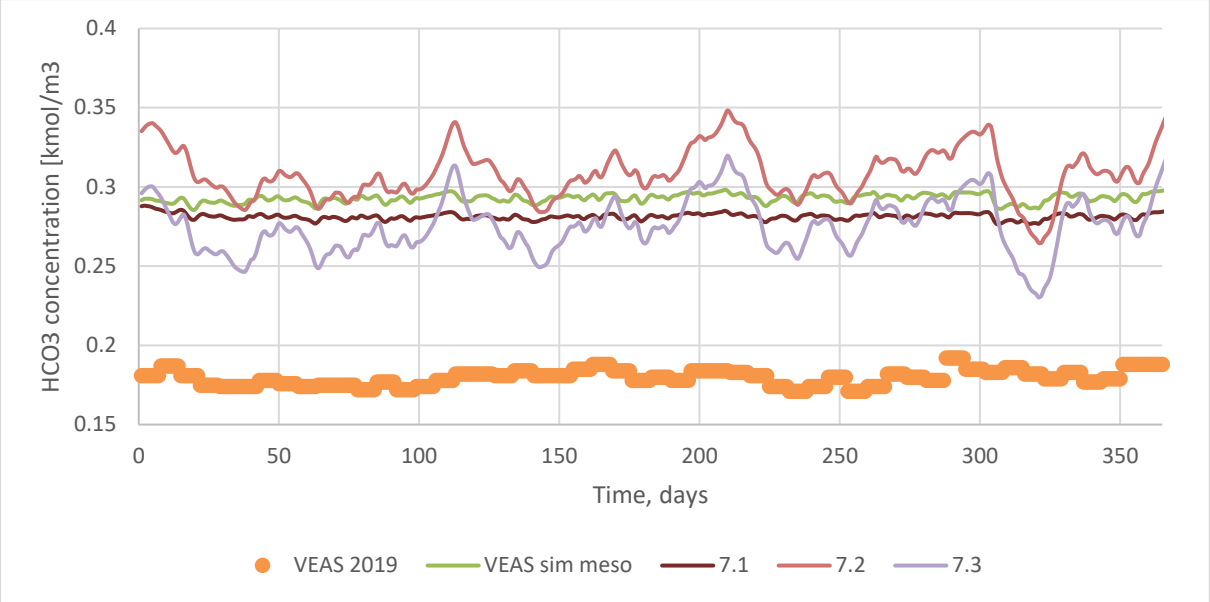

Figure 4.41: Comparison of bicarbonate concentration from VEAS 2019 process data and VEAS process simulation to three VEAS simulations with PGW and additional sludges.

When comparing the relative difference between the VEAS co-digestion simulations and VEAS simulation in Table 4.4, one can see that pH is changing less the 1%. At the same time, acetate has a dramatic increase of more than 1500% for simulations 7.2 and 2.3.

Table 4.4: Comparing some average results values from simulations with PGW and additional sludges against VEAS process simulation. Average values were calculated for the same period of time for all simulations.

Results compared	Relative differences					
	pH [%]	Acetate [%]	HCO3 [%]	NH4 [%]	Methane content [%]	Biogas flow [%]
VEAS sim meso to 7.1	0.53	-28.70	-3.94	-15.57	0.22	-9.27
VEAS sim meso to 7.2	0.61	1511.48	5.55	42.61	-2.88	5.05
VEAS sim meso to 7.3	-0.30	1897.16	-5.75	37.88	-3.49	31.03

4.4 Thermophilic process simulation results

In this work, results from some of the thermophilic simulation are presented, see Table 3.5 in the Results chapter. The results will be shown in the same manner as the results from mesophilic simulations. The chapter compares VEAS data points and the results from the VEAS mesophilic simulation to the results from VEAS thermophilic simulation. After that, three sub-chapters compare some mesophilic and thermophilic simulation results with PWG as co-substrate, additional sludges as co-substrate and a combination of PGW and additional sludges.

Figure 4.42 compares process points from VEAS 2019 process and results from mesophilic and thermophilic simulation for the same process. It is seen from the figure VEAS thermophilic simulation has an increase in biogas production compared to mesophilic simulation.

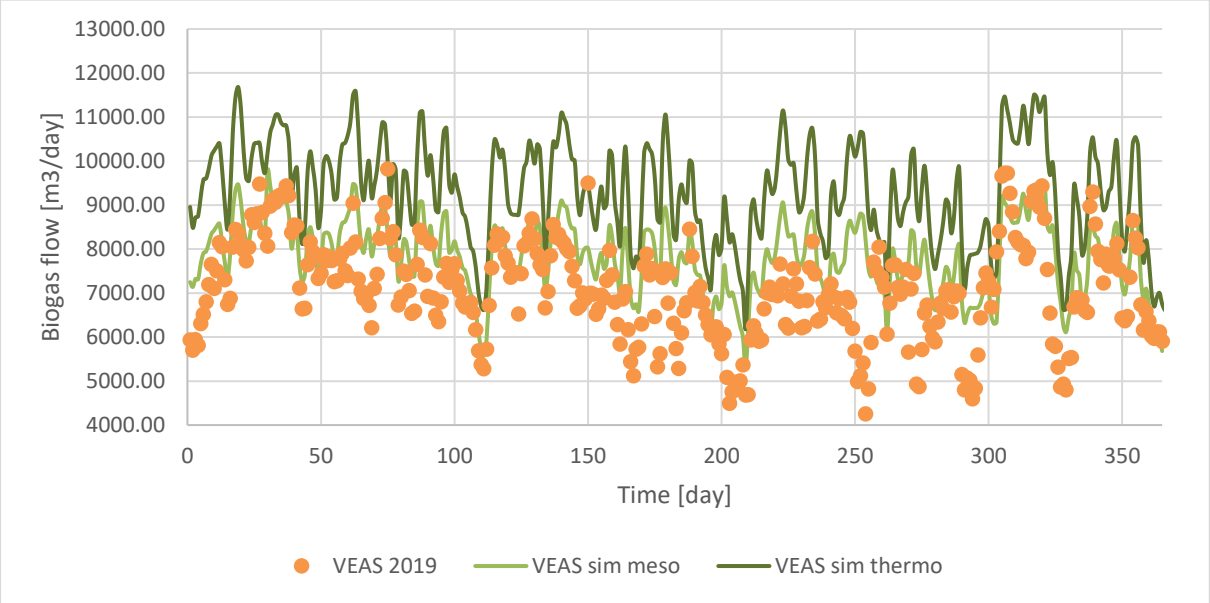

Figure 4.42: Biogas production from VEAS 2019 process data and mesophilic simulation compared to VEAS thermophilic simulation.

Though the biogas production is increased in thermophilic simulation, it is observed from Figure 4.43 that methane content is lower for thermophilic simulation than for mesophilic simulation.

When pH values are compared in Figure 4.44, it is higher for thermophilic simulation than for both VEAS data points and mesophilic simulation.

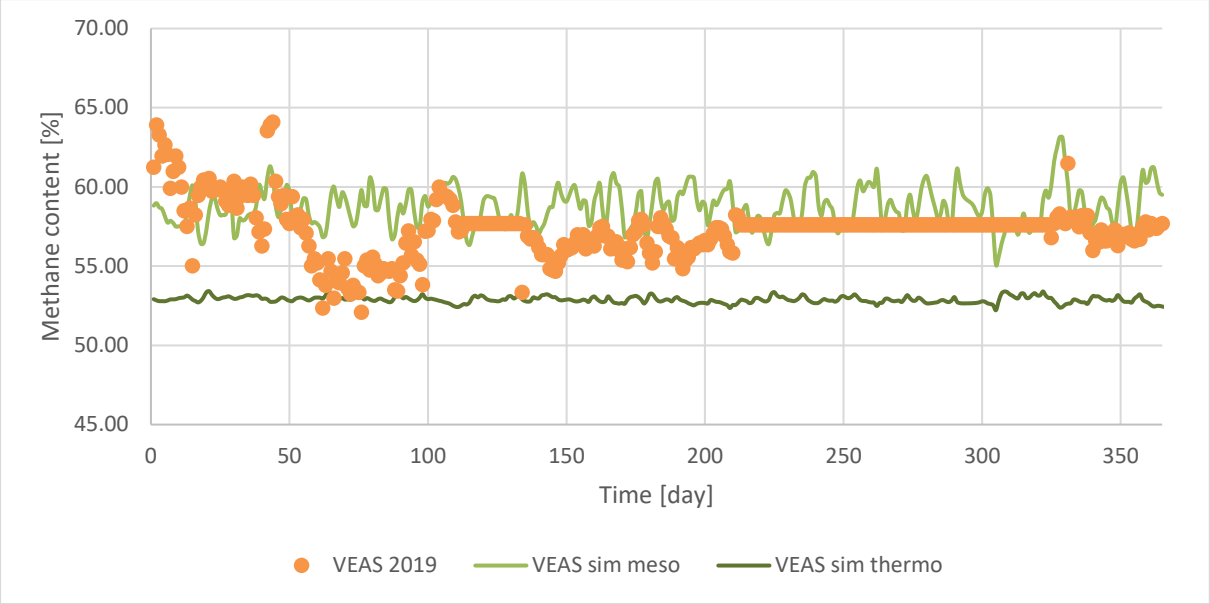

Figure 4.43: Methane content in biogas from VEAS 2019 process data and mesophilic simulation compared to VEAS thermophilic simulation.

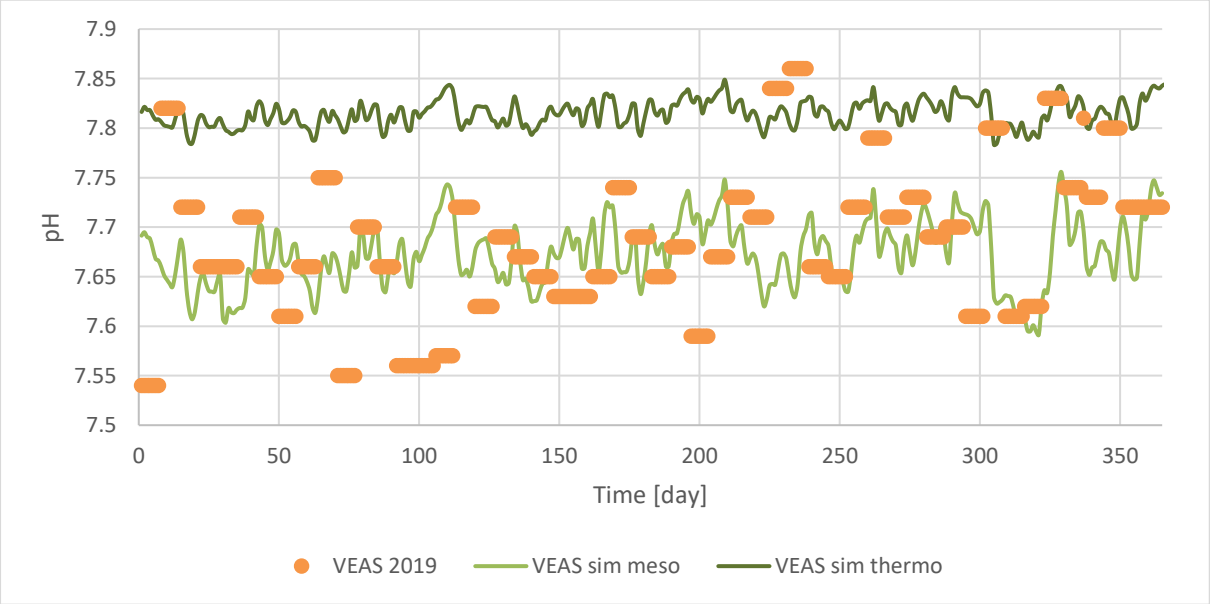

Figure 4.44: pH value from VEAS 2019 process data and mesophilic simulation compared to VEAS thermophilic simulation.

When it comes to simulated acetate concentration for thermophilic case in Figure 4.45, the values are below the 1 kgCOD/m^3. It seems to be even slightly lower than the results from mesophilic simulation. The bicarbonate concentration from the thermophilic simulation is also lower than from mesophilic simulation, see Figure 4.46. though VEAS process data points are still on much lower values.

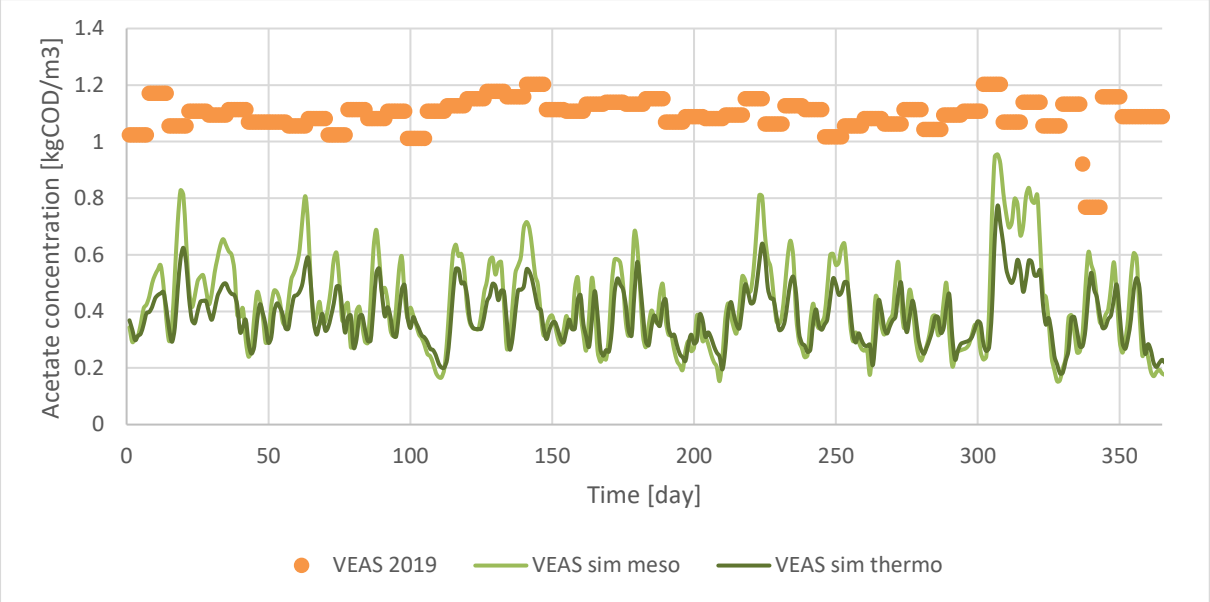

Figure 4.45: Acetate concentration from VEAS 2019 process data and mesophilic simulation compared to VEAS thermophilic simulation.

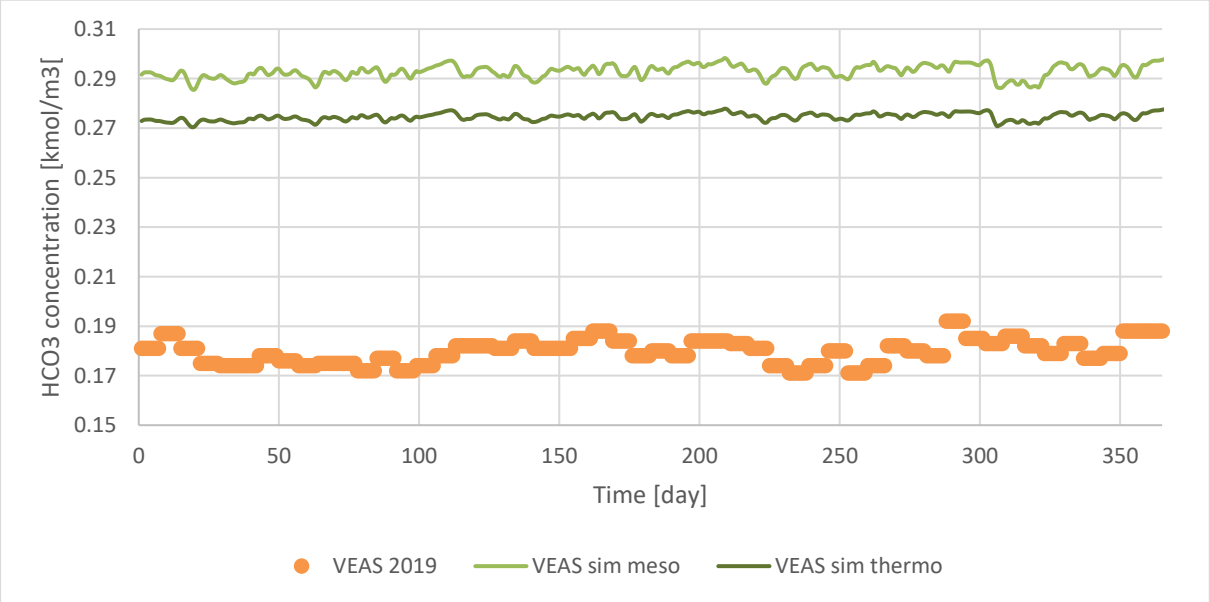

Figure 4.46: Bicarbonate concentration from VEAS 2019 process data and mesophilic simulation compared to VEAS thermophilic simulation.

The simulated IN concentration under the thermophilic and mesophilic conditions are shown in Figure 4.47. Compared to mesophilic condition, the thermophilic simulation shows lower values for the IN concentration, which is around 0.145 - 0.15 kmol/m^3.

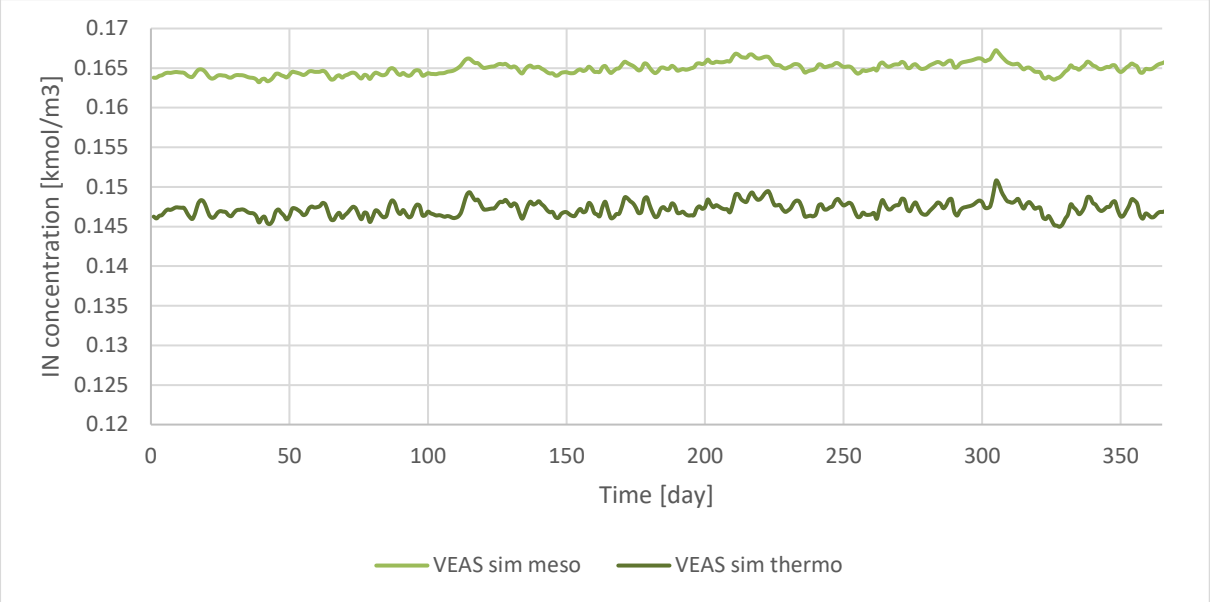

Figure 4.47: IN concentration from VEAS mesophilic simulation compared to VEAS thermophilic simulation.

Table 4.5 summarizes the simulation results, and according to the summary, the average methane flow rate has increased by 14.8% in thermophilic simulation compared to mesophilic. The simulated average methane content drops by 10%. Average pH value rises only by 2%, and average acetate and bicarbonate concentrations drop by 10% and 6%, respectively.

Table 4.5: Comparison of average values for mesophilic and thermophilic VEAS simulations together with the relative difference between them. Average values calculated for the same time period for all simulations.

Results compared	VEAS 2019 simulation mesophilic	VEAS 2019 simulation thermophilic	Relative difference
Biogas flow rate	8016 [m3/day]	9203 [m3/day]	14.8 %
Methane content	58.8%	52.9%	-10%
pH	7.67	7.82	2%
Acetate concentration	0.42 [kgCOD/m3]	0.38 [kgCOD/m3]	-10%
HCO3	0.29 [kmol/m3[	0.27 [kmol/m3[	-6%

4.4.1 Thermophilic process simulation with propylene glycol

This section of the report is presenting results from thermophilic simulation no. 9 summarised in Table 3.5. Simulation 9 is compared to simulation 6.3 as well as VEAS mesophilic and thermophilic.

The simulated results of biogas flow in Figure 4.48 show an increase in simulation 9 results compared to other simulations in the same graph. It also seems that simulation 6.3 has increased gas flow compared to VEAS mesophilic; the same is for simulation 9 and VEAS mesophilic.

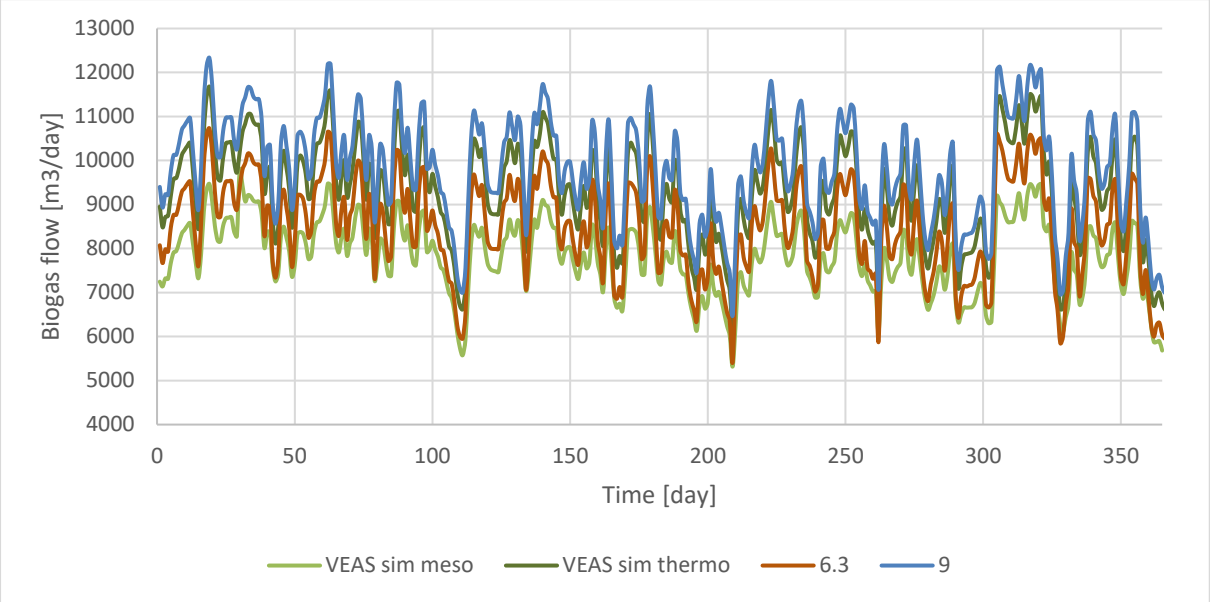

Figure 4.48: Comparison of simulated biogas flow from VEAS mesophilic simulation, mesophilic simulation with PGW (6.3) to VEAS thermophilic simulations and thermophilic simulations with PGW (9).

Figure 4.49 shows simulated values of methane content for four simulations, VEAS mesophilic and thermophilic process simulations and 6.3 mesophilic simulations with PGW and 9 thermophilic simulations with PGW.

According to simulation results, VEAS mesophilic simulation and simulation 6.3 are in approximately the same range, and VEAS thermophilic and simulation 9 have are in lower methane content range. Though simulation 9 has slightly higher values.

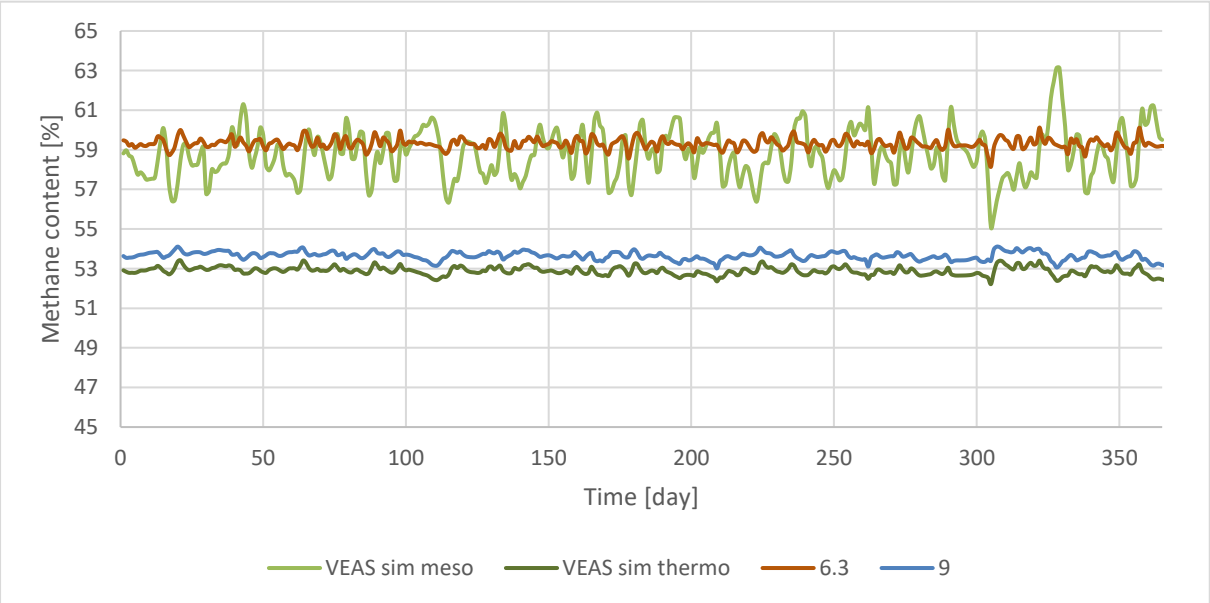

Figure 4.49: Comparison of simulated methane content in biogas from VEAS mesophilic simulation with and without PGW to VEAS thermophilic simulations with and without PGW.

The same is happening in Figure 4.50 for pH. Both mesophilic 6.3 and VEAS are within the same range, while thermophilic, 9, and VEAS thermophilic simulations are within another range. The pH is higher for both thermophilic simulations, where simulation 9 has a slightly

lower pH than VEAS thermophilic simulation. However, the difference is not that significant between all simulations.

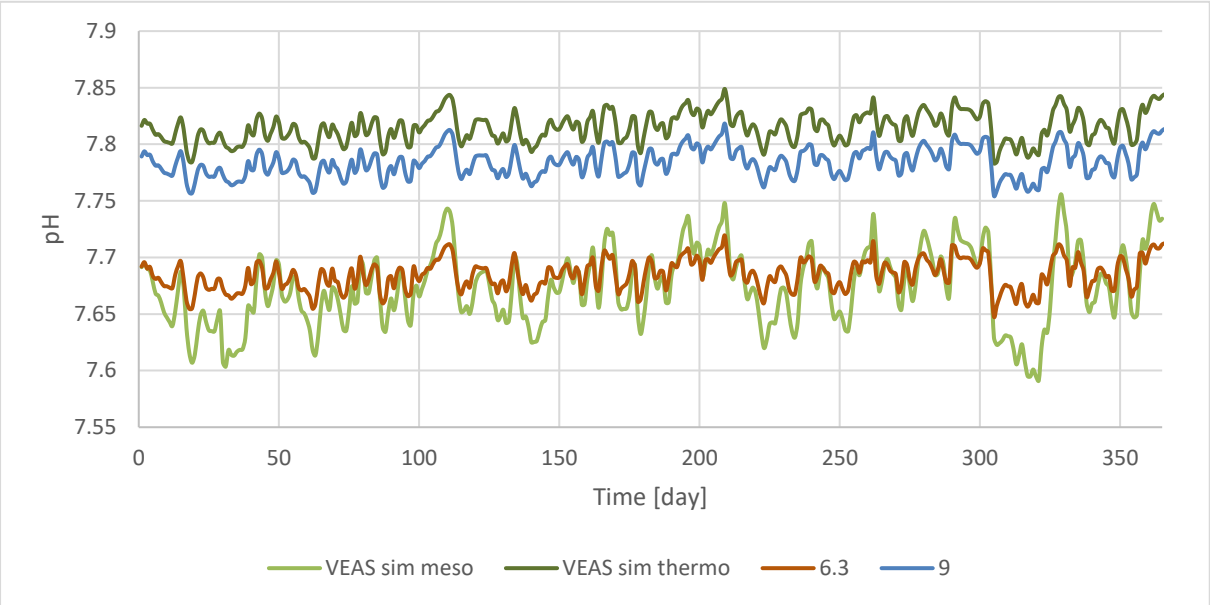

Figure 4.50: Comparison of simulated pH from VEAS mesophilic simulation with and without PGW to VEAS thermophilic simulations with and without PGW.

The simulated acetate concentrations in Figure 4.51 seem to be lower for simulations 6.3 and 9, with PGW added. However, all simulations group together and do not have a big difference between them.

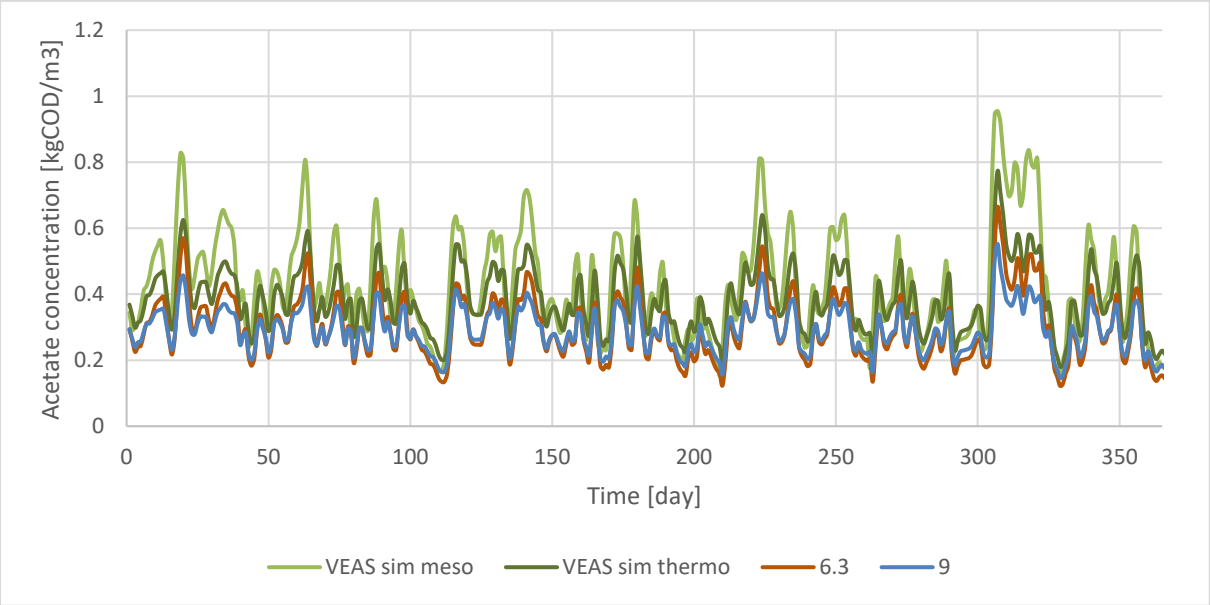

Figure 4.51: Comparison of simulated acetate concentration from VEAS mesophilic simulation with and without PGW to VEAS thermophilic simulations with and without PGW.

As for simulated bicarbonate concentrations in Figure 4.52, simulation 9 has the lowest values for the period comparing to other simulations in the graph. It also can be noticed that 6.3 and 9 simulations with PWG added have lower concentrations than the VEAS mesophilic and thermophilic simulations.

Then Figure 4.53 shows simulated IN concentration. In the figure, IN concentration for VEAS thermophilic simulation and simulation 6.3 are approximately the same. Further, the modelled results from simulation 9 have the lowest values of all four simulations, with VEAS mesophilic having the highest values.

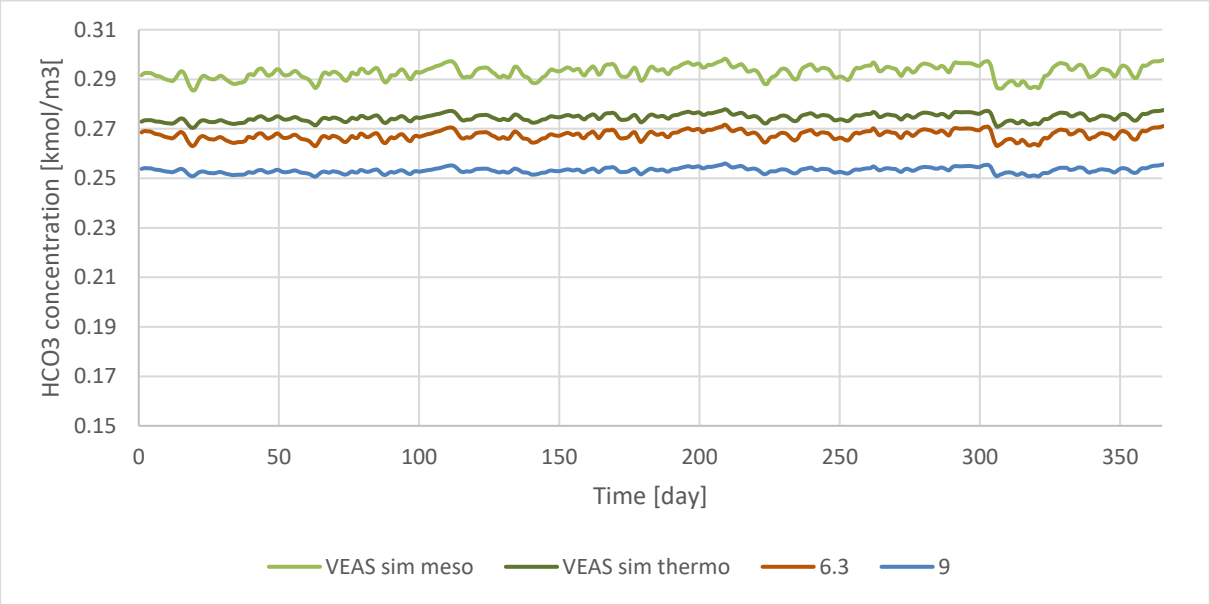

Figure 4.52: Comparison of simulated bicarbonate concentration from VEAS mesophilic simulation with and without PGW to VEAS thermophilic simulations with and without PGW.

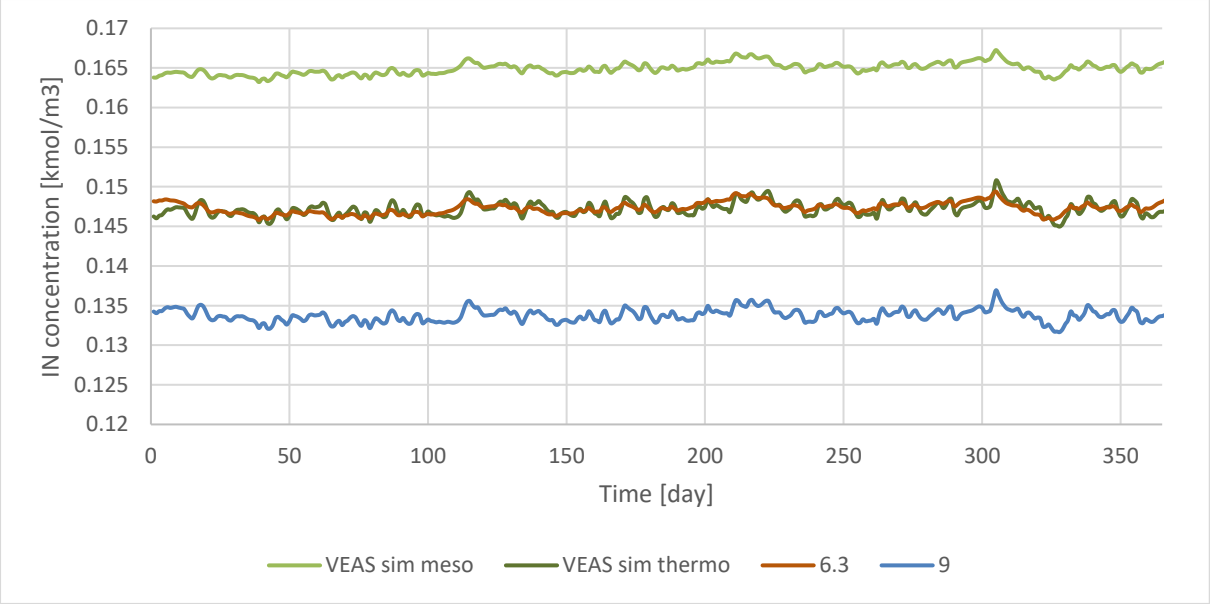

Figure 4.53:Comparison of simulated IN concentration from VEAS mesophilic simulation with and without PGW to VEAS thermophilic simulations with and without PGW.

The relative difference calculated from the average values for this chapter's simulations is compared in Table 4.6. When comparing VEAS thermophilic simulation to simulation 9, one can see the decrease in simulated acetate, bicarbonate and IN concentration. Though the pH has decreased as well, the decrease is below 1%. The increase of average methane content and biogas flow was not very high, 1.5% for methane content and 6.4% for biogas flow. By

comparing simulations 6.3 and 9, the most noticeable difference is in 11.8% increase of average biogas flow. However, the average methane content is decreased by almost 10%.

Table 4.6: Comparing the relative difference between chosen parameters for some simulations. They were calculated from average values for the same time period in simulations.

Simulation compared	Relative differences					
	pH [%]	Acetate [%]	HCO3 [%]	NH4 [%]	Methane content [%]	Biogas flow [%]
VEAS sim thermo to 9	-0.4	-23.8	-7.8	-9.2	1.5	6.4
6.3 to 9	1.3	-1.97	-5.3	-9.2	-9.6	11.8

Since propionate degraders can be inhibited by hydrogen in the PWG degradation pathway, average values of propionate degraders inhibition by hydrogen are presented in Table 4.7 for both mesophilic (6.1, 6.2, 6.3) simulation with PGW and thermophilic (9) simulation with PGW. Propionate degraders show no sign of increasing inhibition by hydrogen, as it can be observed in Table 4.7. The inhibition is the same for the simulated VEAS 2019 mesophilic process and simulations 6.1, 6.2 and 6.3 with increasing PGW ratio. Same for VEAS 2019 thermophilic process simulation and simulation 9, no increase in inhibition is observed.

Table 4.7: Average value for $I_{h2,\,pro}$ (inhibition function) showing inhibition by hydrogen in ADM1 for propionate degraders where 1 is no inhibition 0 is fully inhibited.

Simulation	Average $I_{h2,\,pro}$	Substrates	Substrate ratios
VEAS meso	0.92	SS	-
6.1	0.92	PGW:SS	7.5:192.5
6.2	0.92	PGW:SS	10.8:189.2
6.3	0.92	PGW:SS	14:186
VEAS thermo	0.84	SS	-
9	0.84	PGW:SS	14:186

4.4.2 Thermophilic process simulation with additional sludges

The chapter presents simulated results from thermophilic simulations with additional sludge, simulations 8.1 – 8.4 in Table 3.5. These simulations were compared to VEAS thermophilic simulation and mesophilic simulations 5.1 – 5.4, also described in Table 3.5.

It seems like all simulations with additional sludges predict a decrease in biogas flow compared to VEAS thermophilic simulation, see Figure 4.54. A qualitative comparison of simulations in this chapter presented in Table 4.8.

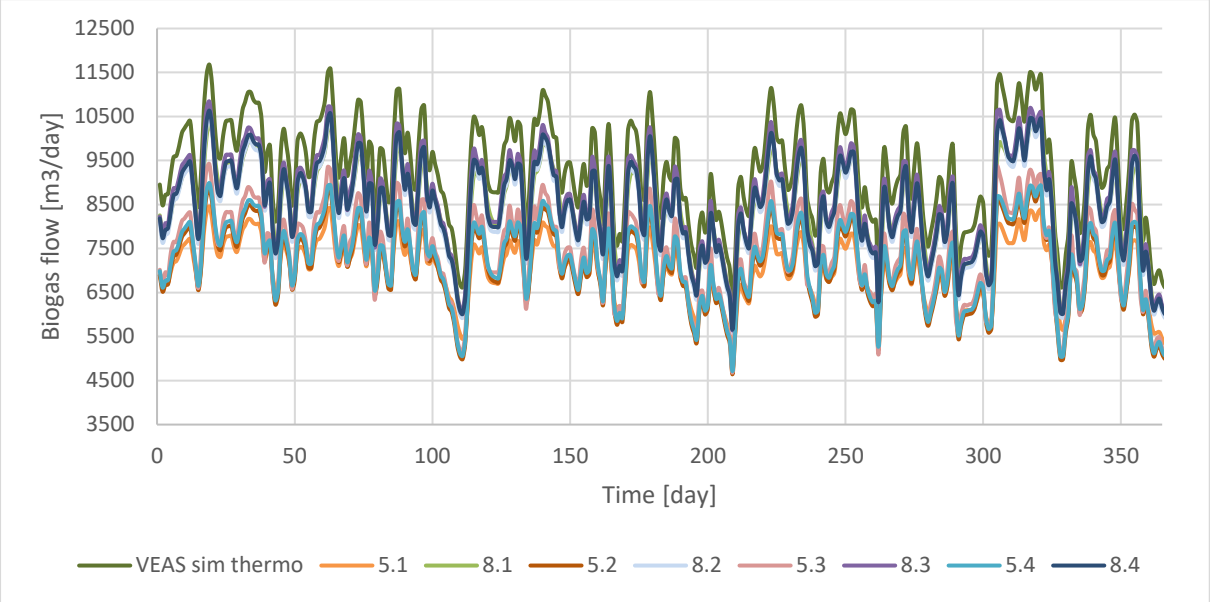

Figure 4.54: Comparison of simulated biogas flow from VEAS thermophilic simulations with and without additional sludge.

Figure 4.55: Comparison of simulated methane content in biogas from VEAS thermophilic simulations with and without additional sludge.Simulated methane content for simulations 5.1-5.4 is clustered in the 61-56% range, but 8.1-8.4 simulations clustered in the lower range – 54 to 51% methane, see Figure 4.55. Additionally, simulations 8.1, 8.2 and 8.4 are in the 54 – 53% range, and 8.3 is in the 52% range.

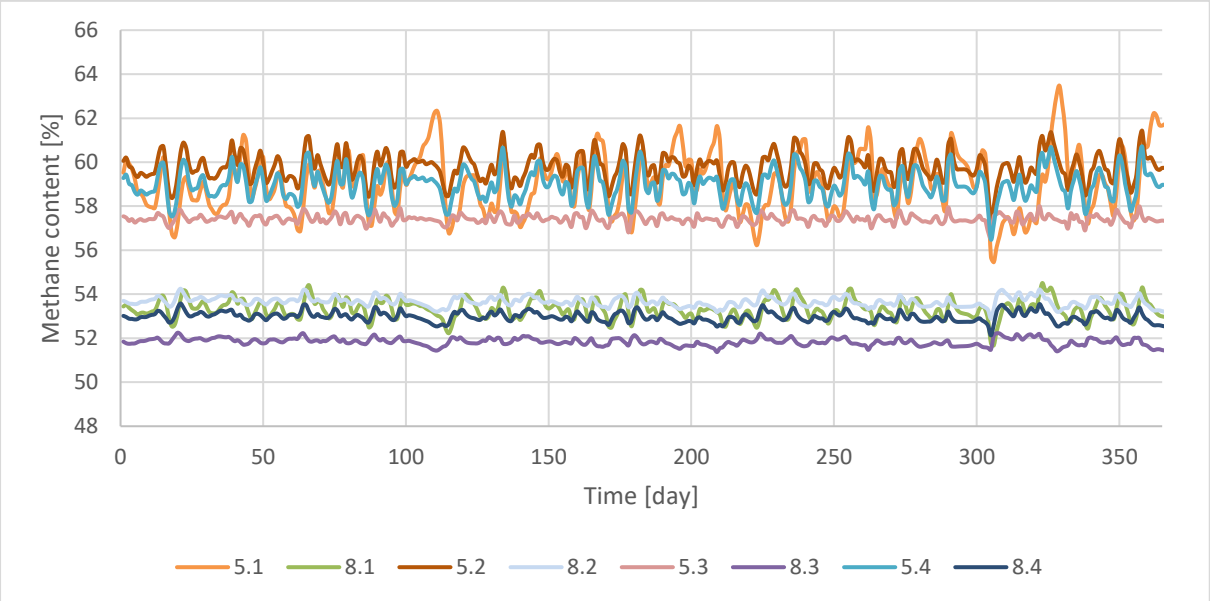

Figure 4.55: Comparison of simulated methane content in biogas from VEAS thermophilic simulations with and without additional sludge.

According to Figure 4.56, it is observed very high simulate acetate concentration for simulation 5.1 as it was also shown in chapter 4.3.2. However, simulated acetate concentration for the same simulation parameters only in thermophilic temperature range, 8.1, is in a much lower range. Though it still peaks over 1 kgCOD/m^3; and the rest of the simulations are below.

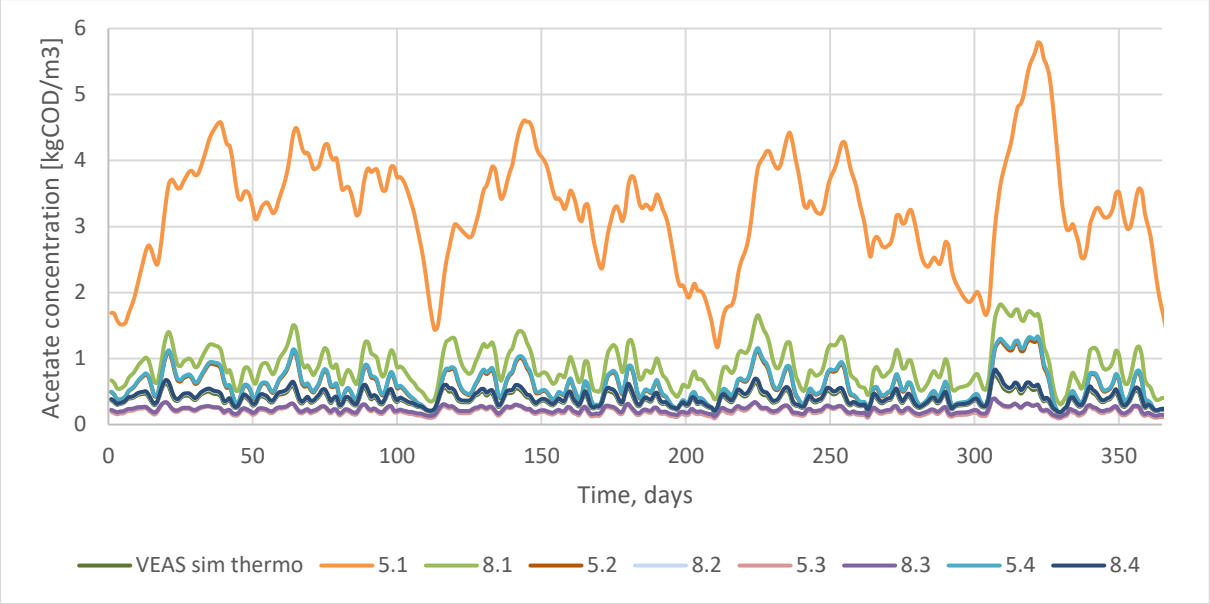

Figure 4.56: Comparison of simulated acetate concentration from VEAS thermophilic simulations with and without additional sludge.

Simulated bicarbonate concentration for all simulations in Figure 4.57 is in the range between 0.25 and 0.32. The lowest values are for simulation 8.3, followed by the 5.3 simulation. The 8.4 simulation is in a slightly higher range, above the VEAS thermophilic simulation. Then above that comes 8.2, and 8.1 is overlapping with 5.2 in 0.3 to 0.32 range.

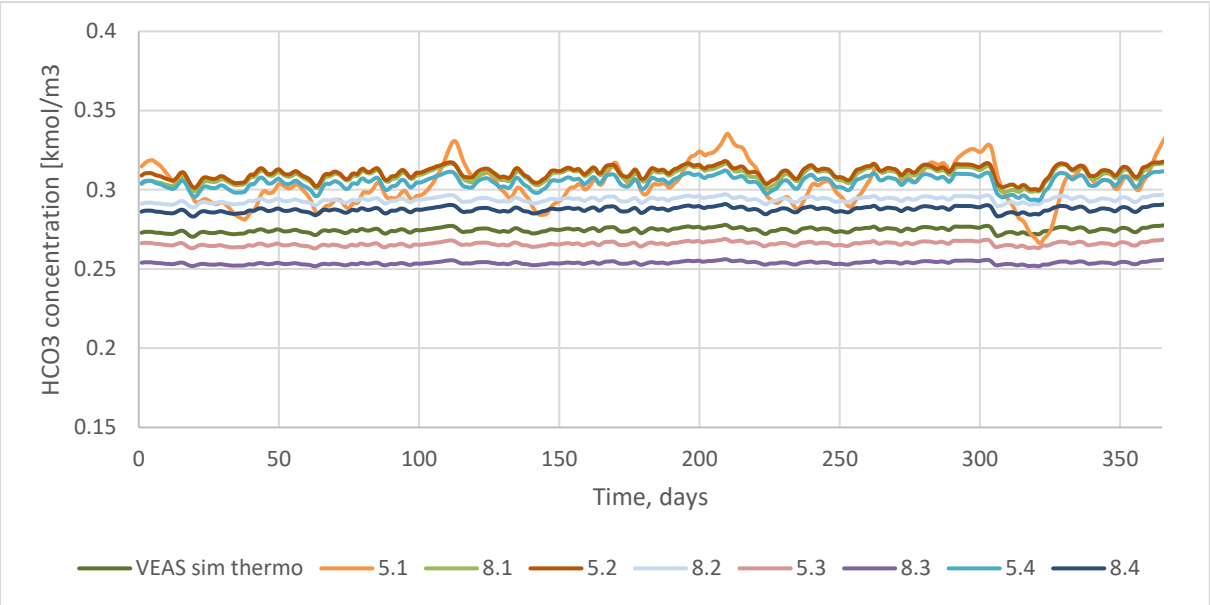

Figure 4.57: Comparison of simulated bicarbonate concentration from VEAS thermophilic simulations with and without additional sludge.

The simulated pH values in Figure 4.58 can be divided into three groups of ranges. The 7.9-7-8 pH range with simulations 8.1, 8.2, 8.4 and VEAS thermophilic, followed by pH range between 7.8 and 7.7 with simulations 8.3, 5.2, 5.4 and 5.1. However, the 5.1 simulation is fluctuating more than the others. Then the last pH range is between 7.7 and 7.65 with simulation 5.3.

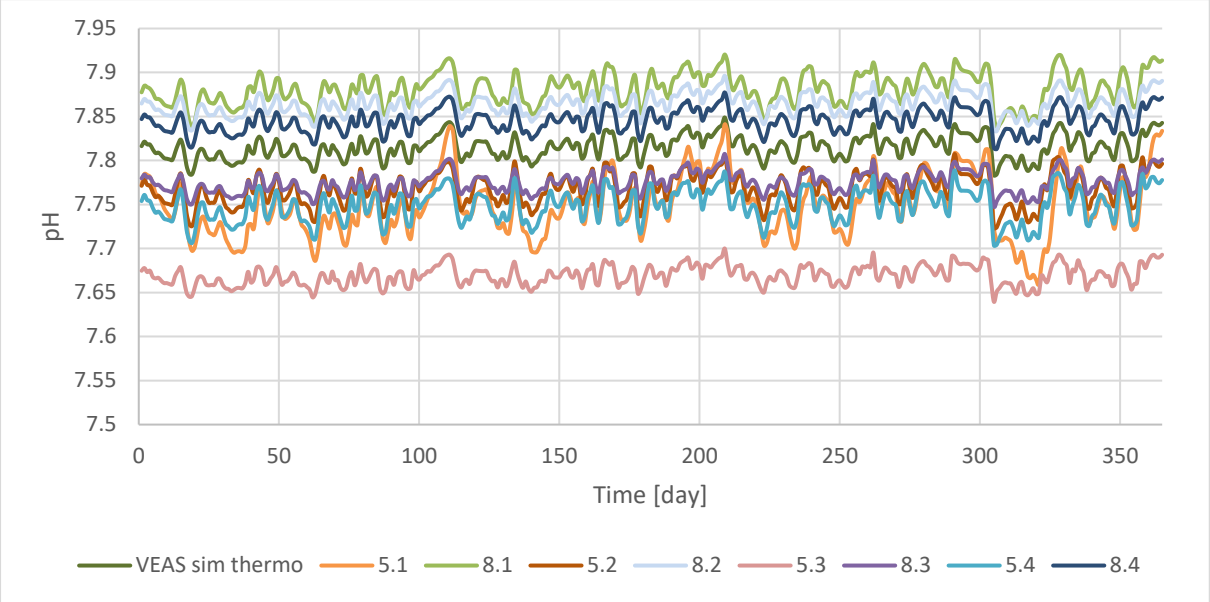

Figure 4.58: Comparison of simulated pH from VEAS thermophilic simulations with and without additional sludge.

By looking at Figure 4.59, all simulations seem to spread in the range between 0.21 and 0.11 kmol/m^3 with VEAS thermophilic almost in the middle. The simulations 8.4, 8.2, 5.3 and 8.3 are below VEAS simulation, and simulations 5.2, 5.4, 8.1 and 5.1 are over VEAS simulation.

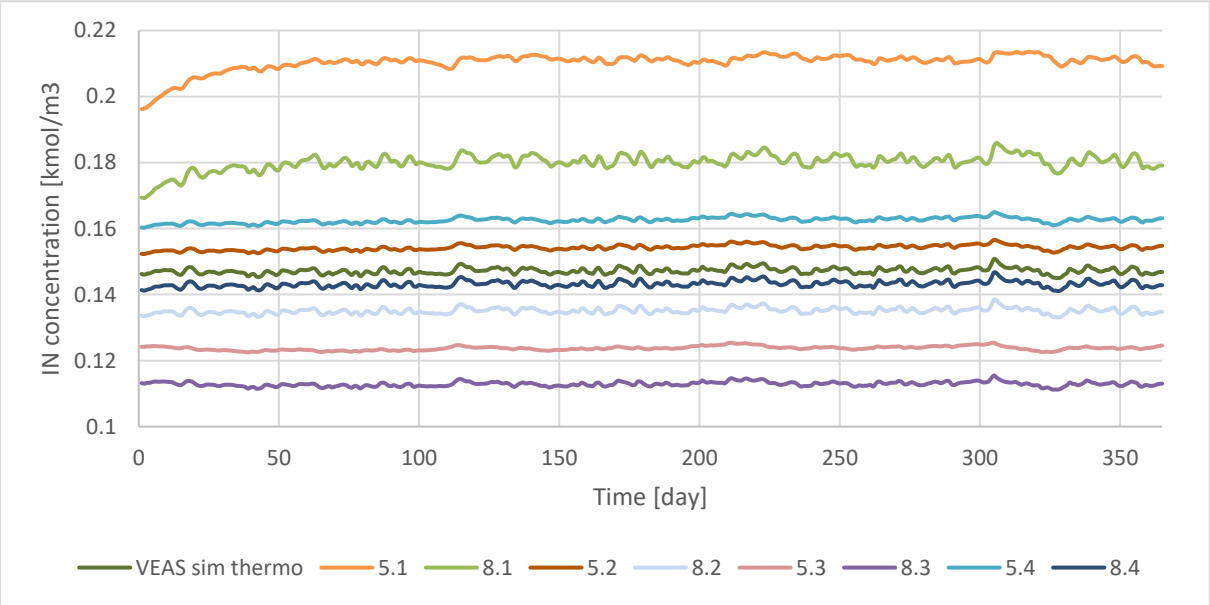

Figure 4.59: Comparison of simulated biogas flow from VEAS thermophilic simulations with and without additional sludge.

In Table 4.8 comparison of average values for simulations are presented. Relative differences were calculated for parameters: pH, acetate, bicarbonate and NH4 concentrations, methane concentrations, and biogas flow. Simulations were compared in pairs where the only difference between compared simulations is temperature.

When comparing the 5.1 simulation to 8.1 in Table 4.8, biogas flow is increased by 16% in 8.1. Furthermore, most noticeably, acetate concentration decreased by 72%. By comparing

simulations 5.2 and 8.2 most visible difference was acetate decrease by 31% and increase in biogas flow by 13%. Also, the comparison shows reductions in NH4 concentration and methane content by 12% and 10%, respectively. Simulations 8.3 and 8.4 had very close changes to the 8.2 simulation with the respective comparisons, except for 8.3 for acetate concentration which raised instead by 13%.

Table 4.8: Chosen simulations compared by relative difference. Calculation of difference based on the average value taken for the same period for all simulations.

Simulations compared	Relative differences					
	pH [%]	Acetate [%]	HCO3 [%]	IN [%]	Methane content [%]	Biogas flow [%]
5.1 to 8.1	1.7	-72.4	1.7	-14.4	-9	16
5.2 to 8.2	1.3	-31	-5.5	-12.4	-10	13
5.3 to 8.3	1.4	13	-4.6	-8.8	-10	12
5.4 to 8.4	1.3	-31	-5.7	-11.9	-10	11

4.4.3 Thermophilic process simulation with propylene glycol and sludges

The subchapter will present results from two VEAS thermophilic simulations with both PGW and additional sludges as co-substrates. The simulation parameters were shown before in Table 3.5 for simulation numbers 10.1 and 10.2. These two simulations are compared to simulations 7.1 and 7.3. The difference between simulation 10.1 and 7.1 and 10.2 and 7.3 is operating temperature. For 10.1 and 10.2, it is thermophilic, and 7.1 and 7.3, it is mesophilic.

When comparing biogas flow in Figure 4.60 from simulations 10.1 and 10.2, one can see that they have higher simulated biogas flow than their respective comparison. When 10.2 has the most increased simulated biogas flow.

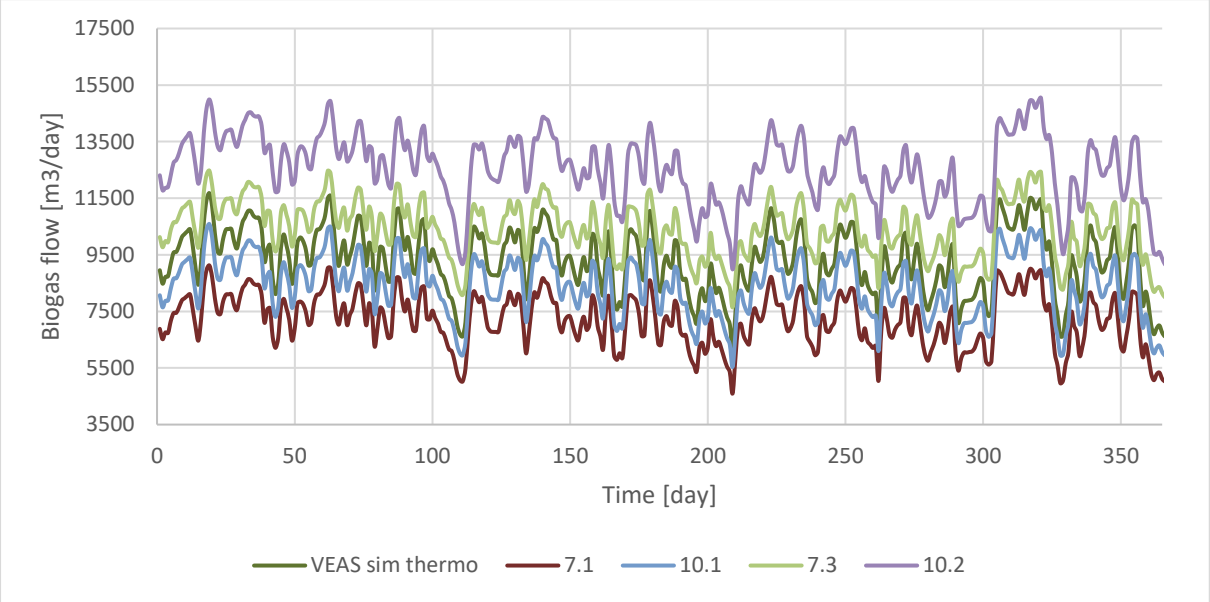

Figure 4.60: Comparison of simulated biogas flow from VEAS thermophilic and mesophilic simulations with PWG and additional sludges.

As for simulated methane content in Figure 4.61, simulation 10.1 is in the same value region as 10.2, only less oscillating. Also, the 10.1 and 10.2 simulations show lower values than 7.1 and 7.3.

In Figure 4.62, with simulation results for acetate concentration, it can be observed that simulation 10.1 is overlapping with simulation 7.1 and do not exceed the concentration of 1 kgCOD/m^3. But when looking at simulation results from 10.2, one can observe that it reaches values up to 4 kgCOD/m^3. Though it is much lower than values for 7.3(substrate ratio 200:14:14:14:14) wich has a maximum value of 11.5 kgCOD/m^3.

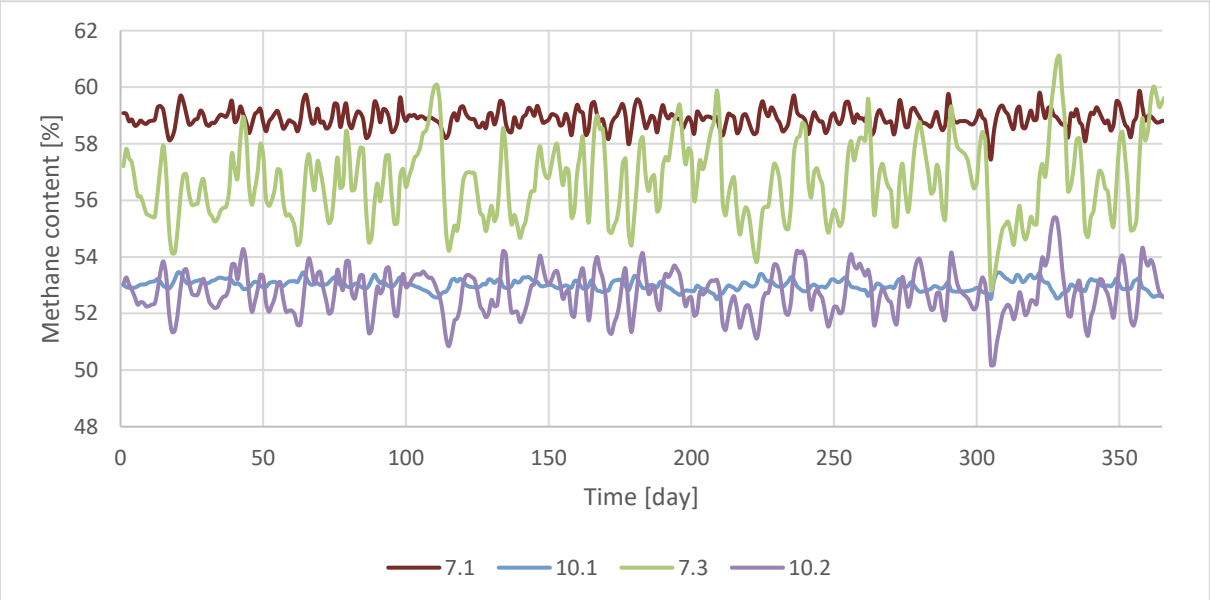

Figure 4.61: Comparison of simulated methane content in biogas from VEAS thermophilic and mesophilic simulations with PWG and additional sludges.

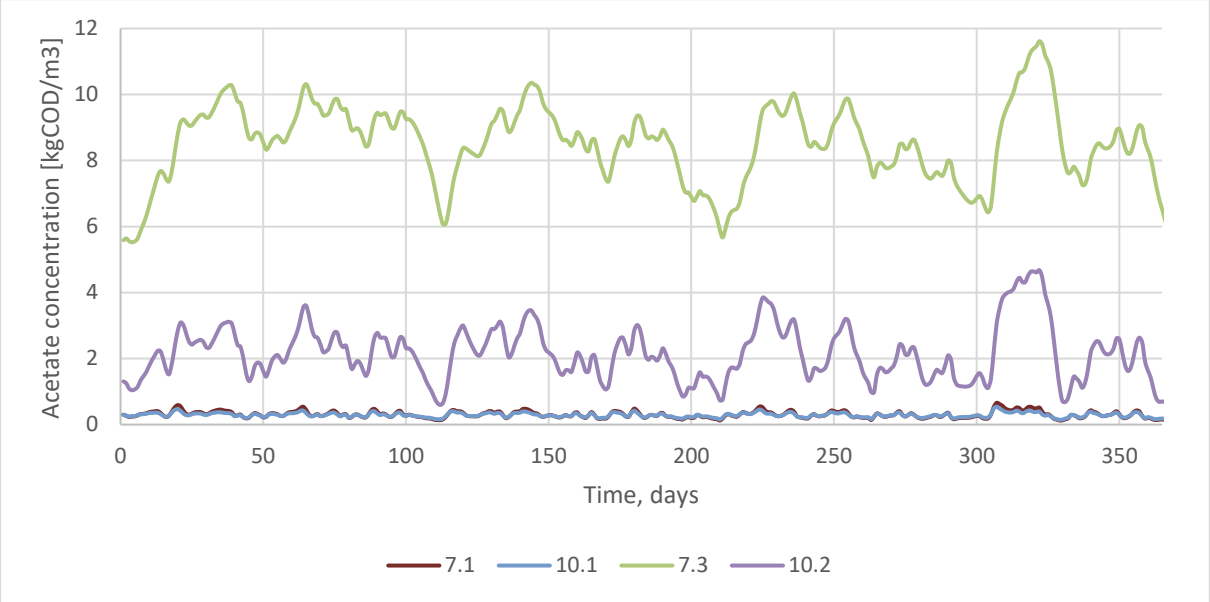

Figure 4.62: Comparison of simulated acetate concentration from VEAS thermophilic and mesophilic simulations with PWG and additional sludges.

In Figure 4.63, simulation results for bicarbonate concentration are presented. The figure shows that simulation 10.2 and 7.3 show very similar pattern, and simulation 10.2 suggests higher bicarbonate concentration in thermophilic temperature. However, simulations 10.1 and 7.1 show a different pattern, where simulation 10.1 with mesophilic temperature has lower simulated concentrations than 7.1.

In the case with simulated IN concentration in Figure 4.64, both simulation 10.1 and 10.2 show decreased concentration compared to 7.1 and 7.3, respectively.

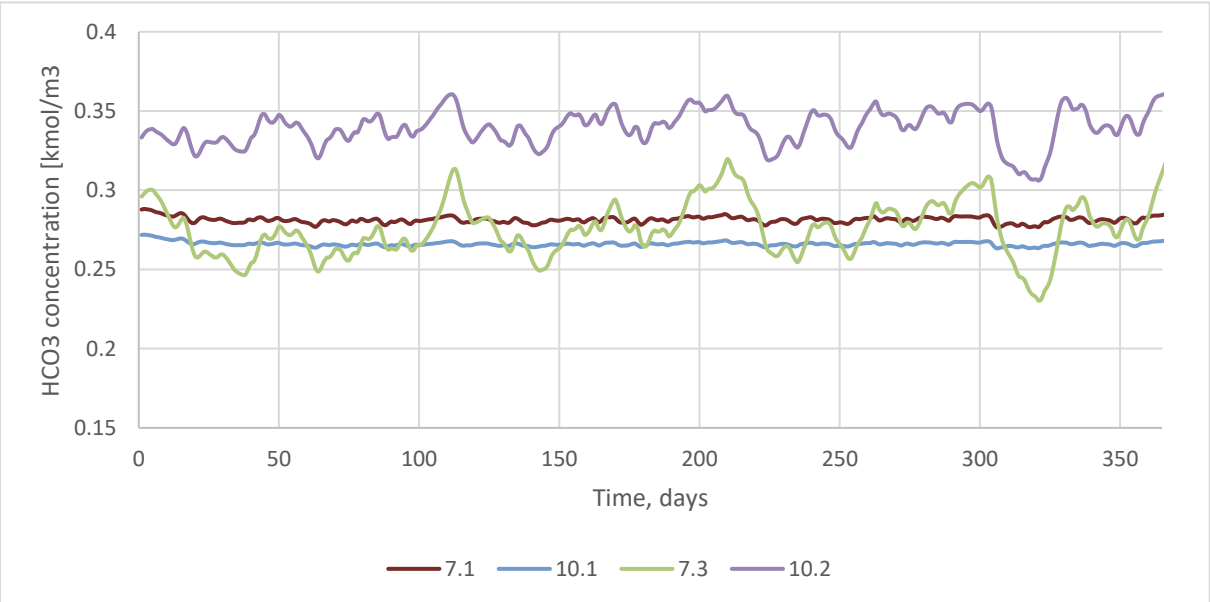

Figure 4.63: Comparison of simulated bicarbonate concentration from VEAS thermophilic and mesophilic simulations with added PWG and additional sludges.

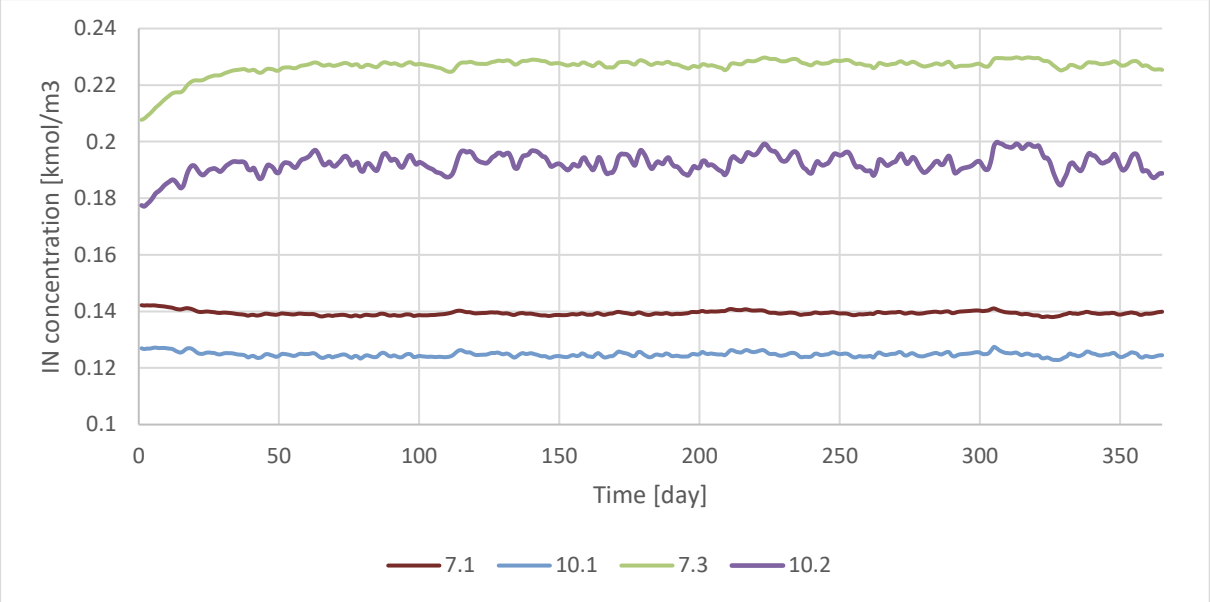

Figure 4.64: Comparison of simulated IN concentration from VEAS thermophilic and mesophilic simulations with added PWG and additional sludges.

Figure 4.65 shows the simulated pH value for the chosen cases. It seems like simulations 10.1 and 10.2 with thermophilic operating temperature predict higher pH values than 7.1 and 7.3.

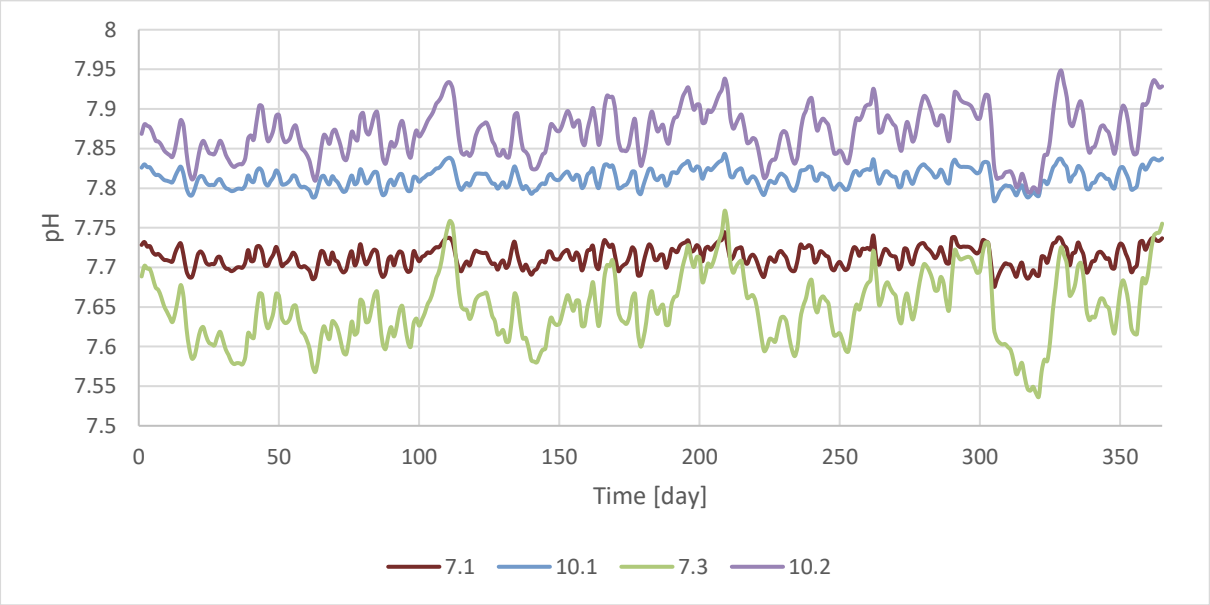

Figure 4.65: Comparison of simulated pH from VEAS thermophilic and mesophilic simulations with added PWG and additional sludges.

Table 4.9 compares the relative difference for some parameters between simulation pairs. When comparing simulation 10.1 to 7.1, one can observe biogas flow increased by 12% and a drop in methane content by 10%.

By comparing 10.2 to 7.3, the most noticeable is a drop in average acetate concentration by 74.8% and an increase in average biogas flow by 25%.

Table 4.9: Comparison of relative difference for the chosen simulations. Difference calculated from the average values for the same period for 7.1, 7.3, 10.1 and 10.2.

Simulations compared	Relative differences					
	pH [%]	Acetate [%]	HCO3 [%]	NH4 [%]	Methane content [%]	Biogas flow
7.1 to 10.1	1.3	-4.6	-5.4	-10.5	-10	12
7.3 to 10.2	2.9	-74.8	23	-15	-7	25

4.5 Methane yield and production

This chapter will present a methane yield from both VEAS 2019 process data and predicted by simulations done in this thesis. Furthermore, simulated methane production and calculated methane production From VEAS process data will be compared.

Figure 4.66 supports the results from chapter 4.3 that VEAS process simulation is not accurately predicting VEAS 2019 process data. When comparing the methane yield between VEAS 2019 and VEAS mesophilic simulation, simulation has a higher yield. By comparing yield from different simulations to VEAS mesophilic simulation, some simulations show higher yield and some lower. Simulations with PGW, 6.1-6.3 and 9, both mesophilic and thermophilic condition, show a higher yield than VEAS mesophilic simulation. Mesophilic simulations 5.1 – 5.4 with additional sludges show either decrease or equal yield as VEAS mesophilic simulation, though this is not the case for the same thermophilic simulations. They seem to increase in yield except for 8.4, which is equal in methane yield with VEAS mesophilic simulation. Though when compared to VEAS thermophilic simulation, the yield is lower for simulations 8.1 – 8.4. The lowest simulated yield compared to VEAS mesophilic simulation, which is corresponding to simulations 7.1 and 10.1. The highest yield is for simulation 10.2 at the value of 0.307 $m^3CH_4/kgCOD$.

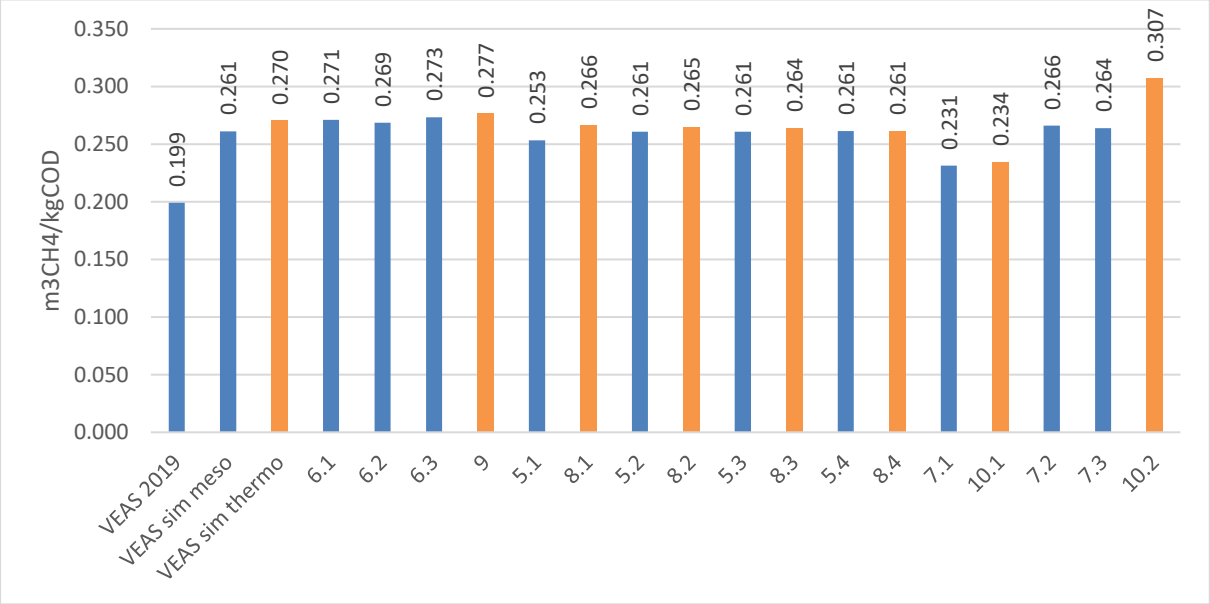

Figure 4.66: Methane yield for VEAS 2019 process and all simulations (blue mesophilic process, orange thermophilic).

A comparison of calculated methane production per year is presented in Figure 4.67, from VEAS process data and simulated data. Again, VEAS mesophilic simulation is overpredicting methane production compared to VEAS 2019 data. What can be noticed also is that VEAS thermophilic simulation, simulations 6.1 – 6.3, 9, 7.3 and 10.2 give higher methane production than VEAS mesophilic simulation. When simulations 5.1 – 5.4, 8.1 – 8.4, 7.1 – 7.2 and 10.1 predict methane production lower than VEAS mesophilic simulation.

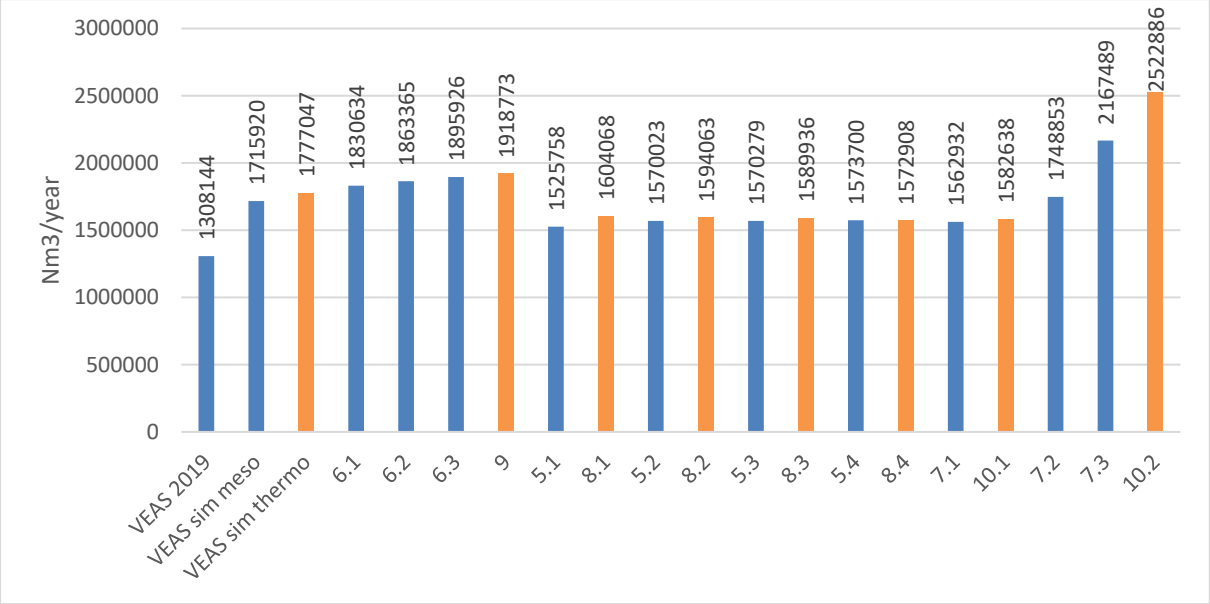

Figure 4.67: Volume of methane (STP) produced per year by VEAS in 2019 and simulated production for all simulations (blue mesophilic process, orange thermophilic).

When calculating potential energy from methane in Figure 4.68, it is evident that not all simulations predict an increase in energy production when compared to the VEAS mesophilic simulation. Unsurprisingly, the same result is observed in Figure 4.68 as it was in Figure 4.67.

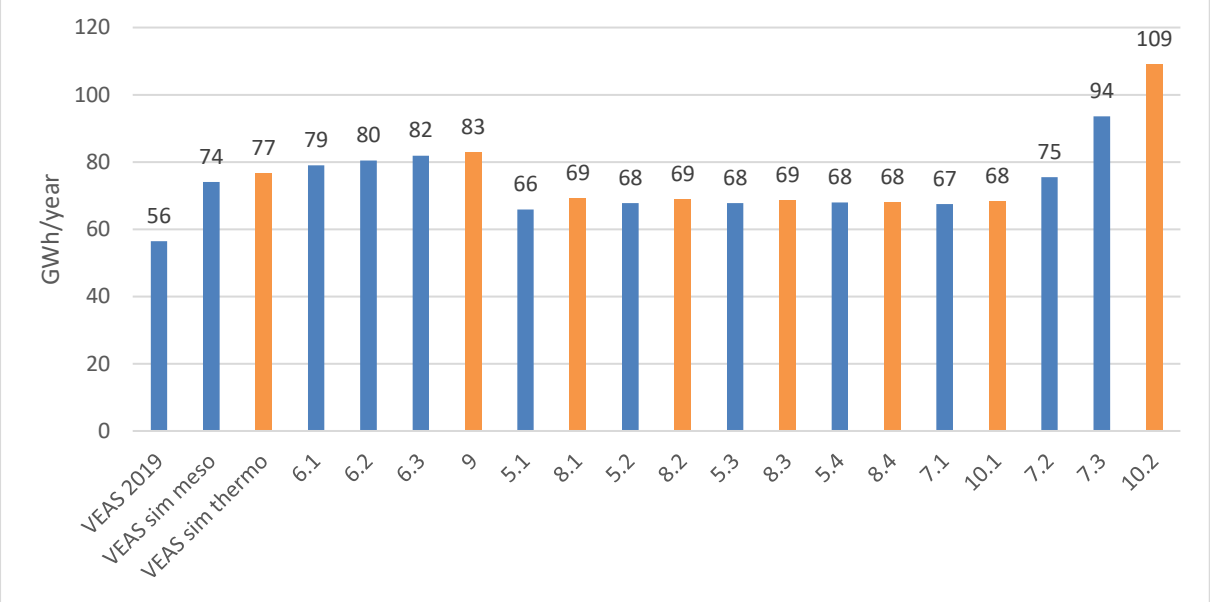

Figure 4.68: Potential energy production from methane for VEAS 2019 and all simulations (blue mesophilic process, orange thermophilic).

Figure 4.69 presents the relative difference in potential energy production of all simulation compared to VEAS mesophilic simulation, which is based on VEAS present operating scenario of the plant. This result may help better understand how much the changes in simulations can theoretically influence energy production.

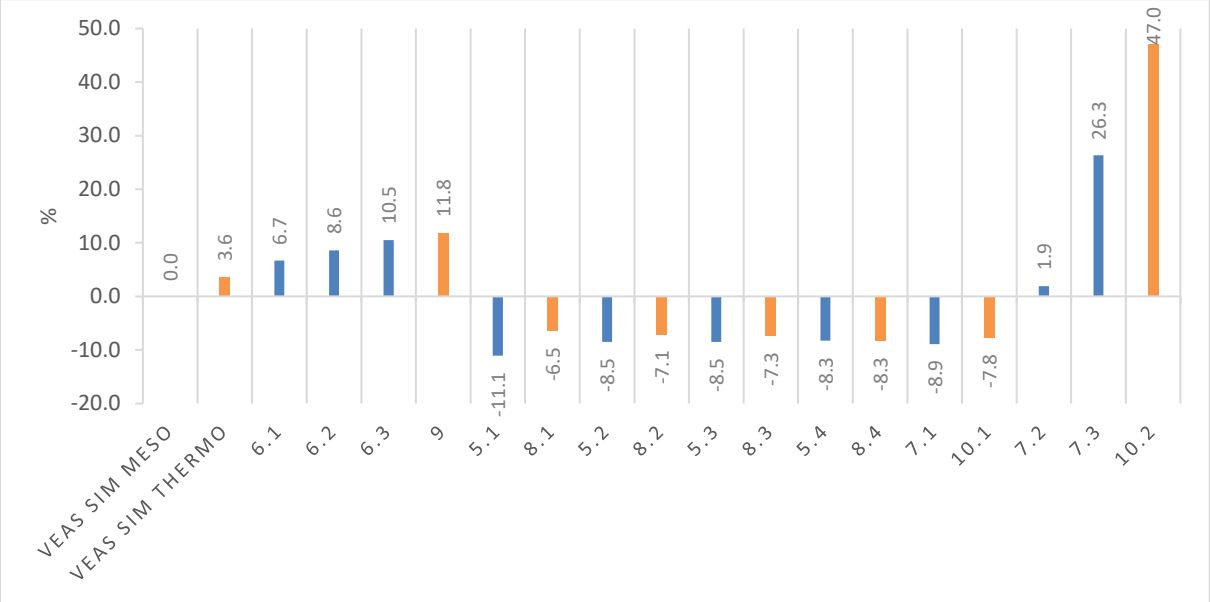

Figure 4.69: Difference in simulated potential energy from methane compared to VEAS mesophilic simulation (blue mesophilic process, orange thermophilic).

5 Discussion

5.1 Temperature transition models

Models ADM1_FTnew and ADM1_CTM1 were validated and tested, and results were presented in chapters 4.1 and 4.2. As was mentioned in chapter 3, the two models were validated against experimental results from two research works ([22] and [24]). Then the models were tested against each other with two different cases summarised in Table 3.5, and results presented in the 4.2 chapter. The results will be discussed in this chapter, and model ADM1_FTnew will be discussed first, then model ADM1_CTM1.

5.1.1 Performance of ADM1_FTnew model

The ADM1_FTnew model was validated via simulating the laboratory-scale experiment presented in [34], [41] and summarized in Table 3.5. The results from simulation, in chapter 4.1.1, were compared to experimental data from the laboratory-scale experiment and showed a generally good match. As shown in Figure 4.1, simulated biogas production had a good fit with the experimental data points. The original model from the research work with the same temperature function implemented showed a better fit to the experimental data. This difference can be explained by the fact that not all parameters were implemented in ADM1_FTne from the research work. One of the biggest differences was leaving the hydrolysis step as it was in the original ADM1. There was also some overestimation for acetate concentration and pH in Figure 4.2 and Figure 4.3, respectively, though the overall dynamic simulation response looks promising.

In chapter 4.2.1, using the ADM1_FTnew model in simulating laboratory-scale experiment in [20], shows a good dynamical response to temperature change. Though there was some overestimation of acetate concentration in Figure 4.9, there were also similarities with the experimental data. The match in simulated methane content and experimental data between days 10 and 40 looks very promising. The same applies to biogas flow simulation as well. It seems like the model matches the dynamics of the experimental data well, even though it is not consistent in estimating the values correctly.

The ADM1_FTnew model was used to simulate VEAS process from 2016-2017, and the results presented in the 4.2.2 chapter. The results show that the model and the Linear model [35] from the previous work are quite similar. With the same temperature in steady-state, the models had very similar results, except for the growth rate of acetate degraders in Figure 4.18. This exception might be possible since the growth rate values in ADM1_FTnew model were taken from research work [34], and k_m is calculated from the research work growth rate values too. In the days of temperature transition, the simulations have surprisingly similar results. Some peak values are more prominent for the ADM1_FTnew model than for the Linear model between days 410 and 550. Nevertheless, the dynamics of the temperature transition in the two simulations are similar.

5.1.2 Performance of ADM1_CTM1 model

The ADM1_CTM1 model was validated via a simulation of a laboratory-scale experiment described in [20]; parameters are also summarised in Table 3.5.

Simulated gas production in Figure 4.4 and methane percentage of biogas in Figure 4.6 did not show the same behaviour as experimental data while the temperature was 47°C. This inconsistency might be due to how the model is built. Since the model calculates new parameter values from the changing temperature and does not account for lag or adaptation times of organisms in the biological system, the changes might be seen earlier in the model. This mechanic may explain why simulated and experimental methane content in Figure 4.6 between days 20 and 26 are different. When discussing the spike in acetate concentration in Figure 4.5, the simulation spikes earlier than experimental data. Here the absence of lag time can also be the reason. This behaviour can also be observed when comparing the ADM1_CTM model to the ADM1_FTnew model in chapter Laboratory scale experiment4.2.1, that the ADM1_CTM1 reacts to temperature change but not with the same dynamics as ADM1_FTnew.

The results obtained from the ADM1_CTM1 model were very similar in days with constant temperature to results of the Linear and ADM1_FTnew models for the VEAS 2016-2017 process simulation (chapter 4.2.2). The simulation shows some deviation from the Linear model when the temperature was changed, but it still shows similar dynamical behavior.

In summary, it seems like all three models, Linear, ADM1_CTM1, and ADM1_FTnew have quite similar performance in predicting VEAS 2016-2017 transition case. However, this may be due to a stop in reactor feed in days when temperature was changed in VEAS 2016-2017 process. This may explain that why models performed well in laboratory-scale experiments more dynamically. When the ADM1_CTM1 and ADM1_FTnew models were compared to each other, it seemed like ADM1_FTnew perform better and was closer to experimental results.

5.2 Effects of co-digestion

The decision to calculate the COD for the additional sludges from TOC will most likely influence the relevance of the results for VEAS. However, since the sludges were modified to be different in lipid, carbohydrate, and protein fractions, it will still be beneficial to compare the effects.

Another point worth noting that even though simulation results for VEAS 2019 mesophilic process without co-substrates has some deviations from VEAS 2019 data points in parameters like biogas production, bicarbonate, IN and acetate concentrations. The fact that simulated pH and methane content has a good fit to VEAS 2019 process data points is considered sufficient to evaluate the results in this work. Still, this inconsistency is something that should be kept in mind. Also, the assumption made for PGW that it is only propylene glycol and water should be remembered.

5.2.1 Propylene glycol as co-substrate

As the results suggest, with adding propylene glycol, the average gas production increase, and average acetate, bicarbonate and NH4 concentrations decrease. This result is not surprising since the PGW was modelled as a carbon source. It was shown in research that PG is easily converted to methane, and reported COD removal of PG could be up to 95% at mesophilic condition[42], [21], [23]. PG has a ThOD value of 1680 kg/m3 [12], making it a good source of easily convertible COD to produce methane. Though, due to the lack of nutrients and other

substances in PG based de-icing fluid, it is suggested to use it as a co-substrate with substrates high in nutrients, like WWS [42].

The simulation results predict a stable process for all three simulations with mesophilic and thermophilic temperature and increasing OLR. It was shown that co-digestion was sustainable with diluted aircraft de-icing fluid at OLR as high as 1.6 kgCOD/(m^3*d) [23]. In the simulation cases of the thesis highest OLR of PGW was around 0.47 kgCOD/(m^3*d), which is well on the safe side and, in theory, can be increased even more if there is an opportunity. The one thing worth attention also is the adaptation time of the microorganisms to the new substrate. Time is needed for microorganisms to adapt to PG[43].

Though simulation shows a good potential of PWG, one also must remember that simulation of the PGW was simplified. In reality, AD can be influenced by other products that are used to de-ice the concreate in the plane de-icing area. In the case of Torp airport, products containing sodium and potassium formate are used. Also, additives in a de-icing fluid can influence the AD[44], in addition to substances washed with rainwater from the airport area.

Maybe it is also worth mentioning that propionate conversion to acetate is sensitive to hydrogen levels. Since the PG degradation pathway has propionate and hydrogen as intermediates, elevated hydrogen concentration can inhibit propionate degraders[21]. Though, the simulation results showed no increase in inhibition of propionate degraders by hydrogen at PG concentrations simulated compared to simulation results of VEAS process.

5.2.2 C/N ratio in additional sludges

It is prominent from the results in chapters 4.3.2 and 0 that the C/N ratio impacts the process. Though all simulations predict somewhat normal pH, the acetate and IN concentrations were increased to high levels in simulations with a low C/N ratio, with simulation 5.1 having the highest values. The average predicted value of IN by simulation 5.1 was 3.16 kg/m^3 with a C/N ratio of 3.7, when a value of more than 3 kg/m^3 of total ammonia nitrogen is a strongly inhibitory concentration, according to [1]. Also, the C/N ratio of 3.7 is way below the suggested value, 9-30, for organic waste[11]. It may also be noticed that simulated acetate concentration is relatively high for an actual AD to work stably. The value of VFA concentration that was suggested for stable AD should not increase above 0.3 kg/m^3 [45]. Though for simulation 5.1, the average simulated VFA concentration seems to be excessive, around 3.2 kgHAc/m^3. Even the simulation 5.4 with a C/N ratio of 6.1 shows elevated acetate concentrations that sometimes reach values of VEAS 2019 data points with an average of 1.2 kgHAc/m^3. This might suggest that the actual process may also be unstable without an additional carbon source. Though VFA/Alkalinity ratio for simulation 5.1 is 0.17, which is in the suggested range between 0.05 to 0.25 [4].

5.3 THP

THP is a known pre-treatment process that has proven its efficiency in increasing gas production in AD, increased solubilization of particulate material in substrate and increasing disintegration and hydrolysis rate. Though to successfully implement it in AD model, it is need to know more about how much particulate material is solubilizing and how much hydrolysis rate is increased. And some research has been done to determine solubilization and hydrolysis rate as it was presented in Table 2.3, as well as change for some other parameters like pH,

NH4-N and VFA. The results differ in some values, and also, some experiments have different TS of tested sludge. Also, only WAS was used as a substrate that contains microorganisms and, therefore, may have a higher increase in ammonia after THP than for example PS. In addition, not all research looks into THP effect on hydrolysis rate, so more data may be needed. Though there is sufficient research showing the increase in biogas production and positive effects of THP on AD process.

5.4 Energy production potential

Figure 4.69 in the results chapter showed how much energy production could theoretically be increased by changes assessed in this work. When comparing VEAS thermophilic simulation to mesophilic simulation, the increase in potential energy is only 3.6%. This slight increase may be supported by the fact that thermophilic temperature increases the biochemical reaction rate of the digestion, and impact will be most prominent in shorter HRT or higher OLR[1], [15]. An increase in simulated potential energy production is also seen for simulations with PGW. The fact that PG is easily converted to acetate can be a factor in the energy increase.

Energy potential seems to be lower for simulations involving additional sludges in both mesophilic and thermophilic temperature ranges. These lower values may be due to the low C/N ratio for mesophilic simulations 5.1, 5.3 and 5.4 and thermophilic simulations 8.1, 8.3 and 8.4. However, the simulations with PGW and additional sludges, 7.1 and 10.1, show a decrease in potential energy production also. This may be due to still low carbon content to balance out the nitrogen in sludges. The two processes that exert the ability to increase potential energy production close to 50% seem to be simulation 10.2 with thermophilic temperature when for mesophilic temperature simulation 7.3 shows only a 26% increase compared to VEAS mesophilic simulation. These simulations have an increase in OLR compared to simulations 7.1 and 10.1. These results, that simulation with increased OLR have a more prominent increase in potential energy production than simulations with the same substrates, but lower OLR may suggest that it might be due to OLR and not so much due to co-substrate addition. Which, in this case, can be an indicator to that reactor can manage higher loading rates.

6 Conclusion

Microbial adaptation to temperature change was investigated with purpose to evaluate the temperature change in VEAS 2016-2017 by means of simulation. Two temperature transition models, ADM1_CTM1 and ADM1_FTnew were tested. The simulation done with ADM1_FTnew model fitted fairly closely the experimental data published in [22] and also had a better fit to experimental data in [24] than ADM1_CTM1. This suggesting that ADM1_FTnew model is more suitable to simulate dynamic temperature change.

When it comes to VEAS 2016-2017 process, it has a weak point since the reactor feeding has been stopped during days 19 to 62 and 473 to 514. During these two periods, temperature transition happened. Nevertheless, the recommendation is to continue work with ADM1_FTnew model and include parameters and equations of temperature response for other microorganisms besides methanogens. Furthermore, consider temperature response for hydrolysis step as well.

Co-substrate and pre-treatment effects on AD were evaluated, together with a possibility of a 50% increase of biogas production for VEAS. The study has identified through literature review and simulations that PWG can potentially be a good additional organic source for AD. However, composition analysis of the PGW from Torp airport is recommended to identify the potential substances that can inhibit the AD process. Also, in the star-up period for the new co-substrate, the adaptation time of the organisms in the reactor should be considered.

Different C/N ratios were assessed for the sludges used in this work. Though the simulated cases had somewhat stable pH and gas production, there were still too high values of VFA for a low C/N ratio simulation. The high VFA can be a sign of instability. The study, therefore, advises to adapt appropriate C/N ratios in the feed substrate by blending the low C/N ratio sludges with a carbon-rich substrate. According to simulation results, it is reasonable to suggest a C/N ratio of 9 to be the lowest value sufficient for a stable process. This is comparable to reported values in the literature [11].

The THP pre-treatment is widely used in biogas industry and proved to be an effective strategy to increase biogas yield. The research in this work supports the fact that THP can improve biogas production in VEAS process and increase the use of available reactors capacity. The lack of extensive research on how much THP effects different substrates makes it challenging to implement it in an AD model. Thus, more future work is advised in this part.

The simulation results of the thermophilic process without co-substrate addition showed a 3.6 % increase in potential energy production compared to the mesophilic process. This increase might not be higher than the energy required to maintain a higher reactor temperature at thermophilic conditions. Though with pre-treatment, increased OLR and co-substrates, both mesophilic and thermophilic processes have the potential to increase biogas production closer to 50%.

References

[1] G. Tchobanoglous, Metcalf & Eddy, and AECOM, *Wastewater engineering: treatment and resource recovery : Volume 2*, 5th international ed., vol. Volume 2. New York: McGraw-Hill, 2014, p. XXI, 1059–2018.

[2] "VEAS." https://www.veas.nu/ (accessed Apr. 07, 2021).

[3] Espen Govasmark, "Utråtningskapasitet i RÅT," VEAS, 2020.

[4] G. Tchobanoglous, Metcalf & Eddy, and AECOM, *Wastewater engineering: treatment and resource recovery : Volume 1*, 5th international ed., vol. Volume 1. New York: McGraw-Hill, 2014, p. XXIX, 1058.

[5] IWA Task Group for Mathematical Modelling of Anaerobic Digestion Processes, *Anaerobic digestion model no.1 (ADM1)*, vol. No.13. IWA Publishing, 2002, p. 80.

[6] J. B. van Lier, *Thermophilic anaerobic wastewater treatment: temperature aspects and process stability*.

[7] A. Wellinger, J. D. Murphy, D. Baxter, and R. Braun, *The Biogas Handbook : Science, Production and Applications*, vol. 52. Elsevier Science & Technology, 2013.

[8] M. Takashima, K. Shimada, and R. E. Speece, "Minimum Requirements for Trace Metals (Iron, Nickel, Cobalt, and Zinc) in Thermophilic and Mesophilic Methane Fermentation from Glucose," *Water Environ. Res.*, vol. 83, no. 4, pp. 339–346, Apr. 2011, doi: 10.2175/106143010X12780288628895.

[9] S. A. Neshat, M. Mohammadi, G. D. Najafpour, and P. Lahijani, "Anaerobic co-digestion of animal manures and lignocellulosic residues as a potent approach for sustainable biogas production," *Renew. Sustain. Energy Rev.*, vol. 79, pp. 308–322, Nov. 2017, doi: 10.1016/j.rser.2017.05.137.

[10] O. W. Awe, Y. Zhao, A. Nzihou, D. Pham Minh, and N. Lyczko, "Anaerobic co-digestion of food waste and FOG with sewage sludge – realising its potential in Ireland," *Int. J. Environ. Stud.*, vol. 75, no. 3, pp. 496–517, May 2018, doi: 10.1080/00207233.2017.1380335.

[11] N. J. Horan, Z. Siqqiqui, and K. Anaman, "Optimisation of C:N Ratio for Co-Digested Processed Industrial FoodWaste and Sewage Sludge Using the BMP Test," *Int. J. Chem. React. Eng.*, May 2011, Accessed: Nov. 08, 2020. [Online]. Available: http://eprints.whiterose.ac.uk/42981/

[12] "Troubleshooting: Biogas Plants problems • BiogasWorld," *BiogasWorld*. https://www.biogasworld.com/biogas-plant-troubleshooting/ (accessed May 11, 2021).

[13] Z. Yang, W. Wang, Y. He, R. Zhang, and G. Liu, "Effect of ammonia on methane production, methanogenesis pathway, microbial community and reactor performance under mesophilic and thermophilic conditions," *Renew. Energy*, vol. 125, pp. 915–925, Sep. 2018, doi: 10.1016/j.renene.2018.03.032.

[14] J. Palatsi, A. Gimenez-Lorang, I. Ferrer, and X. Flotats, "Start-up strategies of thermophilic anaerobic digestion of sewage sludge," *Water Sci. Technol.*, vol. 59, no. 9, pp. 1777–1784, May 2009, doi: 10.2166/wst.2009.180.

[15] G. Gebreeyessus and P. Jenicek, “Thermophilic versus Mesophilic Anaerobic Digestion of Sewage Sludge: A Comparative Review,” *Bioengineering*, vol. 3, no. 2, p. 15, Jun. 2016, doi: 10.3390/bioengineering3020015.

[16] L. Kardos, “COMPARING OF MESOPHILIC AND THERMOPHILIC ANAEROBIC FERMENTED SEWAGE SLUDGE BASED ON CHEMICAL AND BIOCHEMICAL TESTS,” *Appl. Ecol. Environ. Res.*, vol. 9, no. 3, pp. 293–302, Oct. 2011, doi: 10.15666/aeer/0903_293302.

[17] R. A. Labatut, L. T. Angenent, and N. R. Scott, “Conventional mesophilic vs. thermophilic anaerobic digestion: A trade-off between performance and stability?,” *Water Res.*, vol. 53, pp. 249–258, Apr. 2014, doi: 10.1016/j.watres.2014.01.035.

[18] U. Tezel, M. Tandukar, M. G. Hajaya, and S. G. Pavlostathis, “Transition of municipal sludge anaerobic digestion from mesophilic to thermophilic and long-term performance evaluation,” *Bioresour. Technol.*, vol. 170, pp. 385–394, Oct. 2014, doi: 10.1016/j.biortech.2014.08.007.

[19] M. A. de la Rubia, L. I. Romero, D. Sales, and M. Perez, “Temperature conversion (mesophilic to thermophilic) of municipal sludge digestion,” *AIChE J.*, vol. 51, no. 9, pp. 2581–2586, 2005, doi: https://doi.org/10.1002/aic.10546.

[20] A. Boušková, M. Dohányos, J. E. Schmidt, and I. Angelidaki, “Strategies for changing temperature from mesophilic to thermophilic conditions in anaerobic CSTR reactors treating sewage sludge,” *Water Res.*, vol. 39, no. 8, pp. 1481–1488, Apr. 2005, doi: 10.1016/j.watres.2004.12.042.

[21] T. Schoenberg, S. Veltman, and M. Switzenbaum, “Kinetics of anaerobic degradation of glycol-based Type I aircraft deicing fluids,” p. 10.

[22] S. Veltman, T. Schoenberg, and M. S. Switzenbaum, “Alcohol and acid formation during the anaerobic decomposition of propylene glycol under methanogenic conditions,” p. 6.

[23] D. Zitomer, N. Ferguson, K. McGrady, and J. Schilling, “Anaerobic Co-Digestion of Aircraft Deicing Fluid and Municipal Wastewater Sludge,” *Water Environ. Res.*, vol. 73, no. 6, pp. 645–654, Nov. 2001, doi: 10.2175/106143001X143376.

[24] D. F. Dwyer and J. M. Tiedje, “Degradation of ethylene glycol and polyethylene glycols by methanogenic consortia.,” *Appl. Environ. Microbiol.*, vol. 46, no. 1, pp. 185–190, Jul. 1983.

[25] P. Phothilangka, M. A. Schoen, M. Huber, P. Luchetta, T. Winkler, and B. Wett, “Prediction of thermal hydrolysis pretreatment on anaerobic digestion of waste activated sludge,” *Water Sci. Technol.*, vol. 58, no. 7, pp. 1467–1473, Oct. 2008, doi: 10.2166/wst.2008.726.

[26] A. Valo, H. Carrère, and J. P. Delgenès, “Thermal, chemical and thermo-chemical pre-treatment of waste activated sludge for anaerobic digestion: Pre-treatment of waste activated sludge,” *J. Chem. Technol. Biotechnol.*, vol. 79, no. 11, pp. 1197–1203, Nov. 2004, doi: 10.1002/jctb.1106.

[27] C. Bougrier, J.-P. Delgenès, and H. Carrère, “Combination of Thermal Treatments and Anaerobic Digestion to Reduce Sewage Sludge Quantity and Improve Biogas Yield,”

Process Saf. Environ. Prot., vol. 84, no. 4, pp. 280–284, Jul. 2006, doi: 10.1205/psep.05162.

[28] R. Cano, S. I. Pérez-Elvira, and F. Fdz-Polanco, "Energy feasibility study of sludge pretreatments: A review," *Appl. Energy*, vol. 149, pp. 176–185, Jul. 2015, doi: 10.1016/j.apenergy.2015.03.132.

[29] "THP Solutions - Cambi - world leader in thermal hydrolysis." https://www.cambi.com/what-we-do/thp-solutions/ (accessed Jan. 15, 2021).

[30] I. Ramirez, A. Mottet, H. Carrère, S. Déléris, F. Vedrenne, and J.-P. Steyer, "Modified ADM1 disintegration/hydrolysis structures for modeling batch thermophilic anaerobic digestion of thermally pretreated waste activated sludge," *Water Res.*, vol. 43, no. 14, pp. 3479–3492, Aug. 2009, doi: 10.1016/j.watres.2009.05.023.

[31] C. Bougrier, J. P. Delgenès, and H. Carrère, "Effects of thermal treatments on five different waste activated sludge samples solubilisation, physical properties and anaerobic digestion," *Chem. Eng. J.*, vol. 139, no. 2, pp. 236–244, Jun. 2008, doi: 10.1016/j.cej.2007.07.099.

[32] S. Y. Jeong *et al.*, "Influence of thermal hydrolysis pretreatment on physicochemical properties and anaerobic biodegradability of waste activated sludge with different solids content," *Waste Manag.*, vol. 85, pp. 214–221, Feb. 2019, doi: 10.1016/j.wasman.2018.12.026.

[33] A. Donoso-Bravo, C. Retamal, M. Carballa, G. Ruiz-Filippi, and R. Chamy, "Influence of temperature on the hydrolysis, acidogenesis and methanogenesis in mesophilic anaerobic digestion: parameter identification and modeling application," *Water Sci. Technol.*, vol. 60, no. 1, pp. 9–17, Jul. 2009, doi: 10.2166/wst.2009.316.

[34] A. Kovalovszki, L. Treu, L. Ellegaard, G. Luo, and I. Angelidaki, "Modeling temperature response in bioenergy production: Novel solution to a common challenge of anaerobic digestion," *Appl. Energy*, vol. 263, p. 114646, Apr. 2020, doi: 10.1016/j.apenergy.2020.114646.

[35] D. Raya, M. Domirani, P. Parhizkarabyaneh, and V. Mikelsone, "Modelling mesophilic and thermophilic digestion with addition of SAOB and cosubstrate for VEAS biogas process.," University of Sout-Estern Norway, Porsgrunn, Group project, Nov. 2020.

[36] R. Girault *et al.*, "A waste characterisation procedure for ADM1 implementation based on degradation kinetics," *Water Res.*, vol. 46, no. 13, pp. 4099–4110, Sep. 2012, doi: 10.1016/j.watres.2012.04.028.

[37] D. Orhon and E. Uba, "COD Fractionation in Wastewater Characterization-The State of the Art," p. 12.

[38] K. Schuchmann *et al.*, "Nonacetogenic Growth of the Acetogen Acetobacterium woodii on 1,2-Propanediol," *J. Bacteriol.*, vol. 197, no. 2, pp. 382–391, Jan. 2015, doi: 10.1128/JB.02383-14.

[39] W. Bergland, D. Botheju, C. Dinamarca, and R. Bakke, "Considering Culture Adaptations to High Ammonia Concentration in ADM," p. 8.

[40] PubChem, "Propylene glycol." https://pubchem.ncbi.nlm.nih.gov/compound/1030 (accessed May 18, 2021).

[41] G. Luo, D. De Francisci, P. G. Kougias, T. Laura, X. Zhu, and I. Angelidaki, “New steady-state microbial community compositions and process performances in biogas reactors induced by temperature disturbances,” *Biotechnol. Biofuels*, vol. 8, no. 1, p. 3, 2015, doi: 10.1186/s13068-014-0182-y.

[42] D. H. Zitomer and G. U. Tonuk, “Propylene Glycol Deicer Biodegradation Kinetics: Anaerobic Complete-Mix Stirred Tank Reactors, Filter, and Fluidized Bed,” *J. Environ. Eng.*, vol. 129, no. 2, pp. 123–129, Feb. 2003, doi: 10.1061/(ASCE)0733-9372(2003)129:2(123).

[43] N. Sezgin and G. U. Tonuk, “Anaerobic Treatability of Wastewater Contaminated with Propylene Glycol,” *Bull. Environ. Contam. Toxicol.*, vol. 91, no. 3, pp. 320–323, Sep. 2013, doi: 10.1007/s00128-013-1063-y.

[44] C. L. Gruden, S. M. Dow, and M. T. Hernandez, “Fate and Toxicity of Aircraft Deicing Fluid Additives Through Anaerobic Digestion,” *Water Environ. Res.*, vol. 73, no. 1, pp. 72–79, Jan. 2001, doi: 10.2175/106143001X138714.

[45] “OPERATOR ESSENTIALS: What every operator should know about anaerobic digestion,” p. 3, 2021.

Appendices

Appendix A: Sludge analysis results and calculated values for ADM1 inputs.

Appendix B: IWA Task Group parameter values for mesophilic and thermophilic process simulations.

Appendix C: Peterson matrix with biological kinetic rates and coefficients.

Appendix D: Gantt chart for the Master Theses.

Appendix E: Project description.

Appendix F: Analysis report from ALS Laboratory Group on sludges from Marker, Aremark and Indre Østfold municipalities.

Appendix G: List of variables and equations added or edited in ADM1_FTnew

PS: The models and supplementary material is in attachment file delivered with the report PDF.

Appendix A: Sludge analysis results and values for simulation parameters.

Table 1-A: VEAS sludge analysis values and input values for simulation.

	Slam 0			**Slam 0**	
tCOD (g/L)	90.73		tCOD (g/L)	90.73	gCOD/L
sCOD (g/L)	9.46		sCOD (g/L)	9.46	gCOD/L
Råfett (g/l)	9.9		Input_X_li	29.2	gCOD/L
Karbohydrater (g/l)	14.1		Input_X_ch	19.1	gCOD/L
Proteiner (g/l)	15.07		Input_X_pr	20.4	gCOD/L
Lactic acid (g/l)	0.02		Input_S_su	0.019	gCOD/L
Formic acid (g/l)	0.01				gCOD/L
Acetic acid (g/l)	3.22		Input_S_ac	3.44	gCOD/L
Propionic acid (g/l)	1.18		Input_S_pro	1.78	gCOD/L
iso-butyric (g/l)	0.12				gCOD/L
butyric acid (g/l)	2.26		Input_S_bu	4.33	gCOD/L
Valeric acid (g/l)	0.12		Input_S_va	0.44	gCOD/L
iso-valeric acid (g/l)	0.09				gCOD/L
Tot VFA (g/l)	7.02		Input_S_I	0	gCOD/L
Tot VFA (g HAc/l)	5.95		Input_X_I	11.2	gCOD/L
BMP (m3 CH4/tonn VS)	512*		Input_S_aa	0	gCOD/L
BMP (m3 CH4/tonn COD)	332*		Input_S_fa		gCOD/L
BMP (tonn COD CH4/tonn COD substrat)	0.876		Input_X_c	0	benytter ikke denne
(m3 biogas/tonn COD)	512*		bruker gjennomsnitt, resten er inert (input_X_I)	79.52	
TAN (mg/L)	942		Input_S_IN	0.0523	
pH	6.34		Input_S_IC	0.18	
TS (%)	7.29		test:		
VS (%)	80.10		sum codt	89.86	
Tot-N (TKN) (% av TS)	4.6		*differanse codt*	*-0.87*	*skal være 0, under 1 er bra nok*
Tot-N (TKN) (g/l)	3.35		sum cods	10.00	
tCOD fra TS, omregningsfaktor	12.45		*differanse cods*	*0.54*	*skal være 0, under 1 er bra nok*
tCOD fra VS, omregningsfaktor	15.54		Input_S_IN	0.0523	
beregnet protein	15.07		Input_S_IC	ukjent, justeres ved simuleringer	
*Utregnet fra driftsdata	20.95875		C/N ratio	9.57	

Table 2-A: Marker municipality WWT plant sludge analysis values and input values for simulation.

Elements	S1 Slam Marker kommune (activated sludge)					
	Units	Measured value	Parameters for ADM1	Units	Values adjusted to COD of TOC	Values adjusted to 7.3% TS
TS	**%**	**0.22**				7.3
TS	**gTS/L**	**2.2**			2.2	73
Lactic acid	**g/L**	**---**				
Formic acid	**g/L**	**---**				
Acetic acid	**g/L**	**0.058**	Input_S_ac	gCOD/L	0.0225	0.7465
Propionic aid	**g/L**	**0.042**	Input_S_pro	gCOD/L	0.0231	0.7674
n-butyric acid	**g/L**	**---**				
Valeric acid	**g/L**	**---**	Input_S_su	gCOD/L		0
iso-valeric acid	**g/L**	**---**	Input_S_aa	gCOD/L		0
Caproic acid	**g/L**	**---**	Input_S_fa	gCOD/L		0
pH						
VS	**g/L**	**1.606**				
TS-VS	**g/L**	**0.594**				
NH4+	**g/L**	**0.039**	input_S_IN	mol/L	0.002	0.0722
TAN	**g/L**	**0.030**				
TN	**g/L**	**0.554**				
Totalt ekstraherbare komponenter	**g/L**	**0.036**				
Total fats and oils	**g/L**	**0.036**	Input_X_li	gCOD/L	0.039	1.2787
TIC	**g/L**	**0.050**	Input_S_IC	mol/L	0.004	0.1393
CO3	**g/L**	**0.251**				
TOC	**g/L**	**0.671**	tCOD	gCOD/L	1.789	59.373
TC	**g/L**	**0.722**				
tCODmeasured	g/L	0.2948	Too low to balance, using COD of TOC			
Proteins	**g/L**	**3.275**	Input_X_pr	gCOD/L	1.611	53.4528
Particulate inert			Input_X_I	gCOD/L	0.094	3.1279
Soluble inert			Input_S_I	gCOD/L	0.000	0.0000
Carbohydrates			Input_X_ch	gCOD/L	0.000	0.0000
Soluble COD			sCOD	gCOD/L	0.046	1.514
C:N						1.2

Table 3-A: Aremark municipality WWT plant sludge analysis values and input values for simulation.

Elements	S2 Slam Aremark kommune (Primary sludge)					
	Units	Measured value	Parameters for ADM1	Units	Values adjusted to COD of TOC	Values adjusted to 7.3% TS
TS	%	4.22				7.3
TS	gTS/L	42.2			42.2	73
Lactic acid	g/L	---				
Formic acid	g/L	---				
Acetic acid	g/L	0.571	Input_S_ac	gCOD/L	0.589	1.0196
Propionic aid	g/L	0.351	Input_S_pro	gCOD/L	0.514	0.8891
n-butyric acid	g/L	---				
Valeric acid	g/L	---	Input_S_su	gCOD/L	0	0
iso-valeric acid	g/L	---	Input_S_aa	gCOD/L	0	0
Caproic acid	g/L	---	Input_S_fa	gCOD/L	0	0
pH						
VS	g/L	29.329				
TS-VS	g/L	12.871				
NH4+	g/L	0.485	input_S_IN	mol/L	0.027	0.0466
TAN	g/L	0.379				
TN	g/L	2.317				
Totalt ekstraherbare komponenter	g/L	4.030				
Total fats and oils	g/L	4.030	Input_X_li	gCOD/L	11.501	19.8943
TIC	g/L	1.300	Input_S_IC	mol/L	0.108	0.1874
CO3	g/L	6.499				
TOC	g/L	13.166	tCOD	gCOD/L	35.110	59.373
TC	g/L	14.475				
tCODmeasured	g/L	3.2916	Too low to balance, using COD of TOC			
Proteins	g/L	12.114	Input_X_pr	gCOD/L	15.884	27.4764
Particulate inert			Input_X_I	gCOD/L	4.931	8.5300
Soluble inert			Input_S_I	gCOD/L	0	0
Carbohydrates			Input_X_ch	gCOD/L	1.692	2.9266
Soluble COD			sCOD	gCOD/L	1.103	1.909
C:N						6.2

Table 4-A: Indre Østfold municipality WWT plant sludge analysis values and input values for simulation.

Elements	S3 Indre Østfold kommune (Primary sludge)					
	Units	Measured value	Parameters for ADM1	Units	Values adjusted to COD of TOC	Values adjusted to 7.3% TS
TS	%	24.4				7.3
TS	gTS/L	244			244	73
Lactic acid	g/L	---				
Formic acid	g/L	---				
Acetic acid	g/L	0.183	Input_S_ac	gCOD/L	0.194	0.058
Propionic aid	g/L	0.156	Input_S_pro	gCOD/L	0.235	0.070
n-butyric acid	g/L	---				
Valeric acid	g/L	---	Input_S_su	gCOD/L		0
iso-valeric acid	g/L	---	Input_S_aa	gCOD/L		0
Caproic acid	g/L	---	Input_S_fa	gCOD/L		0
pH						
VS	g/L	180.316				
TS-VS	g/L	63.684				
NH4+	g/L	0.002	input_S_IN	mol/L	0.002	0.0722
TAN	g/L	0.001				
TN	g/L	7.247				
Totalt ekstraherbare komponenter	g/L	0.798				
Total fats and oils	g/L	0.798	Input_X_li	gCOD/L	2.346	0.702
TIC	g/L	2.879	Input_S_IC	mol/L	0.004	0.1393
CO3	g/L	14.396				
TOC	g/L	76.128	tCOD	gCOD/L	203.008	60.736
TC	g/L	79.056				
tCODmeasured	g/L	10.687	Too low to balance, using COD of TOC			
Proteins	g/L	45.284	Input_X_pr	gCOD/L	61.172	18.302
Particulate inert			Input_X_I	gCOD/L	29.374	8.788
Soluble inert			Input_S_I	gCOD/L	0.000	0.000
Carbohydrates			Input_X_ch	gCOD/L	109.687	32.816
Soluble COD			sCOD	gCOD/L	0.429	0.128
C:N						10.9

Appendix B: Parameter values for mesophilic and thermophilic process simulations.

Table 1-B: Suggested parameter values by IWA Task Group and mathematical equation used to model temperature transition for each parameter in ADM1_CTM1 and ADM1_FTnew models.

Parameters	Mesophilic (35ºC)	Thermophilic (55ºC)	Transition model used for parameters ADM1_CTM1	Transition model used for parameters ADM1_FTnew
k_{dis}(d^{-1})	0.5	1	Linear interpolation	Linear interpolation
k_{hyd_CH}(d^{-1})	10	10	CTM1	Constant
k_{hyd_PR}(d^{-1})	10	10	CTM1	Constant
k_{hyd_LI}(d^{-1})	10	10	CTM1	Constant
k_{dec_all}(d^{-1})	0.02	0.04	Linear interpolation	Linear interpolation
K_{S_NH3}(kmol/m^3)	1x10^{-4}	1x10^{-4}	Constant	Constant
$pH_{UL\ acet/acid}$	5.5	5.5	Constant	Constant
$pH_{LL\ acet/acid}$	4	4	Constant	Constant
k_{m_su} (kgCOD/(kgCOD·d)	30	70	CTM1	Linear interpolation
K_{S-su} (kgCOD/ m^3)	0.5	1	Linear interpolation	Linear interpolation
Y_{su} (COD/COD)	0.1	0.1	CTM1	Constant
k_{m_aa} (kgCOD/(kgCOD·d)	50	70	CTM1	FTref
K_{s_aa} (kgCOD/m^3)	0.3	0.3	Constant	Constant
Y_{aa} (COD/COD)	0.08	0.08	CTM1	Constanta
k_{m_fa} (kgCOD/(kgCOD·d)	6	10	CTM1	FTref
K_{s_fa} (kgCOD/m^3)	0.4	0.4	Constant	Constant
Y_{fa}	0.06	0.06	CTM1	Constant

(COD/COD)				
$K_{I,H2\_fa}$ (kgCOD/m^3)	5x10^{-6}	n/a	Constant	Constant
k_{m_c4+} (kgCOD/(kgCOD·d)	20	30	CTM1	FTref
K_{s_c4+} (kgCOD/m^3)	0.2	0.4	Linear interpolation	Linear interpolation
Y_{c4+} (COD/COD)	0.06	0.06	CTM1	Constant
$K_{I,H2\_c4+}$ (kgCOD/m^3)	1x10^{-5}	3x10^{-5}	Linear interpolation	Linear interpolation
k_{m_pro} (kgCOD/(kgCOD·d)	13	20	CTM1	FTref
K_{s_pro} (kgCOD/m^3)	0.1	0.3	Linear interpolation	Linear interpolation
Y_{pro} (COD/COD)	0.04	0.05	CTM1	Linear interpolation
$K_{I,H2\_pro}$ (kgCOD/m^3)	3.5x10^{-6}	1x10^{-5}	Linear interpolation	Linear interpolation
k_{m_ac} (kgCOD/(kgCOD·d)	8	16	CTM1	FTnew
K_{S_ac} (kgCOD/m^3)	0.15	0.3	Linear interpolation	Linear interpolation
Y_{ac} (COD/COD)	0.05	0.05	CTM1	Constant
pH_{UL_ac}	7	7	Constant	Constant
pH_{LL_ac}	6	6	Constant	Constant
$K_{I,H2\_pro}$ (kgCOD/m^3)	0.0018	0.011	Linear interpolation	Linear interpolation
k_{m_h2} (kgCOD/(kgCOD·d)	35	35	CTM1	Constant
K_{S_h2} (kgCOD/m^3)	7x10^{-6}	5x10^{-5}	Linear interpolation	Linear interpolation
Y_{h2} (COD/COD)	0.06	0.06	CTM1	Constant
pH_{UL_h2}	6	6	Constant	Constant
pH_{LL_h2}	5	5	Constant	Constant

Appendix C: Peterson matrix with biological kinetic rates and coefficients.

Table 1-C: Soluble components with biochemical rate coefficients and kinetic rate equations reproduced from [1] and added coefficient and equations for propylene glycol.

	Component -->	i	1	1a	2	3	4	5	6	7	8	9	10	11	12	
j	Process		S_su	S_pg	S_aa	S_fa	S_va	S_bu	S_pro	S_ac	S_h2	S_ch4	S_IC	S_IN	S_I	Rate (ρ_j, kgCOD/m^3*d)
1	Disintegration														f_SI_xc	k_dis*X_c
2	Hydrolysis Carbohydrate		1													k_hyd_ch*X_ch
3	Hydrolysis of Proteins				1											k_hyd_pr*X_pr
4	Hydrolysis of Lipids		1-f_fa_li			f_fa_li										k_hyd_li*X_li
5	Uptake of Sugar		-1					(1-Y_su)* f_bu_su	(1-Y_su)* f_pro_su	(1-Y_su)* f_ac_su	(1-Y_su)* f_h2_su		- sum(C_i*vi_5) i=1-9,11-24	-(Y_su)* N_bac		km_su*(S_su/(Ks+S_su))*X_su*I_1
5a	**Uptake of propylene glycol**			**-1**					**(1-Y_pg)* f_pro_pg**		**(1-Y_pg)* f_h2_pg**					**km_pg*(S_pg/(Ks+S_pg))*X_pg*I_2**
6	Uptake of Amino Acids				-1		(1-Y_aa)* f_va_aa	(1-Y_aa)* f_bu_aa	(1-Y_aa)* f_pro_aa	(1-Y_aa)* f_ac_aa	(1-Y_aa)* f_h2_aa		- sum(C_i*vi_6) i=1-9,11-24	N_aa-(Y_aa)* N_bac		km_aa*(S_aa/(Ks+S_aa))*X_aa*I_1
7	Uptake of LCFA					-1				(1-Y_fa)* 0.7	(1-Y_fa)* 0.3			-(Y_fa)* N_bac		km_fa*(S_fa/(Ks+S_fa))*X_fa*I_2
8	Uptake of Valerate						-1		(1-Y_c4)* 0.54	(1-Y_c4)* 0.31	(1-Y_c4)* 0.15			-(Y_c4)* N_bac		km_c4*(S_va/(Ks+S_va))*X_c4* (1/(1+(S_bu/S_va)))*)I_2
9	Uptake of Butyrate							-1		(1-Y_c4)* 0.8	(1-Y_c4)* 0.2			-(Y_c4)* N_bac		km_c4*(S_bu/(Ks+S_bu))*X_c4* (1/(1+(S_va/S_bu)))*)I_2
10	Uptake of Propionate								-1	(1-Y_pro)* 0.57	(1-Y_pro)* 0.43		- sum(C_i*vi_10) i=1-9,11-24	-(Y_pro)* N_bac		km_pr*(S_pro/(Ks+S_pro))*X_pro*I_2
11	Uptake of Acetate									-1		(1-Y_ac)	- sum(C_i*vi_11) i=1-9,11-24	-(Y_ac)* N_bac		km_ac*(S_ac/(Ks+S_ac))*X_ac*I_3
12	Uptake of Hydrogen										-1	(1-Y_h2)	- sum(C_i*vi_12) i=1-9,11-24	-(Y_h2)* N_bac		km_h2*(S_h2/(Ks+S_h2))*X_h2*I_1
13	Decay of X_su															kdec_X_su*X_su
13a	**Decay of X_pg**															**kdec_X_pg*X_pg**
14	Decay of X_aa															kdec_X_aa*X_aa
15	Decay of X_fa															kdec_X_fa*X_fa
16	Decay of X_C4															kdec_X_c4*X_c4
17	Decay of X_pro															kdec_X_pro*X_pro
18	Decay of X_ac															kdec_X_ac*X_ac
19	Decay of X_h2															kdec_X_h2*X_h2
			Monosaccharides (kgCOD/m^3)	**Propylene glycol (kgCOD/m^3)**	Amino Acid (kgCOD/m^3)	LCFA (kgCOD/m^3)	Total valerate (kgCOD/m^3)	Total butyrate (kgCOD/m^3)	Total propionate (kgCOD/m^3)	Total Acetate (kgCOD/m^3)	Hydrogen gas (kgCOD/m^3)	Methane gas (kgCOD/m^3)	Inorganic carbon (kmoleC/m^3)	Inorganic nitrogen (kmoleC/m^3)	Soluble inerts	Inhibition factors: I_1=I_pH*I_NH_lim I_2=I_pH*I_NH_lim*I_h2 I_3=I_pH*I_NH_lim*I_NH3_xac

Table 2-C: Particulate components with biochemical rate coefficients and kinetic rate equations reproduced from [1] and added coefficient and equations for propylene glycol.

	Component -->	i	13	14	15	16	17	17a	18	19	20	21	22	23	24	
j	Process		**X_c**	**X_ch**	**X_pr**	**X_li**	**X_su**	**X_pg**	**X_aa**	**X_fa**	**X_c4**	**X_pro**	**X_ac**	**X_h2**	**X_I**	Rate (ρ_j, kgCOD/m^3*d)
1	Disintegration		-1	f_ch_xc	f_pr_xc	f_li_xc									f_XI_xc	k_dis*X_c
2	Hydrolysis Carbohydrate			-1												k_hyd_ch*X_ch
3	Hydrolysis of Proteins				-1											k_hyd_pr*X_pr
4	Hydrolysis of Lipids					-1										k_hyd_li*X_li
5	Uptake of Sugar						Y_su									km_su*(S_su/(Ks+S))*X_su*I_1
5a	**Uptake of propylene glycol**							**Y_pg**								**km_pg*(S_pg/(Ks+S_pg))*X_pg*I_2**
7	Uptake of LCFA									Y_fa						km_fa*(S_fa/(Ks+S_fa))*X_fa*I_2
8	Uptake of Valerate										Y_c4					km_c4*(S_va/(Ks+S_va))*X_c4*(1/(1+(S_bu/S_va)))*I_2
9	Uptake of Butyrate										Y_c4					km_c4*(S_bu/(Ks+S_bu))*X_c4*(1/(1+(S_va/S_bu)))*I_2
10	Uptake of Propionate											Y_pro				km_pr*(S_pro/(Ks+S_pro))*X_pro*I_2
11	Uptake of Acetate												Y_ac			km_ac*(S_ac/(Ks+S_ac))*X_ac*I_3
12	Uptake of Hydrogen													Y_h2		km_h2*(S_h2/(Ks+S_h2))*X_h2*I_1
13	Decay of X_su		1				-1									kdec_X_su*X_su
13a	**Decay of X_pg**		**1**					**-1**								**kdec_X_pg*X_pg**
14	Decay of X_aa		1						-1							kdec_X_aa*X_aa
15	Decay of X_fa		1							-1						kdec_X_fa*X_fa
16	Decay of X_C4		1								-1					kdec_X_c4*X_c4
17	Decay of X_pro		1									-1				kdec_X_pro*X_pro
18	Decay of X_ac		1										-1			kdec_X_ac*X_ac
19	Decay of X_h2		1											-1		kdec_X_h2*X_h2
			Composites (kgCOD/m^3)	Carbohydrates (kgCOD/m^3)	Proteins (kgCOD/m^3)	Lipids (kgCOD/m^3)	Sugar degraders (kgCOD/m^3)	**Propylene glycol (kgCOD/m^3)**	Amino acid degraders (kgCOD/m^3)	LCFA degraders (kgCOD/m^3)	Valerate and butyrate degraders (kgCOD/m^3)	Propionate degraders (kgCOD/m^3)	Acetate degraders (kgCOD/m^3)	Hydrogen egraders (kgCOD/m^3)	Particulate inerts	Inhibition factors: I_1=I_pH*I_NH_lim I_2=I_pH*I_NH_lim*I_h2 I_3=I_pH*I_NH_lim*I_NH3_xac

[1] IWA Task Group for Mathematical Modelling of Anaerobic Digestion Processes, *Anaerobic digestion model no.1 (ADM1)*, vol. No.13. IWA Publishing, 2002, p. 80.

Appendix D: Gantt chart for the Master Theses.

ID	Task Mode	Task Name	Duration	Start	Finish	Predecessors
0		**Master thesis Gantt diagram**	**102 da**	**Wed 06/01/2**	**Thu 27/05/21**	
1		**1 Project schedule and Gantt diagram**	**2 days**	**Wed 13/01/2**	**Thu 14/01/21**	
2		**2 Literature review**	**23 days**	**Wed 06/01/2**	**Fri 05/02/21**	
3		2.1 Modeling parameter transition from mesophilic to thermophilic AD	23 days	Wed 06/01/21	Fri 05/02/21	
4		2.2 Glycol as co-substrate	13 days	Wed 20/01/21	Fri 05/02/21	
5		2.3 Mesophilic to thermophilic transition methods	13 days	Wed 20/01/21	Fri 05/02/21	
6		2.4 THP influence on sludge composition	9 days	Tue 26/01/21	Fri 05/02/21	
7		2.5 Define final project tasks and goals	5 days	Mon 18/01/21	Fri 29/01/21	
8		***3 Meeting 15.01***	***0 days***	***Fri 15/01/21***	***Fri 15/01/21***	***1***
9		***4 Final project description delivery***	***0 days***	***Mon 01/02/2***	***Mon 01/02/21***	***7***
10		***5 Done with main literature review***	***0 days***	***Mon 08/02/2***	***Mon 08/02/21***	***4,5,6,3***
11		***6 Formal meeting***	***0 days***	***Fri 29/01/21***	***Fri 29/01/21***	
12		**7 Model and simulations**	**48 days**	**Mon 08/02/2**	**Wed 14/04/21**	**9,10**
13		7.1 Method to model parameter transition from mesophilic to thermophilic AD	15 days	Mon 08/02/21	Fri 26/02/21	
14		7.2 Composition of de- and anti-icing fluid as co-substrate	5 days	Mon 08/02/21	Fri 12/02/21	
15		7.3 Composition of additional sludge as co-substrate	2 days	Mon 22/02/21	Fri 05/03/21	25
16		7.4 THP implementation into the model	22 days	Mon 08/02/21	Thu 25/03/21	6
17		7.5 Implement parameter transition into the model	20 days	Fri 26/02/21	Thu 25/03/21	13
18		7.6 Implement co-substrates into the model	14 days	Mon 08/03/21	Thu 25/03/21	14,15
19		7.7 Verify model with process data points from VEAS	1 day	Fri 09/04/21	Fri 09/04/21	17,18
20		7.8 Simulation scenarios	6.1 days	Fri 26/03/21	Mon 12/04/21	17,18
21		7.9 Simulate instant temperature transition VEAS 2016-2017	3 days	Mon 12/04/21	Wed 14/04/21	19
22		7.10 Simulate stepwise temperature transition VEAS 2016 - 2017	3 days	Mon 12/04/21	Wed 14/04/21	19
23		7.11 Steady state simulations w/ and w/o co-substrate and THP	4 days	Fri 02/04/21	Tue 13/04/21	18
24		7.12 Transfer simulation results to excel	9 days	Wed 31/03/21	Wed 14/04/21	21FF,22FF
25		***8 Additional sludge composition analysis from Espen***	0 days	Mon 22/02/21	Mon 22/02/21	
26		***9 Formal meeting***	***0 days***	***Fri 05/03/21***	***Fri 05/03/21***	
27		***10 Formal meeting***	***0 days***	***Fri 19/03/21***	***Fri 19/03/21***	
28		***11 Presentation of the project to master students***	***0 days***	***Mon 22/03/2***	***Mon 22/03/21***	
29		***12 Simulation results ready***	***0 days***	***Fri 16/04/21***	***Fri 16/04/21***	***24***
30		**13 Evaluation of simulation results**	**20 days**	**Thu 01/04/21**	**Wed 28/04/21**	
31		13.1 Evaluation of transition methods	16 days	Thu 01/04/21	Wed 28/04/21	
32		13.2 Compare effects of adding co-substrate	16 days	Thu 01/04/21	Wed 28/04/21	
33		13.3 Calculation and evaluation of simulated methane production	11 days	Wed 14/04/21	Wed 28/04/21	31SS,32SS
34		***14 Simulation results evaluated***	***0 days***	***Thu 22/04/21***	***Thu 22/04/21***	***30***
35		**15 Report**	**73 days**	**Mon 08/02/2**	**Wed 19/05/21**	
36		15.1 Introduction	5 days	Thu 01/04/21	Wed 07/04/21	
37		15.2 Theory and literature review	8.2 days	Mon 08/02/21	Mon 10/05/21	
38		15.3 Materials and methods	4 days	Thu 13/05/21	Tue 18/05/21	
39		15.4 Results	11 days	Fri 02/04/21	Fri 30/04/21	
40		15.5 Discussion	7 days	Thu 29/04/21	Fri 07/05/21	
41		15.6 Conclution	3 days	Wed 12/05/21	Fri 14/05/21	
42		15.7 Summary	1 day	Mon 17/05/21	Mon 17/05/21	
43		15.8 Content and reference check	3 days	Mon 17/05/21	Wed 19/05/21	37SS,38SS,3
44		15.9 Spelling check	5 days	Thu 13/05/21	Wed 19/05/21	37SS,38SS,3
45		15.10 Appendices and supplementary materials	3 days	Mon 17/05/21	Wed 19/05/21	37SS,38SS,3
46		***16 Deliver the report in wiseflow***	***0 days***	***Wed 19/05/2***	***Wed 19/05/21***	
47		**17 PowerPoint**	**3 days**	**Fri 21/05/21**	**Tue 25/05/21**	**46FS+1 day**
48		**18 USNExpo video**	**5 days**	**Fri 21/05/21**	**Thu 27/05/21**	

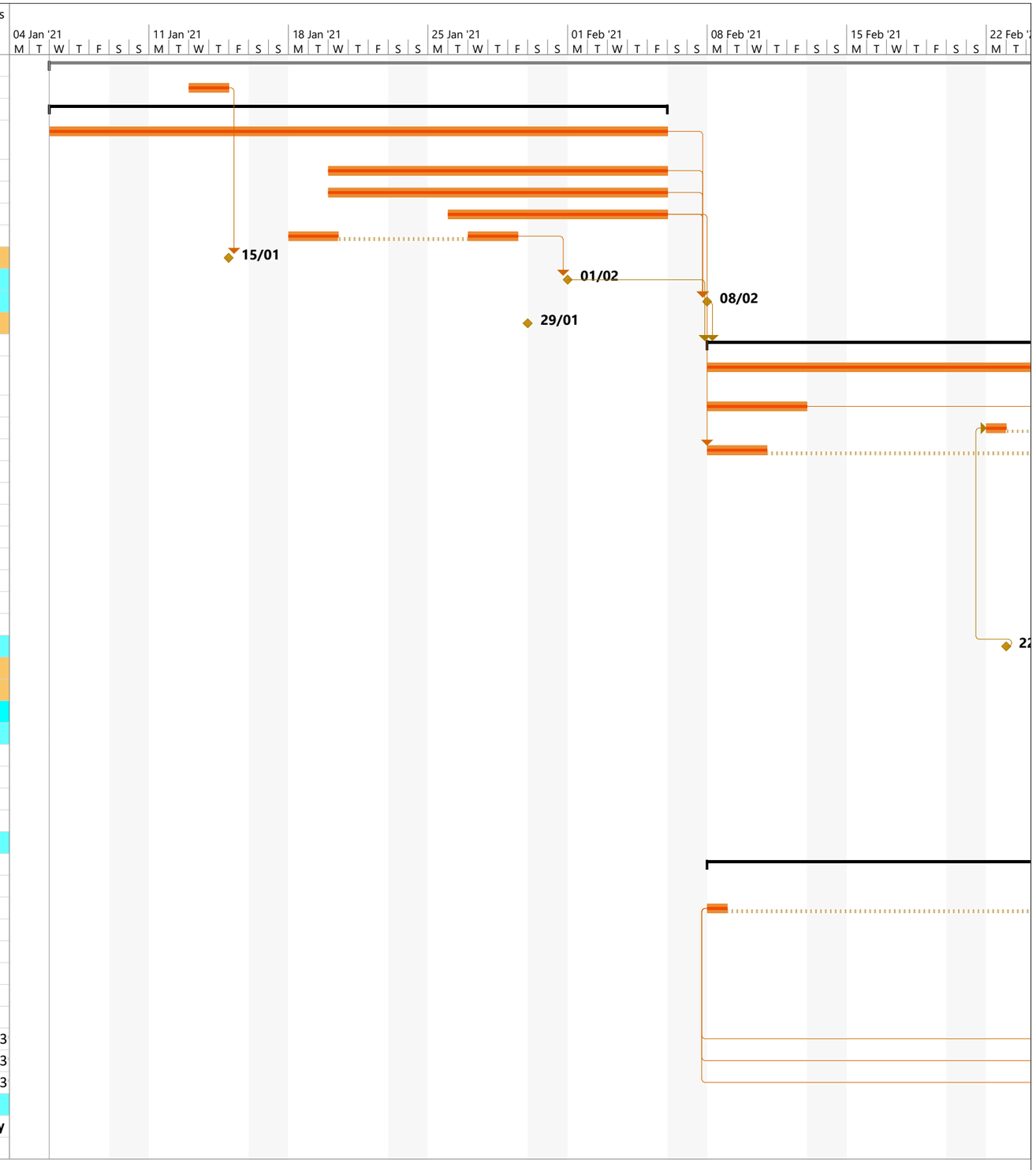

Project: Master thesis Gantt dia
Date: Mon 17/05/21

Task	Project Summary	Manual Task	Start-only	Deadline			
Split	Inactive Task	Duration-only	Finish-only	Late			
Milestone	Inactive Milestone	Manual Summary Rollup	External Tasks	Progress			
Summary	Inactive Summary	Manual Summary	External Milestone	Manual Progress			

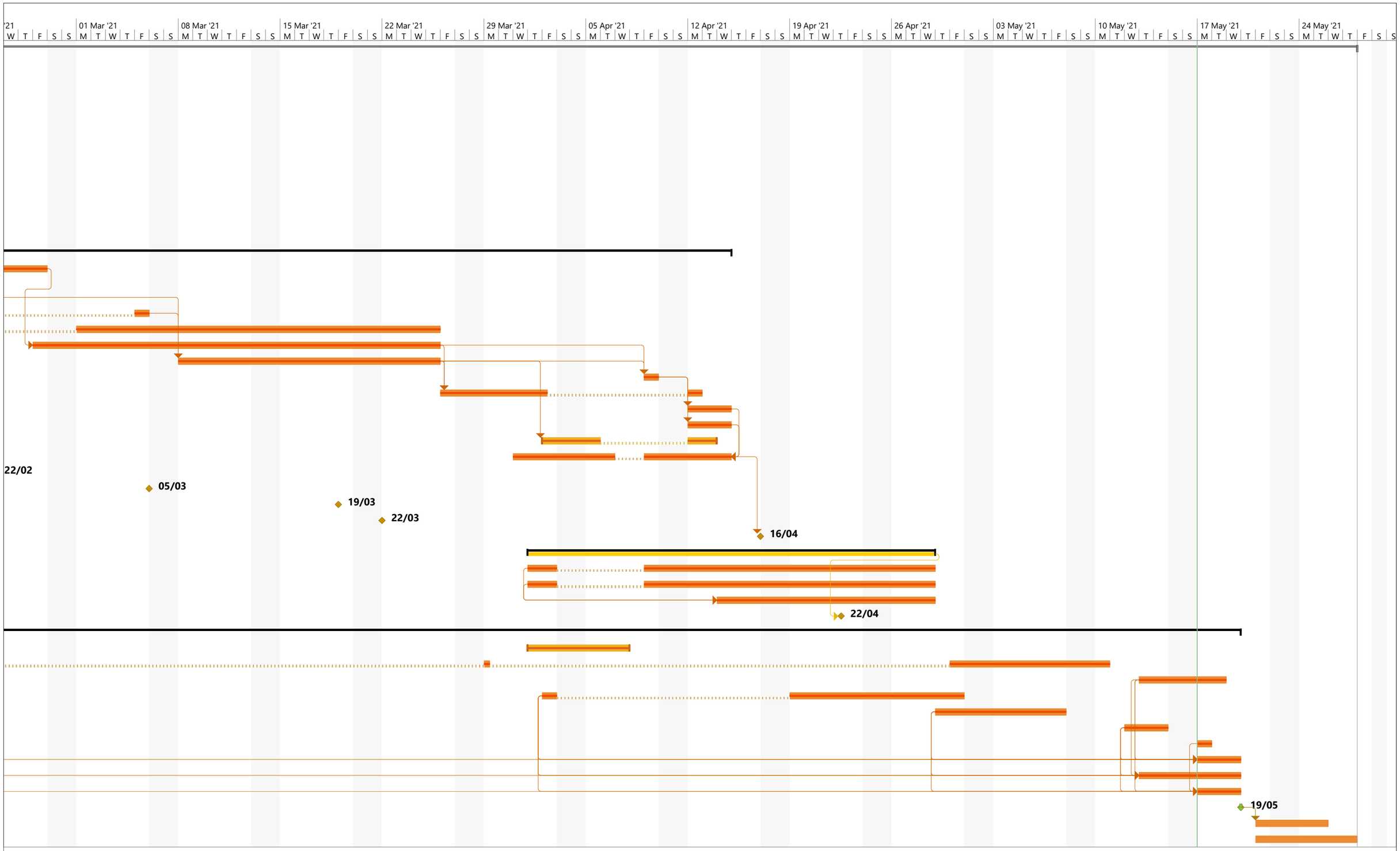

Project: Master thesis Gantt dia Date: Mon 17/05/21	Task		Project Summary		Manual Task		Start-only		Deadline	
	Split		Inactive Task		Duration-only		Finish-only		Late	
	Milestone		Inactive Milestone		Manual Summary Rollup		External Tasks		Progress	
	Summary		Inactive Summary		Manual Summary		External Milestone		Manual Progress	

Appendix E: Project discription.

University of South-Eastern Norway

Faculty of Technology, Natural Sciences and Maritime Sciences, Campus Porsgrunn

FMH606 Master's Thesis

Title: Modelling temperature transition and co-digestion in VEAS biogas process

USN supervisor: Wenche Hennie Bergland and Gamunu S. Arachchige

External partner: Espen Govasmark at VEAS

Task background:
VEAS:
VEAS is the largest wastewater treatment plant in Norway located in Asker in Viken and treats sludge from 760,000 people in Oslo, Asker and Bærum municipalities. The sludge is used to produce biogas for upgrading to liquid biomethane (60 GWh/year). Today's biogas production takes place in 4 bioreactors of 6,000 m^3 by mesophilic digestion (37 °C) and hydraulic residence time (HRT) of 20-25 days on thickened sludge (7% TS) after precipitation with iron, aluminium and synthetic polymer. VEAS aims to increase their biomethane production by up to 50 % where several process changes are evaluated. Increasing the temperature from mesophilic to thermophilic, implementing pre-treatment technology in their mesophilic process and implementing new substrates are all considered.

AD Background:
Anaerobic digestion (AD) processes to produce biogas from many different substrates are a well-established and industrialized technology. AD consists of biological processes involving different microbial communities. Microbial communities are sensitive to technological and operational changes that may cause operational instability in the biogas process. Factors affecting the AD process are often linked to both process parameters and raw materials that collectively affect microbial growth, biogas composition and methane yield.

Relevance for VEAS:
VEAS can use the knowledge from the master's thesis at USN as an aid in predicting behaviour of the AD reactor with the process changes implemented. It may also be useful in the development of business concepts for increased biogas production at VEAS.

Task description:
The thesis work will focus on analysing and quantifying mechanisms related to microbial adaptations when changing from mesophilic operation to thermophilic operation. The simulations of temperature transition schemes will be used to look into a safe way to do the transition. Co-digestion and relevant inhibition issues are also to be analysed. Steady-state simulations will be used to investigate the biogas production in both mesophilic and thermophilic digestion with co-substrate and pre-treatment with Thermal Hydrolysis. Finally, the theses work should also evaluate possible ways of achieving the goal of 50 % increase in biomethane production.

A standard AD model (ADM1) should be adapted to the biogas processes at VEAS for simulations of their processes.

The task includes:

- Literature survey
- Analysing mechanisms in AD
- Modelling and simulation in ADM1 with required modifications
- Suggest and evaluate various operation conditions

Student: Veronika Mikelsone

The task is suitable for online students (not present at the campus): Yes

Practical arrangements:
-

Supervision:
As a general rule, the student is entitled to 15-20 hours of supervision. This includes necessary time for the supervisor to prepare for supervision meetings (reading material to be discussed, etc).

Signatures:

Supervisor (date and signature): 30.01.21 Wenche Bergland

Student (write clearly in all capitalized letters): VERONIKA MIKELSONE

Student (date and signature): Veronika Mikelsone 29.01.21

Appendix F: Analysis report from ALS Laboratory Group on sludges from Marker, Aremark and Indre Østfold municipalities.

ANALYSERAPPORT

Ordrenummer	: **NO2101529**	Side	: 1 av 8
Kunde	: **Vestfjorden Avløpsselskap**	Prosjekt	: Kompostverket
Kontakt	: Pia Ryrfors	Prosjektnummer	: Espen Govasmark
Adresse	: Bjerkåsholmen 125 3470 Slemmestad Norge	Prøvetaker Sted Dato prøvemottak	: ---- : ---- : 2021-02-05 13:25
Epost	: pr@veas.nu	Analysedato	: 2021-02-14
Telefon	: ----	Dokumentdato	: 2021-03-04 08:50
COC nummer	: ----	Antall prøver mottatt	: 3
Tilbuds- nummer	: OF191834	Antall prøver til analyse	: 3

Generelle kommentarer

Denne rapporten erstatter enhver preliminær rapport med denne referansen. Resultater gjelder innleverte prøver slik de var ved innleveringstidspunktet. Alle sider på rapporten har blitt kontrollert og godkjent før utsendelse.

Denne rapporten får kun gjengis i sin helhet, om ikke utførende laboratorium på forhånd har skriftlig godkjent annet. Resultater gjelder bare de analyserte prøvene.

Hvis prøvetakingstidspunktet ikke er angitt, prøvetakingstidspunktet vil bli default 00:00 på prøvetakingsdatoen. Hvis datoen ikke er angitt, blir default dato satt til dato for prøvemottak angitt i klammer uten tidspunkt.

Kommentarer

Leverte prøver 001 og 002 ble behandlet som ferdig sigevann på grunn av det lave innholdet av tørrstoff i den originale prøven.
Prøve(r) NO2101529/003, metode W-NH4-SPC ble / ble filtrert før analyse (filterporøsitet 0,45 um).
Prøve(r) NO2101529/001 - 003, metode S-OACEPP02 - LOT økes på grunn av fortynning.
Prøven for metod S-TC1-IR er tørket ved 105 grader og pulverisert før analyse.
Prøven for metod S-TOC1-IR er tørket ved 105 grader og pulverisert før analyse.

Underskrivere	*Posisjon*
Torgeir Rødsand	DAGLIG LEDER

Laboratorium	: ALS Laboratory Group avd. Oslo	Nettside	: www.alsglobal.no
Adresse	: Drammensveien 264 0283 Oslo Norge	Epost Telefon	: info.on@alsglobal.com : ----

Analyseresultater

Submatriks: **SLAM**

	Kundes prøvenavn	1 Slam Marker kommune Sediment
	Prøvenummer lab	NO2101529001
	Kundes prøvetakingsdato	2021-01-25 00:00

Parameter	Resultat	MU	Enhet	LOR	Analysedato	Metode	Utf. lab	Acc.Key
Tørrstoff								
Tørrstoff	**0.22**	± 0.04	%	0.10	2021-02-14	S-DRY-GRCI	PR	a ulev
Ikke-metalliske Uorganiske Parametere								
P (Fosfor)	**0.154**	± 0.05	% tørrvekt	0.050	2021-02-23	S-P2O5-PHO	CS	a ulev
Ekstraherbare elementer / metaller								
As (Arsen)	<0.56	----	mg/kg TS	0.50	2021-02-16	S-METAXAC1	PR	a ulev
Cd (Kadmium)	<0.11	----	mg/kg TS	0.10	2021-02-16	S-METAXAC1	PR	a ulev
Cr (Krom)	**5.57**	± 1.11	mg/kg TS	0.25	2021-02-16	S-METAXAC1	PR	a ulev
Cu (Kopper)	**74.5**	± 14.90	mg/kg TS	0.10	2021-02-16	S-METAXAC1	PR	a ulev
Hg (Kvikksølv)	<0.22	----	mg/kg TS	0.20	2021-02-16	S-METAXAC1	PR	a ulev
Ni (Nikkel)	**4.8**	± 1.00	mg/kg TS	1.0	2021-02-16	S-METAXAC1	PR	a ulev
Pb (Bly)	**3.6**	± 0.70	mg/kg TS	1.0	2021-02-16	S-METAXAC1	PR	a ulev
Zn (Sink)	**168**	± 33.50	mg/kg TS	5.0	2021-02-16	S-METAXAC1	PR	a ulev
Organiske syrer								
Melkesyre Lactic acid	<18.8	----	mg/kg	7.50	2021-02-15	S-OACEPP02	PR	a ulev
Metansyre (maursyre)	<18.8	----	mg/kg	7.50	2021-02-15	S-OACEPP02	PR	a ulev
Etansyre (eddiksyre)	**58.1**	± 11.60	mg/kg	7.50	2021-02-15	S-OACEPP02	PR	a ulev
Propansyre	**42.1**	± 8.42	mg/kg	7.50	2021-02-15	S-OACEPP02	PR	a ulev
Butansyre sm°rsyre. n-butyric acid (cas 107-92-6)	<18.8	----	mg/kg	7.50	2021-02-15	S-OACEPP02	PR	a ulev
Pentansyre	<18.8	----	mg/kg	7.50	2021-02-15	S-OACEPP02	PR	a ulev
iso-Pentansyre	<18.8	----	mg/kg	7.50	2021-02-15	S-OACEPP02	PR	a ulev
Heksansyre	<19	----	mg/kg	15	2021-02-15	S-OACEPP02	PR	a ulev
Fysikalsk								
pH (H2O)	**5.5**	± 0.20	-	1.0	2021-02-18	S-PHH2O-ELE	CS	a ulev
Glødetap (LOI)	**73.0**	± 3.65	% tørrvekt	0.10	2021-02-19	S-LI550GR	CS	a ulev
Gløderest	**27.0**	± 1.35	% tørrvekt	0.10	2021-02-19	S-LI550GR	CS	a ulev
Næringsstoffer								
Ammonium + Ammoniakk som NH4+	**17800**	----	mg/kg TS	0.50	2021-02-18	S-NH4-SPC	PR	a ulev
Ammonium-N + Ammoniakk-N	**13800**	----	mg/kg TS	0.40	2021-02-18	S-NH4-SPC	PR	a ulev
Total nitrogen (Tot-N)	**252000**	± 50400.00	mg/kg TS	50	2021-02-17	S-NTOT-PHO	CS	a ulev
Andre analyser								
TIC Totalt uorganisk karbon	**2.29**	----	% tørrvekt	0.10	2021-03-04	S-TIC-CC	CS	a ulev
Totalt ekstraherbare komponenter	**36**	± 7.00	mg/kg	20	2021-02-15	S-TEC-IR	PR	a ulev

Submatriks: **SLAM**

	Kundes prøvenavn	1 Slam Marker kommune Sediment
	Prøvenummer lab	NO2101529001
	Kundes prøvetakingsdato	2021-01-25 00:00

Parameter	Resultat	MU	Enhet	LOR	Analysedato	Metode	Utf. lab	Acc.Key
Andre analyser - Fortsetter								
Total Fett og oljer	**36**	± 7.00	mg/kg	20	2021-02-15	S-TEC-IR	PR	a ulev
Totalt organisk karbon (TOC)	**30.5**	± 4.57	% tørrvekt	0.10	2021-02-18	S-TOC1-IR	CS	a ulev
C-total Karbon-total	**32.8**	± 4.91	% tørrvekt	0.10	2021-02-18	S-TC1-IR	CS	a ulev
Karbonater	**11.4**	----	% tørrvekt	0.50	2021-03-04	S-TIC-CC	CS	a ulev

Submatriks: **SLAM**

	Kundes prøvenavn	2 Slam Aremark kommune Sediment
	Prøvenummer lab	NO2101529002
	Kundes prøvetakingsdato	2021-01-25 00:00

Parameter	Resultat	MU	Enhet	LOR	Analysedato	Metode	Utf. lab	Acc.Key
Tørrstoff								
Tørrstoff	**4.22**	± 0.28	%	0.10	2021-02-14	S-DRY-GRCI	PR	a ulev
Ikke-metalliske Uorganiske Parametere								
P (Fosfor)	**0.206**	± 0.05	% tørrvekt	0.050	2021-02-23	S-P2O5-PHO	CS	a ulev
Ekstraherbare elementer / metaller								
As (Arsen)	<0.50	----	mg/kg TS	0.50	2021-02-16	S-METAXAC1	PR	a ulev
Cd (Kadmium)	<0.10	----	mg/kg TS	0.10	2021-02-16	S-METAXAC1	PR	a ulev
Cr (Krom)	**8.28**	± 1.66	mg/kg TS	0.25	2021-02-16	S-METAXAC1	PR	a ulev
Cu (Kopper)	**295**	± 59.00	mg/kg TS	0.10	2021-02-16	S-METAXAC1	PR	a ulev
Hg (Kvikksølv)	<0.20	----	mg/kg TS	0.20	2021-02-16	S-METAXAC1	PR	a ulev
Ni (Nikkel)	**8.8**	± 1.80	mg/kg TS	1.0	2021-02-16	S-METAXAC1	PR	a ulev
Pb (Bly)	**6.0**	± 1.20	mg/kg TS	1.0	2021-02-16	S-METAXAC1	PR	a ulev
Zn (Sink)	**263**	± 52.60	mg/kg TS	5.0	2021-02-16	S-METAXAC1	PR	a ulev
Organiske syrer								
Melkesyre Lactic acid	<188	----	mg/kg	7.50	2021-02-15	S-OACEPP02	PR	a ulev
Metansyre (maursyre)	<188	----	mg/kg	7.50	2021-02-15	S-OACEPP02	PR	a ulev
Etansyre (eddiksyre)	**571**	± 114.00	mg/kg	7.50	2021-02-15	S-OACEPP02	PR	a ulev
Propansyre	**351**	± 70.20	mg/kg	7.50	2021-02-15	S-OACEPP02	PR	a ulev
Butansyre sm°rsyre. n-butyric acid (cas 107-92-6)	<188	----	mg/kg	7.50	2021-02-15	S-OACEPP02	PR	a ulev
Pentansyre	<188	----	mg/kg	7.50	2021-02-15	S-OACEPP02	PR	a ulev
iso-Pentansyre	<188	----	mg/kg	7.50	2021-02-15	S-OACEPP02	PR	a ulev
Heksansyre	<188	----	mg/kg	15	2021-02-15	S-OACEPP02	PR	a ulev
Fysikalsk								
pH (H2O)	**6.1**	± 0.20	-	1.0	2021-02-18	S-PHH2O-ELE	CS	a ulev
Glødetap (LOI)	**69.5**	± 3.48	% tørrvekt	0.10	2021-02-19	S-LI550GR	CS	a ulev

Submatriks: **SLAM**

	Kundes prøvenavn	2 Slam Aremark kommune Sediment
	Prøvenummer lab	NO2101529002
	Kundes prøvetakingsdato	2021-01-25 00:00

Parameter	Resultat	MU	Enhet	LOR	Analysedato	Metode	Utf. lab	Acc.Key
Fysikalsk - Fortsetter								
Gløderest	**30.5**	± 1.52	% tørrvekt	0.10	2021-02-19	S-LI550GR	CS	a ulev
Næringsstoffer								
Ammonium + Ammoniakk som NH4+	**11500**	----	mg/kg TS	0.50	2021-02-18	S-NH4-SPC	PR	a ulev
Ammonium-N + Ammoniakk-N	**8970**	----	mg/kg TS	0.40	2021-02-18	S-NH4-SPC	PR	a ulev
Total nitrogen (Tot-N)	**54900**	± 11000.00	mg/kg TS	50	2021-02-17	S-NTOT-PHO	CS	a ulev
Andre analyser								
TIC Totalt uorganisk karbon	**3.08**	----	% tørrvekt	0.10	2021-03-04	S-TIC-CC	CS	a ulev
Totalt ekstraherbare komponenter	**4030**	± 805.00	mg/kg	20	2021-02-15	S-TEC-IR	PR	a ulev
Total Fett og oljer	**4030**	± 805.00	mg/kg	20	2021-02-15	S-TEC-IR	PR	a ulev
Totalt organisk karbon (TOC)	**31.2**	± 4.69	% tørrvekt	0.10	2021-02-18	S-TOC1-IR	CS	a ulev
C-total Karbon-total	**34.3**	± 5.15	% tørrvekt	0.10	2021-02-18	S-TC1-IR	CS	a ulev
Karbonater	**15.4**	----	% tørrvekt	0.50	2021-03-04	S-TIC-CC	CS	a ulev

Submatriks: **SLAM**

	Kundes prøvenavn	3 Indre Østfold kommune Sediment
	Prøvenummer lab	NO2101529003
	Kundes prøvetakingsdato	2021-01-25 00:00

Parameter	Resultat	MU	Enhet	LOR	Analysedato	Metode	Utf. lab	Acc.Key
Tørrstoff								
Tørrstoff	**24.4**	± 1.50	%	0.10	2021-02-14	S-DRY-GRCI	PR	a ulev
Ikke-metalliske Uorganiske Parametere								
P (Fosfor)	**0.189**	± 0.05	% tørrvekt	0.050	2021-02-23	S-P2O5-PHO	CS	a ulev
Ekstraherbare elementer / metaller								
As (Arsen)	<0.50	----	mg/kg TS	0.50	2021-02-15	S-METAXAC1	PR	a ulev
Cd (Kadmium)	**0.11**	± 0.02	mg/kg TS	0.10	2021-02-15	S-METAXAC1	PR	a ulev
Cr (Krom)	**8.15**	± 1.63	mg/kg TS	0.25	2021-02-15	S-METAXAC1	PR	a ulev
Cu (Kopper)	**93.9**	± 18.80	mg/kg TS	0.10	2021-02-15	S-METAXAC1	PR	a ulev
Hg (Kvikksølv)	<0.20	----	mg/kg TS	0.20	2021-02-15	S-METAXAC1	PR	a ulev
Ni (Nikkel)	**5.8**	± 1.20	mg/kg TS	1.0	2021-02-15	S-METAXAC1	PR	a ulev
Pb (Bly)	**3.4**	± 0.70	mg/kg TS	1.0	2021-02-15	S-METAXAC1	PR	a ulev
Zn (Sink)	**189**	± 37.70	mg/kg TS	5.0	2021-02-15	S-METAXAC1	PR	a ulev
Organiske syrer								
Melkesyre Lactic acid	<188	----	mg/kg	7.50	2021-02-15	S-OACEPP02	PR	a ulev
Metansyre (maursyre)	<188	----	mg/kg	7.50	2021-02-15	S-OACEPP02	PR	a ulev
Etansyre (eddiksyre)	**748**	± 150.00	mg/kg	7.50	2021-02-15	S-OACEPP02	PR	a ulev

Submatriks: **SLAM**

	Kundes prøvenavn	3 Indre Østfold kommune Sediment
	Prøvenummer lab	NO2101529003
	Kundes prøvetakingsdato	2021-01-25 00:00

Parameter	Resultat	MU	Enhet	LOR	Analysedato	Metode	Utf. lab	Acc.Key
Organiske syrer - Fortsetter								
Propansyre	**639**	± 128.00	mg/kg	7.50	2021-02-15	S-OACEPP02	PR	a ulev
Butansyre sm°rsyre. n-butyric acid (cas 107-92-6)	<188	----	mg/kg	7.50	2021-02-15	S-OACEPP02	PR	a ulev
Pentansyre	<188	----	mg/kg	7.50	2021-02-15	S-OACEPP02	PR	a ulev
iso-Pentansyre	<188	----	mg/kg	7.50	2021-02-15	S-OACEPP02	PR	a ulev
Heksansyre	<188	----	mg/kg	15	2021-02-15	S-OACEPP02	PR	a ulev
Fysikalsk								
pH (H2O)	**7.1**	± 0.20	-	1.0	2021-02-19	S-PHH2O-ELE	CS	a ulev
Glødetap (LOI)	**73.9**	± 3.70	% tørrvekt	0.10	2021-02-22	S-LI550GR	CS	a ulev
Gløderest	**26.1**	± 1.30	% tørrvekt	0.10	2021-02-22	S-LI550GR	CS	a ulev
Næringsstoffer								
Ammonium + Ammoniakk som NH4+	**7.13**	----	mg/kg TS	0.50	2021-02-18	S-NH4-SPC	PR	a ulev
Ammonium-N + Ammoniakk-N	**5.53**	----	mg/kg TS	0.40	2021-02-18	S-NH4-SPC	PR	a ulev
Total nitrogen (Tot-N)	**29700**	± 5930.00	mg/kg TS	50	2021-02-19	S-NTOT-PHO	CS	a ulev
Andre analyser								
TIC Totalt uorganisk karbon	**1.18**	----	% tørrvekt	0.10	2021-03-04	S-TIC-CC	CS	a ulev
Totalt ekstraherbare komponenter	**3270**	± 653.00	mg/kg TS	20	2021-02-15	S-TEC-IR	PR	a ulev
Total Fett og oljer	**3270**	± 653.00	mg/kg TS	20	2021-02-15	S-TEC-IR	PR	a ulev
Totalt organisk karbon (TOC)	**31.2**	± 4.68	% tørrvekt	0.10	2021-02-19	S-TOC1-IR	CS	a ulev
C-total Karbon-total	**32.4**	± 4.86	% tørrvekt	0.10	2021-02-19	S-TC1-IR	CS	a ulev
Karbonater	**5.90**	----	% tørrvekt	0.50	2021-03-04	S-TIC-CC	CS	a ulev

Submatriks: **ELUAT**

	Kundes prøvenavn	1 Slam Marker kommune Sediment
	Prøvenummer lab	NO2101529001
	Kundes prøvetakingsdato	2021-01-25 00:00

Parameter	Resultat	MU	Enhet	LOR	Analysedato	Metode	Utf. lab	Acc.Key
Andre analyser								
KOF-Cr	**134000**	± 20200.00	mg/kg TS	50	2021-02-17	W-COD-SPC	PR	a ulev

Submatriks: ELUAT	Kundes prøvenavn	2 Slam Aremark kommune Sediment
	Prøvenummer lab	NO2101529002
	Kundes prøvetakingsdato	2021-01-25 00:00

Parameter	Resultat	MU	Enhet	LOR	Analysedato	Metode	Utf. lab	Acc.Key
Andre analyser								
KOF-Cr	**78000**	± 11700.00	mg/kg TS	50	2021-02-17	W-COD-SPC	PR	a ulev

Submatriks: ELUAT	Kundes prøvenavn	3 Indre Østfold kommune Sediment
	Prøvenummer lab	NO2101529003
	Kundes prøvetakingsdato	2021-01-25 00:00

Parameter	Resultat	MU	Enhet	LOR	Analysedato	Metode	Utf. lab	Acc.Key
Andre analyser								
KOF-Cr	**43800**	± 6580.00	mg/kg TS	50	2021-02-18	W-COD-SPC	PR	a ulev

Dette er slutten av analyseresultatdelen av analysesertifikatet

Kort oppsummering av metoder

Analysemetoder	Metodebeskrivelser
S-LI550GR	CZ_SOP_D06_07_047.A (CSN EN 15169, CSN EN 15935, CSN EN 13039, CSN 72 0103, CSN 46 5735) Bestemmelse av aske gravimetrisk og bestemmelse av glødetap ved utregning fra målte verdier.
S-NTOT-PHO	CZ_SOP_D06_07_102 (CSN ISO 11261) Bestemmelse av total nitrogen ved modifisert Kjeldahl metode spektrofotometrisk.
S-P2O5-PHO	CZ_SOP_D06_07_138 (CSN 72 0116-1) Bestemmelse av P2O5 in silika prøvemateriale etter dekomponering spektrofotometrisk.
S-PHH2O-ELE	CZ_SOP_D06_07_113 (CSN ISO 10390, CSN EN 12176:1999, CSN EN 13037, CSN EN 15933, CSN 46 5735 ZMENA 1, ÖNORM L1086-1, US EPA Metode 9045D; US EPA SW-846 Metode 9040 (Liquid) og sW-846 Metode 9045 (Jord)) Bestemmelse av pH elektrokjemisk i jordsuspensjonen i vann, KCl, CaCl2, BaCl2.
S-TC1-IR	CZ_SOP_D06_07_121.A (CSN ISO 29541, CSN EN ISO 16994, CSN EN ISO 16948, CSN EN 15407, CSN ISO 19579, CSN EN 15408, CSN ISO 10694, CSN EN 13137) Bestemmelse av totalt karbon (TC), totalt organisk karbon (TOC), total svovel og hydrogen ved forbrenningsmetode ved bruk av IR,-bestemmelse av total nitrogen ved forbrenningsmetode ved bruk av TCD og bestemmelse av oksygen ved utregning og totalt uorganisk karbon (TIC) og karbonater ved utregning fra målte verdier.
S-TIC-CC	CZ_SOP_D06_07_121.A (CSN ISO 29541, CSN EN ISO 16994, CSN EN ISO 16948, CSN EN 15407, CSN ISO 19579, CSN EN 15408, CSN ISO 10694, CSN EN 13137) Bestemmelse av totalt karbon (TC), totalt organisk karbon (TOC), total svovel og hydrogen ved forbrenningsmetode ved bruk av IR,-bestemmelse av total nitrogen ved forbrenningsmetode ved bruk av TCD og bestemmelse av oksygen ved utregning og totalt uorganisk karbon (TIC) og karbonater ved utregning fra målte verdier.
S-TOC1-IR	CZ_SOP_D06_07_121.A (CSN ISO 29541, CSN EN ISO 16994, CSN EN ISO 16948, CSN EN 15407, CSN ISO 19579, CSN EN 15408, CSN ISO 10694, CSN EN 13137) Bestemmelse av totalt karbon (TC), totalt organisk karbon (TOC), total svovel og hydrogen ved forbrenningsmetode ved bruk av IR,-bestemmelse av total nitrogen ved forbrenningsmetode ved bruk av TCD og bestemmelse av oksygen ved utregning og totalt uorganisk karbon (TIC) og karbonater ved utregning fra målte verdier.
S-DRY-GRCI	CZ_SOP_D06_01_045 (CSN ISO 11465, CSN EN 12880, CSN EN 14346), CZ_SOP_D06_07_046 (CSN ISO 11465, CSN EN 12880, CSN EN 14346, CSN 46 5735) Bestemmelse av tørrstoff gravimetrisk og bestemmelse av vanninnhold ved utregning fra målte verdier.
S-METAXAC1	CZ_SOP_D06_02_001 (US EPA 200.7, ISO 11885, US EPA 6010, SM 3120, prøver opparbeidet i henhold til CZ_SOP_D06_02_J02 (US EPA 3050, CSN EN 13657, ISO 11466) kap. 10.3 to 10.16, 10.17.5, 10.17.6, 10.17.9 to 10.17.14), Bestemmelse av elementer ved AES med ICP og støkiometriske utregninger av konsentrasjonen til aktuelle forbindelser fra målte verdier. Prøven ble homogenisert og mineralisert med salpetersyre i autoklav under høyt trykk og temperatur før analyse.
S-NH4-SPC	CZ_SOP_D06_02_019 Bestemmelse av sum av Ammoniakk og ammoniumioner, nitritt og totale oksiderte nitrogenioner ved diskret spektrofotometri (basert på CSN ISO 11732, CSN ISO 13395). Målt i eluat, rekalkulert for tørrstoff.
S-OACEPP02	CZ_SOP_D06_03_188.B (Lumex manual, Kudrjaskeova, M.: Kapillær electrophoretic monitoring av microbial growth: -bestemmelse av organiske syrer, COPYRIGHT 2004 Estonian Academy Publishers, June, 2004 Source Volume: 53 Source Issue: 2, ISSN: 1406-0124) Bestemmelse av organiske syrer ved kapillær electrophoresis metode med UV deteksjon
S-TEC-IR	CZ_SOP_D06_02_058 (ISO/TR 11046) Bestemmelse av ekstraherbare og upolare ekstraherbare forbindelser ved IR og bestemmelse av polar ekstraherbare stoffer ved utregning fra målte verdier.
W-COD-SPC	CZ_SOP_D06_02_076 (CSN ISO 15705) Bestemmelse av kjemisk oksygenforbruk (KOF) ved bruk av dikromat (KOF-Cr) fotometrisk. / CZ_SOP_D06_02_076.A / CZ_SOP_D06_07_040 (CSN ISO 6060, CSN ISO 15705) Bestemmelse av kjemisk oksygenforbruk (KOF) ved bruk av dikromat (KOF-Cr) ved titrering.

Prepareringsmetoder	Metodebeskrivelser
*S-PPHOM.07	CZ_SOP_D06_07_P01 Prøvepreparering av faste prøver for analyse (knusing, kverning og pulverisering).
*S-PPHOM0.3	CZ_SOP_D06_07_P01 Prøvepreparering av faste prøver for analyse (knusing, kverning og pulverisering).
*S-PPHOM10	CSN EN 12457-4 Sikting og knusing av prøve med kornstørrelse < 10 mm.
*S-PPHOM2	Tørking og sikting av prøve med kornstørrelse < 2 mm
S-PPL24CE	CSN EN 12457-4 (CZ_SOP_D06_07_P04) Karakterisering av avfall - Eluering - Utlekkingstest av granulert avfall, materialer og slam - Part 4: Ett-stegs test ved væske to solid ratio 10 L/kg for prøvemateriale med partikkelstørrelse under 10 mm (uten or med størrelsesreduksjon). Liquid to Solid ratio var 10:1.
*S-PPL24INS	CZ_SOP_D06_07_P03 Prøvepreparering av eluat. Solid to væske ratio (S:L) var 1:10 (S per kg tørrstoff).

Nøkkel:

LOR = Rapporteringsgrenser representerer standard rapporteringsgrenser for de respektive parameterne for hver metode. Merk at rapporteringsgrensen kan bli påvirket av f.eks nødvendig fortynning grunnet matriksinterferens eller ved for lite prøvemateriale

MU = Måleusikkerhet

a = A etter utøvende laboratorium angir akkreditert analyse gjort av ALS Laboratory Norway AS

a ulev = A ulev etter utøvende laboratorium angir akkreditert analyse gjort av underleverandør

* = Stjerne før resultat angir ikke-akkreditert analyse.

< betyr mindre enn

> betyr mer enn

n.a. – ikke aktuelt

n.d. – Ikke påvist

Måleusikkerhet:

Måleusikkerhet skal være tilgjengelig for akkrediterte metoder. For visse analyser der dette ikke oppgis i rapporten, vil dette oppgis ved henvendelse til laboratoriet.

Måleusikkerheten angis som en utvidet måleusikkerhet (etter definisjon i "Evaluation of measurement data - Guide to the expression of uncertainty in measurement", JCGM 100:2008 Corrected version 2010) beregnet med en dekningsfaktor på 2 noe som gir et konfidensinterval på om lag 95%.

Måleusikkerhet fra underleverandører angis ofte som en utvidet usikkerhet beregnet med dekningsfaktor 2. For ytterligere informasjon, kontakt laboratoriet.

Utførende lab

	Utførende lab
CS	*Analysene er utført av:* ALS Czech Republic, s.r.o., Bendlova 1687/7 Ceska Lipa 470 01
PR	*Analysene er utført av:* ALS Czech Republic, s.r.o., Na Harfe 336/9 Prague 9 - Vysocany 190 00

Appendix G: List of variables and equations added or edited in ADM1_FTnew

---

Edit Variables

---

alpha_aa: regression coefficient for amino acids
0.1176
alpha_ac: regression coefficient for acetate
0.01128
alpha_c4: regression coefficient for valerate and butyrate
0.01248
alpha_fa: regression coefficient for LCFA
0.01008
alpha_pro: regression coefficient for propionate
0.00888
km_aa: maximum uptake rate amino acid degrading organisms
F_Tref_aa/Y_aa
km_ac: maximum uptake rate for acetate degrading organisms
F_Tnew_ac/Y_ac
km_c4: maximum uptake rate for c4 degrading organisms
F_Tref_c4/Y_c4
km_fa: maximum uptake rate for long chain fatty acid degrading organisms
F_Tref_fa/Y_fa
km_pro: maximum uptake rate for propionate degrading organisms
F_Tref_pro/Y_pro
mue_max_aa: 6.384
mue_max_ac: 0.624
mue_max_c4: 0.684
mue_max_fa: 0.552
mue_max_pro: 0.48

S_hg_ac: F_Tnew - constant of change in degrees Celsius
3
T_a: Real List Variable (t)
T_max_aa: Maximum temperature for amino acid degraders
338
T_max_ac: Maximum temperature for acetate degraders
338
T_max_c4: Maximum temperature for valerate and butyrate degraders
343
T_max_fa: Maximum temperature for LCFA degraders
338
T_max_pro: Maximum temperature for propionate degraders
338
T_opt_aa: Optimal temperature for amino acid degraders
328
T_opt_ac: Optimal temperature for acetate degraders
328

T_opt_c4: Optimal temperature for valerate and butyrate degraders
333
T_opt_fa: Optimal temperature for LCFA degraders
328
T_opt_pro: Optimal temperature for propionate degraders
326
Sigma_ac: F_Tnw - bell-shape parametr of the curve
(-S_hg_ac^2/(-1.3863))^0.5
mue_X_ac: maximum specific growth rate for acetoclastic methanogens
F_Tnew_ac*S_ac/(Ks_ac+S_ac)*I_ph_ac*I_nh3_ac*I_NH_limit
F_dyn_ac: dynamic part of microbial growth rate
exp(-(T-T_a)^2/(2*Sigma_ac^2))

F_ss_ac: steady state part of microbial growth rate
if T_a>T_opt_ac then mue_max_ac*(T_max_ac-T_a)/(T_max_ac
-T_opt_ac) else mue_max_ac-alpha_ac*(T_opt_ac-T_a) endif

F_Tnew_ac: temperature dependent maximum growth rate
F_ss_ac*F_dyn_ac
F_Tref_aa: steady state part of microbial growth rate
if T>T_opt_aa then mue_max_aa*(T_max_aa-T)/(T_max_aa-T_o
pt_aa) else mue_max_aa-alpha_aa*(T_opt_aa-T) endif
F_Tref_c4: steady state part of microbial growth rate
if T>T_opt_c4 then mue_max_c4*(T_max_c4-T)/(T_max_c4-T_o
pt_c4) else mue_max_c4-alpha_c4*(T_opt_c4-T) endif
F_Tref_fa: steady state part of microbial growth rate
if T>T_opt_fa then mue_max_fa*(T_max_fa-T)/(T_max_fa-T_o
pt_fa) else mue_max_fa-alpha_fa*(T_opt_fa-T) endif
F_Tref_pro: steady state part of microbial growth rate
if T>T_opt_pro then mue_max_pro*(T_max_pro-T)/(T_max_pro
-T_opt_pro) else mue_max_pro-alpha_pro*(T_opt_pro-T) endif